AD_____

Award Number: DAMD17-96-1-6239

TITLE: Clinical and Technical Performance Evaluation of a Digital Mammography System

PRINCIPAL INVESTIGATOR: Ronald Schilling, Ph.D.

CONTRACTING ORGANIZATION: Primex General Imaging Corporation
Carlsbad, California 92008

REPORT DATE: July 2000

TYPE OF REPORT: Final

PREPARED FOR: U.S. Army Medical Research and Materiel Command
Fort Detrick, Maryland 21702-5012

DISTRIBUTION STATEMENT: Approved for Public Release;
Distribution Unlimited

REPORT DOCUMENTATION PAGE

Form Approved
OMB No. 074-0188

1. AGENCY USE ONLY (Leave blank)	2. REPORT DATE	3. REPORT TYPE AND DATES COVERED
	July 2000	Final (17 Jun 96 - 16 Jun 00)

4. TITLE AND SUBTITLE
Clinical and Technical Performance Evaluation of a Digital Mammography System

5. FUNDING NUMBERS
DAMD17-96-1-6239

6. AUTHOR(S)
Ronald Schilling, Ph.D.

7. PERFORMING ORGANIZATION NAME(S) AND ADDRESS(ES)
Primex General Imaging Corporation
Carlsbad, California 92008

E-MAIL:
71461.3440@compuserv.com

8. PERFORMING ORGANIZATION REPORT NUMBER

9. SPONSORING / MONITORING AGENCY NAME(S) AND ADDRESS(ES)
U.S. Army Medical Research and Materiel Command
Fort Detrick, Maryland 21702-5012

10. SPONSORING / MONITORING AGENCY REPORT NUMBER

11. SUPPLEMENTARY NOTES

12a. DISTRIBUTION / AVAILABILITY STATEMENT
Approved for public release; distribution unlimited

12b. DISTRIBUTION CODE

13. ABSTRACT ***(Maximum 200 Words)***

A slot-scanning digital mammography system was designed, constructed and tested to determine if improved image quality can improve the diagnostic quality of mammograms or to show that the same image quality can be provided at a lower patient dose. Technical evaluation of image data showed improved image quality over screen-film mammography. Not all of the design parameters of the system were met and further improvements in spatial resolution and scanning speed can be obtained through recommended changes to the design. A 2-patient clinical study was performed demonstrating the feasibility of obtaining full-field digital mammograms with a slot-scanning system. Slot scanning is perhaps the lowest cost design for digital mammography due to the small detector area required. A promising new material (thallium bromide) was evaluated as a photoconductor that can be applied directly to the surface of a semiconductor sensor array. Results indicate that thallium bromide can provide superior performance over existing phosphors and photoconductors for many applications in digital x-ray imaging.

14. SUBJECT TERMS	15. NUMBER OF PAGES
Mammography, slot-scan, digital, solid-state	108
	16. PRICE CODE

17. SECURITY CLASSIFICATION OF REPORT	18. SECURITY CLASSIFICATION OF THIS PAGE	19. SECURITY CLASSIFICATION OF ABSTRACT	20. LIMITATION OF ABSTRACT
Unclassified	Unclassified	Unclassified	Unlimited

FOREWORD

Opinions, interpretations, conclusions and recommendations are those of the author and are not necessarily endorsed by the U.S. Army.

JRC Where copyrighted material is quoted, permission has been obtained to use such material.

JRC Where material from documents designated for limited distribution is quoted, permission has been obtained to use the material.

JRC Citations of commercial organizations and trade names in this report do not constitute an official Department of Army endorsement or approval of the products or services of these organizations.

N/A In conducting research using animals, the investigator(s) adhered to the "Guide for the Care and Use of Laboratory Animals," prepared by the Committee on Care and use of Laboratory Animals of the Institute of Laboratory Resources, national Research Council (NIH Publication No. 86-23, Revised 1985).

JRC For the protection of human subjects, the investigator(s) adhered to policies of applicable Federal Law 45 CFR 46.

N/A In conducting research utilizing recombinant DNA technology, the investigator(s) adhered to current guidelines promulgated by the National Institutes of Health.

N/A In the conduct of research utilizing recombinant DNA, the investigator(s) adhered to the NIH Guidelines for Research Involving Recombinant DNA Molecules.

N/A In the conduct of research involving hazardous organisms, the investigator(s) adhered to the CDC-NIH Guide for Biosafety in Microbiological and Biomedical Laboratories.

JRC FOR 6/16/00

PI - Ronald B. Schilling Date

Table of Contents

Introduction

The objective of the effort conducted under this grant was to demonstrate and evaluate the diagnostic sensitivity, specificity and accuracy in the detection of breast cancer by a low dose, primary x-ray, digital mammography system. Digital mammography systems have the potential to provide improved image quality and/or the same image quality at a lower patient dose than existing film-base mammography systems. It is a further objective of this study to determine if improved image quality will improve the diagnostic quality of mammograms or to show that the same image quality can be provided at a lower patient dose. This project was a collaborative effort among the applicant organization, PrimeX General Imaging Corporation (PGI), Carlsbad, California; Fischer Imaging Corporation, Denver, Colorado; the University of California at San Diego; and the University of Arizona at Tucson. The project was organized into three tasks: 1) System Integration, 2) Engineering and Technical Studies and 3) Clinical Studies.

The system integration effort was performed to complete the development of two digital slot-scanning mammography systems that were initially designed and partially developed through funding obtained from the National Institutes of Health with two Small Business Innovative Research (SBIR) grants (phase I and phase II grant no. 2R44CA59104-02AI). The engineering and technical studies were conducted at the University of Arizona to determine optimal spatial resolution, tube loading factors and a number of other parameters required to optimize system performance. Two clinical studies were to be performed involving a total of 1,100 women to determine the clinical efficacy of this digital mammography system in detecting breast cancer.

On March 15, 1999 Dr. John Cox of PGI and Dr. Tom Vogelsong of InfiMed, Inc. made a presentation to Dr. Mishra and staff at Ft. Detrick. During this presentation, an overview of the progress of this grant was made. A proposal was also presented for a change-of-scope request for an IDEA grant awarded to Xicon Technologies, Inc., a subsidiary of InfiMed, Inc. A discussion was held at this meeting regarding a number of problems encountered with the subcontractors working on this project, which has led to significant delays in progress. A recommendation was made to request a no-cost extension. On April 5, 1999 a request was made to obtain a 1-year no-cost extension for this grant. On May 7, 1999 our request was granted (Modification No. P90001), extending the performance period to June 16, 2000.

Our request to change the scope of Xicon's IDEA grant was based on difficulties Xicon was having with one of their subcontractors. We proposed to change the scope of the remaining effort to apply the thallium bromide photoconductor material to the surface of the sensor arrays developed in connection with this grant. A change of scope request was submitted by Xicon and was approved by the Army. A copy of the proposal submitted to the Army in connection with the change-of-scope request is attached in Appendix D. A complete description of the scope of this effort and the extent of PGI's involvement is provided. Results obtained from this effort are incorporated herein.

Body

The motivation for conducting the research funded by this grant as well as a description of the DXM-1 prototype slot-scanning digital mammography system is provided in Appendix A. The statement of work for this 3-year, $1.6 million study is shown below:

TASK 1: System Integration and System Optimization

Task 1.1. (Months 1-3): Integrate DXM-1 sensors and build test-bed prototype.

Milestones: Delivery of system to U of A for testing.

(Month 4-9): Integrate & test second Prototype for clinical studies.

Milestones: Deliver Prototype to UCSD Medical Center.

Task: 1.2 Objectives: Optimize system parameters.

Task 1.2.1. (Months 4-9): Determine, optimize system Dynamic Range:

Task 1.2.2. (Months 4-9): Determine, optimize Tube Loading Factor.

Task 1.2.3 (Months 4-9): Determine, optimize Sensor Bias and Lateral Motion of Electrons, Affecting Spatial Resolution:

Task 1.2.4. (Months 4-9): Noise Analysis:

Task 1.2.5 (Months 4-9): Determine optimum x-ray Energy:

Milestones: Deliver optimized prototype to UCSD Medical Center.

TASK 2: Engineering and Technical Evaluations of DXM-I system:

Task 2.1 Objectives: Determine imaging performance parameters

Task 2.1.1. (Month 10-18): Determine system Characteristic Curve and Sensitivity:

Task 2.1.2.(Month 10-18): Determine system spatial resolution in terms of modulation transfer function (MTF):

Task 2.1.3. (Month 10-18): Determine system noise power spectrum.

Task 2.1.4. (Month 10-18): Determine system Detective Quantum Efficiency (DQE).

Task 2.1.5. (Month 10-18): Determine system Display Signal-to-Noise Ratio.

Task 2.2. (Month 19-24): Objectives: Conduct Contrast Detail Studies using CDMAM phantom.

Task 2.3. (Month 19-24):Objectives: Clinical evaluations to determine observer performance digital vs. Film-screen mammograms.

Task 2.4. (Month 25-30): Objectives: Evaluation of CAD performance; film-Screen versus digital mammograms:

Task 3: Clinical Studies to assess efficacy of DXM-I digital mammography system.

Task 3.1 (Month 10-12): Objectives: Clinical Study Part A to acquaint and train radiologists to read digital mammograms.

Milestones: Radiologists familiarity with the digital mammography system.

Task 3.2 (Month 13-18): Objectives: Clinical Study Part B to assure system safety and efficacy by imaging patients with known abnormal mammograms.

Milestones: Establish DXM-I safety and assurance of its performance at least equal to film screen.

Task 3.3 (Month 19-36): Objectives: (Clinical Studies Part C) Prospective clinical trial of screening digital mammography versus conventional film-screen mammography:

Milestones: Establish clinical efficacy of DXM-I for digital mammography. Quarterly reports on objectives achieved.

Task 1 Accomplishments

The goal of this task was to complete the routine integration of two prototype DXM-1 digital mammography systems. The DXM-1 as described in Appendix A required critical components from a number of outside vendors. Significant delays were encountered from each to these vendors that had the effect of significantly limiting the accomplishments obtained for this project. While this task was scheduled to be completed during the first 3 months of this project several significant delays were encountered that ultimately had a major impact on the amount of clinical studies that were done. The strategy employed to accomplish all of the goals set forth for this project was based on the extensive use of sub-contractors to provide components for the DXM-1. This strategy was employed to try to minimize cost and time.

As stated in Appendix A, the sensors were developed during a previously funded effort and were in the process of being re-designed to improve performance. Newly re-designed and fabricated sensors were not functional. The entire wafer lot containing more than 200 sensors produced only 2 functional die. This created a severe problem in that there was no way to tell if the poor yield was due to design error or fabrication problems. Several meetings were held at the foundry to try and determine the nature of the problem. Ultimately another lot was run using the older design. The yield improved somewhat and several working sensor dies were produced. We subsequently learned that problems with the foundry were the cause of the poor yield. Additional delays were encountered when two of the other sub-contractors were late in delivering components. The mammography gantry was delivered almost a year late and the digital signal processor was about 15 months late. Eventually all of the components were delivered and tested.

System parameters of the DXM-1 prototype were measured that primarily determine image quality. There are three areas of concern; the signal generation, the generation of noise and the removal of artifacts produced from the analog and digital signal processors. The signal generation parameters measured were: x-ray absorption of the diode substrate material (silicon) and the effective energy of the x-ray generator. As shown in Appendix B, Figures B1 - B4, three detector substrates were placed in front of a phosphor-coated fiberoptic taper coupled to a Charge Coupled Device (CCD) camera. Images were acquired with this camera using an x-ray generator. Three different x-ray spectra were used to obtain these images: 80 kVp, 30 kVp and 26 kVp. Using specific filters in connection with these spectra well-characterized effective x-ray energy is produced. For the 80 kVp spectra, the effective energy is 50.5 keV, for the 30 kVp spectra, 19 keV and 14.9 keV for the 26 kVp spectrum. The total absorption measured with these energies is shown in the table below and compared with data calculated from first principles:

Effective X-ray Energy	Calculated Absorption	% Absorption (1.53mm of Si)
50.5 keV	14%	12.3%
19 keV	76%	73.3%
14.9 keV	96%	86.9%

These data suggest that an absorption efficiency of 73 to 86% can be expected for typical mammography spectra using a 1.53 mm silicon detector substrate. These values correlate well with the calculated values. The calculated values assume a mono-energetic, collimated beam of x-rays.

The x-ray generator that will be used in connection with this study was characterized to determine its effective energy at two energy settings, with and without an absorber (to simulate tissue). The effective energy was determined as described by Johns and Cunningham [56] and by Hillen, et al [43]. The results of this study are shown in Figures B5 - B7 and are summarized in the table below:

Energy Spectra	No Absorber	3.9 cm Plexiglas
26 kVp	14.89 keV (E-eff)	18.73 keV (E-eff)
30 kVp	15.55 keV (E-eff)	17.99 keV (E-eff)

These data show that the effective energy of the generator is approximately half of the peak tube voltage with no absorber. Beam hardening through the Plexiglas absorber increases the effective energy. Accordingly, the absorption efficiency of the detector

substrate will decrease from 87% to 73% with a 26kVp spectra due to absorption and beam hardening in the breast tissue.

Results obtained from task 2 indicated that resolution was being degraded in the in-scan axis of the image. After subsequent analysis, it was determined that the chip design allowed for parasitic capacitance or charge sharing among the TDI summing capacitors on the sensor readout chip. To correct these problems, the sensor chip was redesigned, a new mask set was generated and another lot run was initiated. This lot run produced poor results and a meeting with the wafer fabrication vendor (Orbit Semiconductor, Sunnyvale, CA) was held. The source of the problems resulting in poor yield was not established. The lot runs fabricated to that point were made on Orbit's 4-inch wafer fab line, which was in the process of being phased out. Orbit has set up a 6-inch wafer fab line and they agreed to re-run the lot on the new line. A new mask set was made to adapt to the 6-inch format and a lot run was made. The yield on the new lot run was significantly improved and many working chips were produced. A photograph of an assembled and packaged sensor is shown in Figure B8.

The 2-channel DSP unit required several modifications in order to operate at the desired speed (i.e., 10 MHz) using a software-implemented image formation algorithm. The contractor that was chosen to design and fabricate the DSP units was Berkeley Camera Engineering, Inc. They designed, fabricated and delivered a 2-channel DSP unit that only worked at 8 MHz.

Fischer Imaging Corporation delivered the Senoscan mammography gantry that was used for the technical and clinical evaluation tasks. The gantry and its SUN workstation were modified to accommodate and operate the DXM-1 imaging system. Figure B9 shows the assembled detector module with its eight sensor chips. Underneath the sensors are two printed circuit boards containing the analog signal processor where the sensor output is digitized and sent to the DSP unit. Figures B10 and B11 show the Senoscan unit with the generator housing removed. In these two views, the generator and collimator are exposed. Figures B12 and B13 show the gantry fully assembled. Figure B13 shows the gantry next to an engineer to give the reader a perspective on the size of the gantry.

The Fischer x-ray system is constructed with an embedded microprocessor. This embedded processor controls the x-ray generator, a Galil motion controller, and the filter wheel. The x-ray generator, which also has an embedded processor, is connected to the microprocessor through a serial interface. The microprocessor sends commands to the x-ray generator to control tube current, kVp and exposure time. The Galil is a programmable motor controller that controls the rotation, elevation, breast compression plate and scan arm motion. The Galil is connected to the microprocessor through a custom parallel interface. The microprocessor sends commands to the Galil to adjust elevation, rotation, and compression, and to initiate and control the scan velocity. The Galil sends position information to the microprocessor from a rotation sensor and a compression thickness sensor. The filter wheel assembly has it's own controller connected to the microprocessor through a serial interface. The microprocessor sends

commands to the filter controller to select one of three different filters. Currently the filters available are rhodium, molybdenum and aluminum.

Fischer Imaging provided a custom microprocessor configuration with a programmable tube current, kVp, x-ray exposure time, filter position, and scan velocity, with a dumb terminal over a serial interface. Compression thickness, rotation position and other system status codes are accessible through the serial interface as well. A foot pedal and a manual knob, located on the x-ray system, control breast compression. Thumb switches, also located on the x-ray system, control rotation and elevation. X-ray and scan initiation is controlled by a standard dead-man switch configuration.

Software for a graphic user interface (GUI) was written that allows the operator of the system to enter the desired x-ray technique parameters from the host computer, currently a Sun Ultra 10 workstation. This GUI sends the proper ASCII commands to the microprocessor emulating a dumb terminal output and receives and displays the technique parameters.

A safety interlock was designed and built that consists of an interlock board that plugs into the parallel port of the host computer. The host computer sends a heartbeat signal to the interlock board. The heartbeat signal consists of two, eight bit words that alternate at one-second intervals. The heartbeat signal is sent to the interlock board only if the technique parameters received by the host computer match the parameters entered by the operator. The host computer monitors the x-ray tube heat loading and will disrupt the heartbeat signal if the tube heat loading exceeds specifications. If the heartbeat signal is not present, the interlock board disconnects power to the dead-man switch on the x-ray system, disabling x-ray initiation. The heart beat signal provides an intrinsically safe interlock for such things as computer glitches and unauthorized access.

An image restoration program was written to stitch together the 16 individual image strips acquired (one for each of 2 banks of pixels on each of the 4 sensors). The assembled image is formatted for storage using a file format compatible with any of several image-processing programs that will permit the radiologist to enhance, display, archive or print the acquired image. The GUI program described above will permit the radiologist to control the operating parameters of the mammography gantry and acquire images.

A study of the sensor design was undertaken to try to determine the nature of the performance deficiencies discovered during task 2. This effort was frustrated by the poor performance of the wafer foundry early in the program. Once we were able to determine the nature of the fabrication problems at the foundry, our sensor design subcontractor using the newly fabricated ICs and the DXM-1 prototype undertook an exhaustive evaluation of the sensor chip design. Several design errors were detected and our subcontractor furnished a report. This report is attached in Appendix C. The design errors manifest themselves in a loss of resolution in the in-scan axis of the image. The readout ICs perform an on-chip 4-pixel Time Delay and Integration (TDI) during image acquisition. Pixels in the cross-scan axis are read out without any such processing.

During the technical evaluation of the images produced, it was discovered that the sensor array produces full resolution in the cross-scan axis but has less than half the resolution in the in-scan axis.

Task 2 Accomplishments

Initially three parameters that affect the performance of the DXM- I imager were measured: Mean and Standard Deviation, Signal-to-Noise Ratio (SNR), noise power spectrum (NPS) and dark signal generation. To analyze the Mean and Standard Deviation, the mean analog-to-digital units (ADU) were measured and plotted vs. relative exposure in mAs. These measurements were made by acquiring x-ray images with the DXM-1. An area of interest (AOI) was selected in the image containing approximately 10,000 pixels. Each pixel consists of a gray-level value produced by the digitized TDI sum of the detector elements on the sensor array. Each pixel contains a 16-bit digital word to represent its gray level value, thus each pixel has a capacity of 16,384 ADUs or gray levels. It is important to note that the Mean increases linearly with exposure.

The DXM-1 sensor arrays contain two separate banks of detectors offset by half a pixel in the in-scan and cross-scan direction. Results obtained with both banks of sensors were plotted as shown in Figure B14. As shown bank 2 consistently has a higher sensitivity than bank 1 and both banks show an increased output as exposure is increased. The root-mean square (RMS) of the ADU was plotted vs. exposure for both banks of sensors and is shown in Figure B15. Note that the RMS increases as the square root of the exposure. The Signal-to-Noise Ratio (SNR) calculated by dividing the mean with the RMS, is plotted vs. exposure in Figure B16. As shown, the SNR is about 45:1 at an exposure of 25 mA and increases with increasing exposure to about 85:1 at an exposure of 130 mA. Also note that the SNR increases as the square root of the exposure as well.

The Mean (ADU) of the sensor array AOI was measured without x-ray exposure as a function of time for both banks of sensors. The results are shown in Figure B17. As shown, the mean dark signal in as a function of time for both banks of sensors. Bank I has a higher dark current generation rate than Bank 2. The increase in dark current generation is attributed to the temperature rise experienced by the camera and sensor array due to heat generated while the system is on.

The noise power spectrum (NPS) of the sensor arrays was determined as described by Dainty, et al [57] and Roehrig, et al [53] and is plotted as a function of frequency from 0 to 10 line pairs/mm (lp/mm). Data was obtained with and without x-ray exposure. The results of this study are shown in Figures B18 and B19. As shown in Figure B18, the NPS of both banks of sensors decreases slightly as frequency increases for both cases (with and without x-ray exposure). As shown in Figure B19, the NPS was obtained under four exposure conditions with the accreditation phantom. The NPS decreases with increased exposure and frequency.

Images were acquired of the accreditation phantom to characterize the amount of fixed pattern noise and other artifacts created by the camera and DSP system. Images

obtained are shown in Figures B20 and B21. A schematic of the accreditation phantom is shown in Figure B22. As shown in Figure B20, at an exposure of 75 mA, mass groups 13 - 15 are visible, while 16 is not. Figure B21 shows the same mass groups taken at an exposure of 100 mA. At this exposure mass group 16 is not visible either. These images were produced with a dark-subtraction and flat-fielding algorithm applied to the raw image data.

Several images were acquired with the first DXM-1 prototype using only two of the required eight sensor chips. Although this system has only 1/4 of the total imaging area, several images were acquired and were analyzed. The data so produced has been used to complete the development of the system and make the required changes to the sensor chips and DSP unit. These images have been printed on a laser film printer and photographed with a Minolta digital still camera. The digital images were imported into Adobe Photoshop where some contrast enhancements and cropping was performed. These images were then printed on an inkjet printer with 300 dots-per-inch resolution. Figure B23 shows a photograph of the prototype 2-channel imaging system. As shown the gantry is a simplified version of the Senoscan unit and contains a lower power x-ray generator. The SUN workstation and DSP unit used to acquire images is shown in Figure B24. As shown the DSP unit is connected to the analog signal processor by several ribbon cables. Images are acquired and displayed on the SUN workstation.

Figure B25 shows an image acquired of a cadaver breast imbedded in wax. This image was acquired with10 line-pairs-per-millimeter (lp/mm) resolution. Figure B26 shows and enlarged portion of the cadaver breast where some micro-calcifications (50 – 200 microns in diameter) have simulated by placing ground up oyster shells into the breast tissue. As shown the particles are easily visible and can be seen in the upper central portion of the image. It should be noted here that the steps taken to reproduce these images for this report have significantly reduced the quality of the acquired images and consequently, the quality of these images cannot be fully appreciated here.

Figure B27 shows an image acquired of the American College of Radiology (ACR) Accreditation Phantom. The ACR accreditation phantom is described in detail by DeParedes, et al [58], Hendrick, et al [59], and McLelland, et al [60]. Figure B28 shows the same phantom imaged with traditional film/screen techniques. A schematic of the accreditation phantom is shown in Figure B22. To review, images of the phantom acquired with the DXM-1 prototype at an exposure of 75 mAs, mass groups 13 - 15 were visible, while 16 was not. Mass group 16 was not visible at an exposure of 100 mAs. These images were produced with a dark-subtraction and flat-fielding algorithm applied to the raw image data.

Figure B29 shows an image acquired of the CDMAM phantom. As shown the phantom consists of a gold foil containing a grid. Each square in the grid contains two gold disks of varying thickness and diameter. One of the disks is placed in the center of each square with the second disk placed in one of the four corners in a random pattern. A portion of the phantom can be viewed electronically that shows disks that are barely resolvable with the DXM-1 prototype. The disks imaged here indicate that the DXM-1

prototype has excellent contrast resolution. These disks are the smallest in the grid indicating that 100% of the disks are visible. By comparison, a typical mammographic stereotactic biopsy system using a CCD camera can only see about 50 - 60% of these disks.

Task 3 Accomplishments

As a result of the delays encountered from the late delivery of components from the sub-contractors used on this project and the poor performance of the sensors, the clinical studies portion of this project were greatly curtailed. The resolution of the DXM-1 system is only 5 lp/mm in the in-scan axis and 10 lp/mm in the cross-scan axis. This deficiency prevented the use of the interpolation and over-sampling routine designed into the system to increase the spatial resolution to 20 lp/mm. Accordingly, many of the goals set forth for this task were no longer obtainable. However, a two-patient study was conducted with the DXM-1 prototype supervised by Dr. Linda Olson, a radiologist at UCSD. The original IRB approval was modified and approved for this abbreviated study. An example of a full-field breast image obtained from one of the two patients studied is show in Appendix B, Figure B-30.

Xicon IDEA Grant (thallium bromide) Accomplishments

The goal of this effort was to determine the feasibility of applying a layer of Thallium bromide directly on the surface of the sensor readout IC. The motivation to do this is based on the potential of the thallium bromide coating to dramatically increase the sensitivity and lower the cost of the sensor arrays designed in connection with this effort. The existing design employs a silicon PiN diode array that is bump bonded to the readout IC with an array of indium bumps. The silicon PiN diode array is fabricated using an exotic silicon starting material that has a very high impedance (>5kOhm-cm). This material is quite expensive and difficult to obtain. The indium bumping process is also expensive and there are only a few facilities left in the world that can perform such a service.

The primary concern in establishing the feasibility of applying thallium bromide to the surface of an integrated circuit was the corrosive effects of thallium bromide on the IC. Another concern was the adhesion properties of the thallium bromide and its propensity to delaminate from surfaces during the cool-down phase of its deposition. A series of experiments were set up and conducted to determine the extent of these potential problems and to find remedies for them. At the time this effort began, all of the readout ICs on hand had indium bumps applied. The first step was to develop a process to strip off the indium bumps to prevent contamination of the thallium bromide.

The following process was developed to remove the indium bumps:

Step 1: The wire bondpads of the ICs are coated with a photoresist.
Step 2: After the photoresist has dried, the ICs are placed in a dilute solution of nitric acid (0.1 N) and left to soak for 12 hours

Step 3: The ICs are removed from the solution and washed with distilled water
Step 4: The ICs are then visually inspected with a boom microscope to determine if all of the indium has successfully been remove and that no degradation of the bondpads or vias has occurred
Step 5: The photoresist is then removed
Step 6: The ICs are then given a final visual inspection

Only a few functional readout ICs were on hand at the start of this effort. To make the most use of these ICs, all of the techniques used were first developed using non-functional ICs. Several non-functional ICs were sent to Xicon where a layer of thallium bromide was deposited on each of them. They were returned to PGI for inspection.

The inspection procedure involves cleaving the coated arrays and inspecting them with a scanning electron microscope. Scanning electron microscope images acquired from cleaved sensor arrays providing a cross-sectional view of the coated sensor arrays are shown in Appendix E. Figure 1 shows a view of the sensor array at a 14,000 X magnification. As shown in the upper portion of the image, the thallium bromide layer has been peeled back from the surface of the sensor array exposing the pixel bond pad via. There is no observable corrosion or degradation of the surface of the sensor array. Figure 2 shows another cross-sectional view at a higher magnification (25,000 X). As shown a layer of titanium-tungsten a few thousand Angstroms thick covers the pixel bond pad via. Beneath the metal layer is a layer of overglass or passivation layer. A layer of glass and a layer of aluminum follow this layer. There is little or no observable corrosion or damage to any of these layers. There seems to be a pocket of missing material in the lower right hand portion of the via. This may have been caused by cleaving the die or from poor fabrication and does not appear to be caused by the thallium bromide. Figure 3 shows another cross-sectional view of a pixel bond pad. In this view, some of the indium bump material is shown. This indicates that the process developed to remove this material does not remove all of the indium. Subsequently we increased the soak time used in the removal process to make sure that all of the indium is removed.

Two functional readout ICs were stripped of their indium bumps and sent to Xicon for thallium bromide coating. A 50-micron coating thickness was desired. After coating, the thickness of each coating was measured to be 40 microns and 80 microns. It was never determined why the coating thicknesses were not the same or 50 microns thick. These sensors were sent to PGI for packaging and wire bonding. A process to attach a bond wire to the top electrode of a thallium bromide coated sensor array was developed as follows. Due to the soft texture of the thallium bromide and the thin layer of nickel, it was necessary to attach the bond wire to the nickel with a conductive epoxy. This bond wire will provide a bias voltage to the thallium bromide

Upon visual inspection of the coated sensor arrays it became evident that the nickel coating had inadvertently made contact with an exposed portion of the sensor array. This caused a short circuit between the top electrode and the ground plane of the sensor substrate. The wire-bonded sensors were probed with an ohmmeter to determine

the resistance from the nickel layer to ground. An impedance of 660K ohms was measured for the 80-micron thick layer and 11K ohms was measured for the 40-micron thick layer. These values are too low. A bias voltage was applied and the current draw was excessive burning out the current limiting resistors on the sensor substrate. Two additional sensors were then sent to Xicon for another coating attempt. Efforts were made to ensure that the nickel layer does not extend past the surface of the thallium bromide. When these sensor arrays were attached to the camera electronics and exposed to visible light without any bias voltage a signal response was observed. This indicated that the thallium bromide coating did not degrade the sensor and that it was capable of functioning.

Sensors were mounted on the camera driver electronics board of the DXM-1 prototype and exposed to x-rays for comparison tests between the thallium bromide sensors and silicon PIN diode sensors. The test parameters and results are as follows:

X-ray source - Mo x-ray tube target with a Mo filter.
Bias voltage for Si PIN diode sensor = 220vdc
Bias voltage for 80 micron TlBr sensor = 9.9vdc to create a 1.5v offset in the output
Bias voltage for 40 micron TlBr sensor = 7.0vdc to create a 1.5v offset in the output

Test-1
39kvp 125ma
Plexiglas attenuator thickness = 28.2mm
1mm thick Si PIN diode response apprx. = 1.5v
80 micron TlBr response apprx. = 1.2v
40 micron TlBr response apprx. = .5v

Test-2
39kvp 125ma
Plexiglas attenuator thickness = 37.3mm
1mm thick Si PIN diode response apprx. = 1v
80 micron TlBr response apprx. = .8v
40 micron TlBr response apprx. = .4v

Test-3
27kvp 125ma
Plexiglas attenuator thickness = 9.5mm
1mm thick Si PIN diode response apprx. = 1.5v
80 micron TlBr response apprx. = .6v
40 micron TlBr response apprx. = .5v

Test-4
27kvp 125ma
Plexiglas attenuator thickness = 19mm

1mm thick Si PIN diode response apprx. = .75v
80 micron TlBr response apprx. = .3v
40 micron TlBr response apprx. = .3v

The response of the 80-micron TlBr sensor at the higher energy level was close to the Si PIN diode sensor. However it was a little bit less. It is likely that the response of the 80-micron TlBr will be better than the Si PIN diode at higher energies, like over 60 kVp. (39kvp is the maximum capability of the x-ray source.)

There is a shift in the dark current of the TlBr when it is exposed to x-rays. For the 80 micron TlBr, the output shifts about 0.4v in the first half second of the exposure. After the exposure the dark current returns to it's original state in about two seconds. We don't know what would cause this.

A conference call was held to discuss these results. The consensus reached from this call was that because the TlBr was being operated at room temperature, the impedance of the TlBr layer was sufficiently low that the bias voltage was limited to less than 10 volts. This low bias voltage resulted in a low electric field gradient that was insufficient to prevent electron-hole pair recombination and therefore reduced x-ray sensitivity. In order to verify that this is the case it was suggested that a measurement of the TlBr impedance be made at room temperature and at 20 degrees C below room temperature to try and extrapolate the impedance at –15 degrees C where most of the previous work had been conducted. This would allow us to compare the dark current to previous data and determine if the problem being encountered is due solely to low impedance. If so, then the sensor arrays will have to be operated at a lower temperature.

A series of images was acquired with the thallium bromide coated sensors using a 32 kVp x-ray source of a lead foil penetrameter with steps varying from 0.5 – 10.0 lp/mm. The technique factors used to acquire these images were: 32 kVp, 125 mA, 63 cm SID, 250-micron Al filter, 300-micron Mo filter and an exposure time of 93 milliseconds/pixel. These images are shown in Appendix E. As shown in Figures E4 and E%, the limiting spatial resolution of the thallium bromide coated sensor approaches 10 lp/mm, the limiting resolution of the readout IC.

The Modulation Transfer Function (MTF) of this sensor was computed using the square wave response function [61]. The data used to compute the MTF was taken from the images in Figures E4 and E5. The MTF is shown in Figure E6. Despite the low bias voltage used, the MTF appears nominal and is not degraded significantly.

Key Research Accomplishments

- A low-dose slot-scanning digital mammography system was built and tested
- Superior image quality over film-screen mammography was demonstrated
- Clinical digital mammographic images were obtained
- The feasibility of producing a high-performance low-cost digital mammography system was demonstrated
- The feasibility of applying a layer of thallium bromide photoconductor material to an integrated circuit detector array was demonstrated

Reportable Outcomes

- RSNA InfoRAD Exhibit 1996, Chicago, IL Nov 27-Dec 4, 1996 – Poster Session
- RSNA InfoRAD Exhibit 1997, Chicago, IL, Nov 28 – Dec 5, 1997 – Poster Session
- RSNA InfoRAD Exhibit 1998, Chicago, IL Nov 29-Dec 46 1998 – Poster Session
- Schilling, R.B., Sharma, S.R. and Cox, J.D., "Advanced Digital Mammography", Society for Computer Applications in Radiology (SCAR) Annual Meeting, Houston June 4-6, 1998. (Invited paper)
- Cox, J.D. and Schilling, R.B., "Technologies for Digital Mammography", Computer Assisted Radiology and Surgery (CARS) '99, June 23-26, Paris, France. (invited paper).

  Copies of the manuscripts for the SCAR and CARS papers are attached in Appendix F. The 3 RSNA presentations were given in poster form and as such there are no published documents.

Conclusions

The primary goal of this research effort was to demonstrate that the detection of breast cancer could be improved using digital mammography. This goal was based on preliminary evidence that showed that a digital mammography system has superior spatial and contrast resolution than screened film mammography. While a full-field digital mammography system was designed, assembled and tested as a result of this effort, an adequate clinical study was not performed to fully demonstrate the stated goal of this effort.

The primary reason for not completing the clinical study was poor performance and delays created from sub-contractors working on this project. In retrospect the goals set forth in this project were very optimistic and required the cooperation of several different companies in order to obtain the results and goals set forth. Nevertheless, the feasibility of producing superior quality images using a digital mammography system was established but the prospects for utilizing this technology as an alternative to screen-film mammography remain obscure. There are two primary reasons why the benefits of digital mammography remain in doubt. The first reason relates to the need to view digital mammograms on a soft-copy display (i.e., a CRT or monitor). The second reason relates to the higher cost of digital mammography compared with film-screen mammography.

Mammography is one of the first defense mechanisms in the fight against breast cancer. A screening mammogram is essentially a "pap smear" of the breast. Radiographic images of the breast are taken as a screening procedure, during follow-up diagnostic examination and are used in biopsies well. Screened film is currently the only method approved by the FDA for screening and diagnostic mammography although stereotactic needle-biopsy imaging systems employ a CCD camera fiber-optically coupled to a phosphor.

Mammographic procedures can be measured in terms of fixed and variable cost. These terms are largely dictated by the throughput and productivity of the way in which mammograms are processed within the hospital or clinical setting. With a given amount of equipment and staffing there are a limited number of patients that can be seen. A typical film-based mammography system costs less than $100,000, although mammograms can be processed, viewed and stored along with other films in the radiology department. A time-and-motion study of mammographic examinations reveals that the rate limiting step in the production of the mammographic image is the time spent by the technician in setting up, taking and developing the radiographic image. The major cost element, however is the time spent by the radiologist reading the exam. Given the long history of reading film-based mammograms, this step has been highly optimized by using a bank of light-boxes, dictation machines, etc. Additional cost factors include the cost of film materials and film processing, warehouse space for film storage, the cost of lost films (and associated expense and dose penalty of re-takes), and film retrieval and transport. These factors create a high-cost environment for mammography.

One of the most difficult challenges in radiology is to identify the minute changes in the anatomy of the breast that first occur in connection with breast cancer. Consequently radiologists routinely use a magnifying glass to read mammograms. Screened film images of the breast can reveal the existence of micro-calcifications and masses associated with breast cancer but often a biopsy procedure is recommended to establish malignancy. This results in a relatively large number of false positives adding to the direct cost of fighting the disease and a great deal of unnecessary anxiety.

The current reimbursement policies for mammography set forth by HCFA and the high cost of processing mammograms have created an environment where radiology departments view mammography as a "loss leader". The present scenario appears to provide a barrier to radiology departments desiring to move to fully digital, film-less departments due to the perceived higher cost of digital mammography. **However, when the focus is placed on the patient, and the yardstick is the cost of total patient care rather than the cost of the mammographic exam in isolation, the benefits of going digital become apparent.** In order to reduce the overall cost, and realize the true benefits of digital mammography, a paradigm shift must take place in both operation and reimbursement.

Direct digital mammography systems are now entering the FDA approval process using solid-state transducers to absorb x-rays and produce a digital signal directly without the use of film. These systems are characterized as providing images equivalent to and even superior to screen-film mammography but are expected to sell for $400,000 and up. There are a variety of systems being developed that use amorphous-silicon flat panel arrays, fiberoptic coupled CCD cameras and PiN diode arrays. Both scanning and projection systems are being developed and are in clinical trials.

Clearly, direct digital systems will only be justified if the overall cost of treating breast cancer can be lowered overcoming any incremental increase in the cost of the mammography exam. This means shifting more of the cost of treating breast cancer to the diagnostic phase of the process thereby reducing the cost of surgical procedures and radiation therapy. It means using tele-presence to "destroy geography" putting patient and expert physician together no matter where they might live. It means using artificial intelligence and neural networks to do the most tedious and demanding task of identifying suspicious lesions via computer aided detection (CAD) and to develop data bases cataloging thousands of similar cases. The ability to provide more accurate diagnosis through the use of digital technology has the potential to reduce the number of false positives and increase the number of malignancies detected at an earlier stage. ***Perhaps it could be argued that for every additional dollar spent (using digital imaging technology) at the screening and diagnostic stage of breast cancer detection, several dollars can be saved by reducing the number of surgical procedures and radiation treatment programs that are now required due to false positives and missed cancer detection.***

To accomplish this goal, digital mammography systems will have to acquire, process, store, transmit, retrieve, and provide for radiographic image review quicker and

more efficiently than screen-film images. Increasing the efficiency of the process can be largely gained if the information content of the initial screening exam is increased without excessive cost. Increasing the information content of a mammogram means acquiring and processing high-resolution images. To provide enough information in a mammogram to not only detect a micro-calcification, but to reveal its shape and other topological features, images must be acquired with pixels on the order of 50 microns. In contrast, a typical chest image is acquired with 140-micron pixels or larger. This means that an 8 inch x 10 inch mammogram requires about 10 or 20 times the image storage and bandwidth capability than what is required for 14 inch x 17 inch chest films.

In the absence of approved digital mammographic acquisition products, radiologists have attempted to gain some of the advantages of going digital by scanning films with a digitizer. These digital images can be used with CAD packages, and the images can be tele-transmitted, stored digitally etc. However, in digitizing the films, resolution and clinical information can be lost, thus moving the "quality of health care" factor in the wrong direction. This is viewed as a non-ideal solution to the real problem limiting increased efficiency with screen-film mammography.

Computing power and transmission bandwidth have increased on almost an exponential scale over the past few decades. The cost of processing images will continue to fall in the future as further improvements are made. The real challenges for digital mammography systems are in the acquisition and presentation of high quality images. The systems must be able to acquire and display a high quality image and do so with an ergonomic and intuitive ease. The real challenge for the radiologists is to change their habits and capitalize on the "higher bandwidth" of direct digital mammography. The challenge for regulatory agencies is to redefine the protocol used to evaluate mammographic screening and diagnostic procedures. Ultimately, reimbursement guidelines for mammography will have to be modified to reflect the inevitable changes that will occur in these procedures as a result of the use of digital technology. ***This will require higher reimbursement fees for radiologists performing digital mammographic procedures and a reduction in the number of biopsies and treatment fees paid as a result of better performance in the radiographic diagnosis of breast cancer.***

The performance of digital mammography imaging systems will be largely measured on the capabilities of its transducer and workstation. The transducer absorbs x rays and produces digital data but must do so with high quantum efficiency and with high spatial and contrast resolution. Mammograms are read with a magnifying glass. This fact establishes the need for high-performance image acquisition and display. The workstation displays the digital data but must do so in a quick and efficient manner. Moreover, it must also interact with Radiology Information Systems and Hospital Information Systems perform tele-radiology functions, interface directly to CAD systems with no image degradation, and a number of other tasks that are not specific to the system's transducer characteristics.

With the capital cost of digital mammography technology likely to be up to 4 times the cost of film systems, the capabilities of digital technology will have to

significantly improve the efficacy of screening and diagnostic functions and rely on the overall reduction in health care costs to be competitive. To accomplish this, digital mammography cannot simply have "**substantial equivalence to film.**" Film equivalency at the higher cost associated with digital imaging is a non-starter for mammography! This is true even though film equivalency for digital chest systems is viable. This implies that all of the information needed for both screening and diagnosis must be acquired at once. Doing this will minimize time, effort and cost. Computer Aided Detection (CAD) systems have to be integrated into the image processing procedures of digital mammography to provide more information content to the radiologist and to afford a "second opinion". Workstations must present the images, CAD findings, and diagnostic data in a fashion that is as fast and easy to interpret as film on a light box, and be able to send and receive these data to networks and tele-radiology systems.

The path to fully implemented digital mammography technology will have to pass through the film-equivalence test and move on to performance superior to film. Digital mammography devices now in FDA trials are struggling with the established protocols for "film equivalency" and it is likely that a new protocol to establish the clinical efficacy for this new modality will have to be created. Radiologists will have to change the way they perform screening and diagnostic procedures to make full use of the higher-diagnostic-content information that can be provided. Reimbursement policies will also have to change to reflect the shift in cost to screening and diagnostic functions.

The digital mammography systems now under development span a wide variety of transducer technologies including fiberoptic coupled CCDs, amorphous silicon flat panel detectors and PiN diode arrays. Amorphous silicon flat-panel detectors are being introduced by General Electric and Siemens. TREX Medical is introducing a full-field mammography system using an array of fiberoptically coupled CCDs. Fischer Imaging Corporation is introducing a slot scanning full-field mammography system using fiberoptically coupled CCDs. PrimeX General Imaging Corp. is developing a slot-scanning full-field mammography system based on PiN diode arrays.

The systems being introduced by GE, Siemens and TREX are "flat-panel" systems that acquire an image in projection geometry much like current film systems do. As such they require a detector that is 8 inch x 10 inch in area. Large-area detectors are intrinsically very expensive and systems using these detectors will struggle to establish cost effectiveness. The TREX system has higher resolution capabilities compared with the GE and Siemens' systems but will cost at least $100,000 more. With a target price of $500,000, it is unlikely that the TREX system will prove to be cost effective.

The amorphous silicon flat-panel detector being introduced by GE has a pixel size of 100 microns. Images produced with this system might work well for screening applications but will probably not provide enough data for diagnostic purposes. As such this system will not provide the total solution to mammography that will most certainly be required to justify the high cost of digital mammography. Reducing the pixel size of this device to 50 microns will cause the fill-factor of the pixel to be reduced to about 15%. With the current approach of applying a Cesium Iodide scintillator on the panel,

such a low fill factor will seriously degrade imaging performance. One possible solution to this problem would be to use a photoconductor such as amorphous selenium in place of the scintillator. Doing this will eliminate the problem of the small fill factor since charge generated in the photoconductor could be concentrated and collected by a small electrode in each pixel. Until a way to get to 50-micron pixels with high performance can be implemented it is unlikely that the amorphous silicon flat panel detectors will offer sufficient performance to achieve the requirements of the total solution.

The slot-scanning mammography system being introduced by Fischer Imaging Corporation appears to have the best performance at the lowest cost of any system currently being shown as "works-in-progress". The scanning approach offers unique advantages in mammography since the breast is immobilized during exposure eliminating most of the motion artifacts encountered with scanning. The detector is less than 1 inch wide, greatly reducing its surface area. This greatly reduces the detector cost although some of these savings are given back to provide higher x-ray tube output and the scanning mechanism. Scatter rejection is an inherent property of scanning systems and affords superior imaging performance over projection systems. The imaging performance displayed by this system has established slot scanning as a viable option for digital mammography and may prove to be optimal.

PrimeX General Imaging Corp. (PGI) developed a slot-scanning digital mammography camera system designed to retrofit into the Fischer slot-scanning mammography gantry in the present effort. This system uses an array of hybrid silicon-based PiN diode arrays that absorb x rays and convert them directly into electrical charge. In contrast, Fischer Imaging is using scintillator-coated fiberoptic coupled CCD arrays. These detectors are more expensive and less efficient than direct-sensing diode arrays. PGI is also developing a second-generation detector array that uses a photoconductor deposited on a Complementary Metal Oxide Semiconductor (CMOS) readout integrated circuit (IC). These devices have the potential to provide the best imaging performance at the lowest cost of any digital mammography system now under development.

The foregoing notwithstanding, the total solution required for digital mammography will not be realized until the display and processing functions of the system are optimized. It is likely that CRT display will not provide an adequate means for displaying mammograms. New flat panel displays are being developed that will solve the ergonomic problems afflicting CRT displays and still provide the brightness, resolution, field of view and contrast required for reading soft copy mammograms. Workstations must be able to display 8 or more images in parallel or in rapid sequence, offer electronic magnification that emulates the capabilities of the magnifying glass used with film, and integrate CAD functions in a way that facilitates diagnostic accuracy and maximizes throughput. Image post-processing can enhance the diagnostic value of a digital mammogram, or even correct for poorly exposed images (and avoid the need for retakes), but these enhancements must be done automatically in order to not reduce the efficiency of the radiologist. These workstations must also be able to send and receive images through a tele-radiology network communicating with a variety of different system designs and imaging modalities so image communication standards are critical.

Mobile mammography systems are being developed by the DOD and are being used to provide mammography services to remote and under-served portions of the population. Screening mammograms are obtained, stored and then forwarded on to remote sites where expert mammographers can read the images. These systems are being developed using technology currently being used to obtain and transmit radiographic images from battlefield, ships and remote bases around the world. This program is paving the way for digital mammography systems meant for clinical use by addressing a myriad of problems being encountered when transmitting and remotely reading mammograms and the subsequent patient follow up.

Telecommunications technology is rapidly developing capabilities that will be required to make digital mammography cost effective. Higher bandwidth transmission systems are becoming available at lower cost with formidable progress. Image processing power and bandwidth is also increasing at an amazing rate. These technologies are integral to digital mammography and will have to be incorporated into the design and function of digital mammography workstations.

Perhaps the best way digital mammography can improve breast cancer detection is to use the acquisition and storage of digital mammograms as a gateway to the establishment of a national database on digital mammography. This database could be set up to allow radiologists to view thousands of cases with similar patient demographics and pathology to determine stastically how other patients with the same demographics and pathology progressed and were treated. By having access to these data, physicians can make more accurate diagnosis and determine appropriate treatment based on results obtained from others in a similar situation.

Digital Mammography is coming of age at a time when technology is rapidly evolving and managed healthcare is a driving force in defining the way in which diagnostic examinations are implemented. New methodologies will have to be created to capitalize on the advantages of digital mammography and mitigate its drawbacks. These methodologies will most certainly have to be developed in the academic centers of excellence in cooperation with industry and regulatory agencies. Manufacturers will have to become intimately familiar with telecommunications technology, incorporate state-of-the-art image processor and display technology and develop workstations with optimized ergonomics guided by needs of high-efficiency radiology. This "total solution" concept is essential to the successful implementation of digital mammography. The essential economics of managed healthcare and the high cost of digital modalities prevent an evolutionary approach to digital mammography. A clinically driven solution to screening and diagnosing breast cancer with digital image data that incorporates the best communication, processing and transducer technology will then emerge to fulfill the destiny of digital mammography.

References

1. Silverberg E., Boring C.C., Squires T.S.: Cancer Statistics, 1990. **CA**, 1990; 40: 9-27.
2. Andersson I., Aspergren L., Janzon L., et al.: Mammographic screening and mortality from breast cancer: the Malmo mammographic screening trial. **Br. Med. J.**, 1988; 297: 943-948.
3. Shapiro S., Venet W., Strax P.H., et al.: Ten to fourteen-year effect of screening on breast cancer mortality. **JNCI**, 1982; 69: 349-355.
4. Tabar L., Gad A., Holmberg L.H., et al.: Reduction in mortality from breast cancer after mass screening with mammography. **Lancet**, 1985; 1: 829-832.
5. Hermann G., Janus C., Schwartz 1.5. et al.: Occult malignant breast lesions in 114 patients: Relationship to age and the presence of microcalcifications. **Radiology**, 1988; 169: 321-324.
6. Sickles E.A.: Mammographic features of 300 consecutive nonpalpable breast cancers. **AJR**,1986; 146: 661-663.
7. Wolfe J.N.: Analysis of 462 breast carcinomas. **AJR**, 1974; 121: 846-853.
8. Millis R.R., Davis R., Stacey A.J.: The detection and significance of calcifications in the breast: A radiological and pathological study. **Br. J. Radiol**. 1976; 49: 12-26.
9. Muir B.B., Lamb J., Anderson T.J.: Microcalcification and its relationship to cancer of the breast: Experience in a screening clinic. **Clin. Radiol.**, 1983; 149: 193-200.
10. Murphy W.A., DeSchryver-Kecskemeti K.: Isolated clustered microcalcifications in the breast: Radiologic-pathologic correlation. **Radiology**, 1978; 127: 335-341.
11. Bassett L.W., Gold R.H.: Breast Cancer Detection: Mammography and Other Methods in Breast Imaging. New York, Grune and Stratton, 1982.
12. Lissner J., Kessler M., Anhalt G.: Developments in methods for early detection of breast cancer. In: J. Zander and J. Baltzer, eds. **Early Breast Cancer**. Berlin: Springer-Verlag: 1985; 93-123.
13. Andersson I.: What can we learn from interval carcinomas? **Recent Results in Cancer Research**, 1984; 90: 161-163.
14. Baines C.J., Miler A.B., Wall C., et al,: Sensitivity and specificity of first screen mammography in the Canadian national breast screening study: A preliminary report from five centers. **Radiology**, 1986; 160: 295-298.
15. Martin J.E., Moskowitz M., Milbrath J.R.: Breast cancers missed by mammography. **AJR**, 1979; 132: 737.
16. Pollei S.R., Mettler F.A., Bartow S.A., et al.: Occult breast cancer: Prevalence and radiographic detectability. **Radiology**, 1987; 163: 459-462.
17. Buchanan JR, Spratt JS, Heuser LS: Tumor growth, doubling times, and the inability of the radiologist to diagnosis certain cancers. **Radiologic Clinics of North America**, 1983; 21:115-126.
18. Holland T., Mrvunac M., Hendrirks J.H.C.L., et al.: So-called interval cancers of the breast: Pathologic and radiographic analysis. **CA**, 1982; 49:2527-2533.
19. Baker L.H.: Breast cancer detection demonstration project: five year summary report. **CA**, 1982; 32: 194-225.

20. Moskowitz M.: Screening for breast cancer: how effective are our tests. A critical review, **CA**, 1983; 33: 26-39.
21. Doi K, Giger ML, Nishikawa RM, MacMahon H, Schmidt RA: "Artificial Intelligence and Neural Networks in Radiology: Application to Computer-aided Diagnostic Schemes". in Hendee WR and Trueblood JR editors "Digital Imaging", **Medical Physics**.
22. Jam, AK: Fundamentals of Digital Image Processing; Englewood Cliffs, NJ; Prentice Hall; 1989.
23. Cook LT, Giger ML, Banitzky S.: Digitized film radiography; **Invest. Radiol.** 1989; 24:910-916.
24. Haus AG: Recent Advances in Screen-Film Mammography. **Radiol. Clinics of North America**, 1987; 25:913-928
25. Chan HP, Doi K, Galhotra S. et al. :Image feature analysis and computer aided diagnosis in digital radiography. 1. Automated detection of microcalcifications in mammography. **Med. Phys.**, 1987; 14:538-548
26. Chan H.-P., Doi K., Vyborny C.J., et al.: Computer-aided detection of microcalcifications in mammograms: Methodology and prelimary clinical study. **Invest. Radiol.**, 1988; 23: 664-671.
27. Chan H.-P., Doi K., Vyborny C.J., et al: Improvement in radiologists' detection of clustered microcalcifications on mannograms: The potential of computer-aided diagnosis. **Invest. Radiol**,. 1990; 25: 1102-1110.
28. Giger M.L., Nishikawa R.M., Doi K., et al.: Development of a "smart" workstation for use in mammography. **Proc. SPIE,** 1991; 1445: 101-103.
29. Giger M.L., Yin F.-F., Doi K., et al.: Investigation of methods for the computerized detection and analysis of mammographic masses. **Proc. SPIE**, 1990; 1233: 183-184.
30. Jiang Y., Nishikawa R.M., Doi K. et al.: Method of extracting signal area and signal thickness of microcalcifications from digital mammograms. **Proc. SPIE**, 1992; 1778: 28-36.
31. Nishikawa R.M., Giger M.L., Doi K., et al.: Computer-aided detection of microcalcifications on digital mammograms. **Medical & Biological Engineering & Computing**, 1993 (in press).
32. Wu Y., Doi K., Giger M.L.: Computerized detection of clustered microcalcifications in digital mammograms. Applications of artificial neural networks. **Med. Phys.**, 1992; 19:5555-560.
33. Wu Y., Giger M.L., Doi K., et al.: Artificial neural networks in mammography: Application to decision making in the diagnosis of breast cancer. **Radiology**, 1993; 187: 8 1-87.
34. Yin F.-F., Giger M.L., Doi K,: Computerized detection of masses in digital mammograms:Analysis of bilateral subtraction images. **Med. Phys.**, 1991; 18: 955-963.
35. Yin F.-F., Giger M.L., Doi K.: Evaluation of imaging properties of a laser film digitizer. **Phys. Med.Biol.**, 1992; 37: 273-280.
36. Piccaro, M. F. and Toker, E., Development and evaluation of a CCD-based digital imaging system for mammography. **SPIE** 1901, 1993.
37. Toker, E. and Piccaro, M. F., Design and development of a fiber optic TDI CCD-

based slot-scan digital mammography system. **SPIE** 2009, 1993.

38. Karellas, A. and Harris, L. J., Charge-coupled device detector: Performance considerations and potential for small-field mammographic imaging applications. **Med. Phys.**, 1992. 19(4),1015-1023.
39. Nishikawa, R. M., Mawdsley, G. E., Fenster, A., Yaffe, M. J., Scanned-projection digital mammography. **Med. Phys.**, 1987. 14(5), 717-727.
40. Mumer, B., Prieur-Drevon, P., Roziere, G. and Chabbal, 1., "High resolution digital x-ray imaging with solid-state linear detectors". In: Medical Imaging VI: Instrumentation, **SPIE** 1651, 1992, 106-115.
41. Zhao, W. and Rowlands, J. A., "A large area solid state detector for radiology using amorphous selenium". In: Medical Imaging VI: Instrumentation, **SPIE** 1651, 1992, 134-143.
42. Korn D. M., Lubinski, A. R. and Owen, J. F. "Storage phosphor systems for computed radiography: 1. destructive scanning, 2. screen optics". In: Applications of Optical Instrumentation to Medicine XIV, **SPIE**, 626, 1986. p. 108(1) and 120(2).
43. Hillen, W., Schiebel, U. and Zaengel, T., Imaging performance evaluation of a digital storage phosphor system. **Med. Phys.**, 1987. 14, p.744.
44. Fujita, H., Ueda, K., Morishita, T., and Ohtsuka, A., Basic imaging properties of a computed radiography system with photostimulable phosphors. **Med. Phys**, 1989. 16, p. 52.
45. Miyahara, J., The image plate: A new radiation imaging sensor. **Chemistry Today**, Oct. 1989,29-36.
46. Korn D. M., Lubinski, A. R. and Owen, J. F., "Method for reading out an image signal stored on a transparent photostimulable phosphor". US patent # 4762998 (1988)
47. Hillen, W., Schiebel, U. and Zaengel, T., "A selenium-based detector system for digital slotradiography". In: Medical Imaging II, **SPIE** 914, 1988, p. 253.
48. Schiebel, U., Hillen, W., and Zaengel, T., "Image quality in selenium-based digital radiography". In: Applications of Optical Instrumentation to Medicine XIV, **SPIE**, 626, 1986. p. 176.
49. Rowlands, J. A., Hunter, D. M. and Araj, N., X-ray imaging using amorphous selenium: A photoinduced readout method for digital radiography. **Med. Phys.**, 18, 1991, 421-431.
50. Karssemeijer N, Frieling JIM, Hendricks JHCL. "Spatial Resolution in Digital Mammography". **Invest Radiol**. 28 413-419 (1993)
51. Karssemeijer N, van Erning LJTHO, Hendricks JHCL. "Comparison of digital and conventional mammography: A ROC study of 270 mammograms" **Med. Inform** 17:125-131;1992
52. Chan, H.P., Vybrony, C.J., MacMahon, H., Metz, C.e., Doi, K., Sickles, E.A.: Digital Mammography: ROC Studies of the Effects of Pixel Size and Unsharp-Mask Filtering on the Detection of subtle Microcalcifications. **Invest Radiol** 1987;22: 58 1-589
53. Roehrig H, Krupinski E, Yu I: "Physical and psycho-physical evaluation of digital systems for mammography", **SPIE** 2436:124-1 34;(1995)

54. Roehrig H, Yu T, Gaalema 5, Minteer JA Sharma SD, Yorke WE: Application of Hybrid Detector Technology for Digital Mammography. **SPIE** 2519, 118-126, (1995)
55. S. R. Dev Sharma, "Low Dose Primary X-ray Digital Mammography", Inforad, RSNA,1994.
56. Johns, H.E. and Cunningham, J.R., **"The Physics of Radiology"**. Third Edition, Seventh Printing, Charles C. Thomas – Publisher, Springfield, IL 1974
57. Dainty, J.C. and Shaw, R., **"Image Science: Principles, Analysis and Evaluation of Photographic-type Imaging Processes"** Academic Press, London, New York, San Francisco, 1974
58. DeParedes, E.S., Frazier, A.B., Harwell, G.D., et al, "Development and Implementation of a Quality Assurance Program for Mammography." **Radiology** 163:83-85, 1987.
59. Hendrick, R.E., "Standardization of Image Quality and Radiation Dose in Mammography.", **Radiology**, 174:648-654, 1990.
60. McLelland, R., Hendrick, R.E., Zinninger, M.D., Wilcox, P.A., "The American College of Radiology Accreditation Program", **AJR** 157:473-479, 1991.
61. Buetel, J., Kundel, H.L., and Van Metter, R., editors, **Handbook of Medical Imaging, Vol.1, Physics and Psychophysics**, SPIE Press, Bellingham, WA, 2000

Bibliography

Publications:

1. RSNA InfoRAD Exhibit 1996, Chicago, IL Nov 27-Dec 4, 1996 – Poster Session
2. RSNA InfoRAD Exhibit 1997, Chicago, IL, Nov 28 – Dec 5, 1997 – Poster Session
3. RSNA InfoRAD Exhibit 1998, Chicago, IL Nov 29-Dec 46 1998 – Poster Session
4. Schilling, R.B., Sharma, S.R. and Cox, J.D., "Advanced Digital Mammography", Society for Computer Applications in Radiology (SCAR) Annual Meeting, Houston June 4-6, 1998. (Invited paper)
5. Cox, J.D. and Schilling, R.B., "Technologies for Digital Mammography", Computer Assisted Radiology and Surgery (CARS) '99, June 23-26, Paris, France. (invited paper).

Personnel Receiving Support:

1. Ronald B. Schilling, Ph.D. – Principal Investigator
2. S.R. Dev Sharma, Ph.D.
3. John D. Cox, Ph.D.
4. William Yorke
5. Donald Williams
6. Louis Morales

Appendix A

Motivation and DXM-1 System Description

Currently the lifetime risk of breast cancer for women is one in nine. The annual death rate from breast cancer in the United States is estimated to be approximately 44,000 women per year [1] Several Studies have shown that asymptomatic screening with mammography can reduce mortality from breast cancer by 20-40% [2-4]. Based on these studies, the American Cancer Society and other medical associations have recommended mammographic screening for women over the age of 40. Consequently, mammography may become one of the largest volume radiographic procedures interpreted by radiologists.

Mammography is the most demanding of all clinical imaging applications. It requires high contrast, high spatial resolution and high signal to noise ratio at the minimum possible x-radiation dose to the patient. Fundamentally, it is often the minimum contrast of the cancer, relative to its surroundings, which determines the detection of the breast cancer. This can be as low as 0.1%, and averages 6 to 8% at the 18 to 20 KeV x-ray beam energies employed in mammography. The detectable contrast of a cancer is inversely proportional to the signal-to noise ratio of the imaging system. Clusters of much higher contrast microcalcifications are a frequent mammographic presentation of breast cancer requiring high image resolution.

Diagnosing cancer from a mammogram requires skillful and meticulous interpretation. The two primary indicators of breast cancer in a mammogram are the presence of a mass and clustered microcalcifications. Microcalcifications are an important indication of breast cancer because they are present in 30-50% of all cancers found mammographically [5-7]. Further, microcalcifications are often visible in the mammogram before a mass can be detected clinically by physical examination [5]. However, microcalcifications are often difficult to detect because, radiographically they appear as tiny areas (as small as 0.2 mm in diameter) slightly brighter than the surrounding background. To detect such subtle lesions, radiologists often use magnifying glass and carefully examine the full breast area of the mammogram which is time consuming and tedious. Although, radiologists do find microcalcifications in 30-50% of cases with breast carcinoma, as much as 80% breast carcinomas reveal microcalcifications in pathologic examination [8-10]

Mammography is the most effective method for early detection of breast cancer [11-12] and yet, 10-30% of women who have breast cancer and undergo mammography have negative mammograms [13-16]. In about two-thirds of these false-negative cases, the radiologist failed to detect a cancer that was evident in retrospect [13,15,17,18]. Low conspicuity of the lesion, eye fatigue, and distraction by other image features are possible causes for these misses. It is expected that if radiologists were alerted to suspicious regions on the mammogram, then the number of missed cancers could be reduced. Furthermore, of the women who are sent to biopsy, only 20-40% actually have breast cancer [19,20]. Quantitative analysis of the radiographic features of microcalcifications and masses may help radiologists improve their specificity.

Recent developments in the areas of information processing, computer vision, artificial intelligence, neural networks and particularly the high speed computers have permitted development of schemes for automated detection of lesions and characterization of normal and abnormal patterns in mammography [21]. Here computer

output is expected to be used as a second opinion to assist radiologists in their interpretation of radiographic images. The basic concept for this approach to automated detection is called computer-aided diagnosis (CAD). The goals of CAD are to improve diagnostic accuracy by drawing the radiologist's attention to potential lesion sites and enhancing the consistency of image interpretation. Recent work in CAD has demonstrated significantly improved accuracy, mainly due to improved computer vision [22], better methods for film digitization [23] and an increase in the image quality of mammograms [24]. It is for this reason, that CAD is expected to enjoy improved accuracy with the advent of digital imaging systems for mammography, because these systems are expected to be superior to conventional film-screen in image quality. Much of the recent work on CAD was developed at the University of Chicago [25-35]. Detection of clustered microcalcifications and masses are approached with different strategies.

Performance tests for detection of microcalcifications were conducted at the University of Chicago with a set of "difficult" mammograms (average size of 0.09 mm^2, 14.3 microcalcification per cluster). The result was a true-positive cluster detection accuracy of 85 % and a false positive detection rate of 1.5 clusters per image [21]. The true-positive detection accuracy for detection of masses was found to be 85 % with a false-positive rate of approximately 3 masses per image [21]. It is of particular interest to note that the performance of radiologists clearly improved when CAD was used for reading of mammograms [21].

The current state-of-the-art in screening and diagnostic mammography is still conventional film-screen mammography. However, efficacy of the film-screen mammography is limited by its limited dynamic range, low contrast resolution, film noise, dose-inefficient scatter reduction and film processing artifacts. It offers low diagnostic specificity in the range of 20% to 30% resulting in a high number of false-positive film-screen initiated biopsies, the cost of which alone is estimated at several hundred million dollars. It is currently estimated that *one out of every four women* screened annually for ten years by film-screen mammography will experience the anxiety and cost of a screening initiated false-positive mammogram (benign biopsy).

Solid-state x-ray sensor technology has the potential to improve the diagnostic quality of mammograms through higher quantum efficiency and spatial resolution than screened film can provide. These improvements in performance can be obtained while lowering the patient exposure dose. The inherently digital output of solid-state detector arrays is ideally suited for PACS (Picture Archiving and Communications Systems) including electronic archiving and image transmission over computer networks, image enhancement and analysis, and computer-aided diagnosis (CAD).

Recently, a significant amount of research has been devoted to the development of x-ray sensor technologies for applications to digital mammography at both the universities and the industry levels. As shown below, the solid-state x-ray sensor technologies under development can be broadly divided into two categories; the *primary* sensors which convert the incident x-radiation directly into usable electrical signal and the *secondary* sensors which require an intermediate step for first converting the x-radiation into visible light using, e.g., a phosphor screen which then converts the visible light to usable electrical signal. Both of these categories can be further subdivided into area sensors and the scanning sensors.

Of these classes, the first x-ray sensors to have found application in commercial mammography equipment are the Charge-Coupled Device (CCD) based systems [36-38]. These systems use CCD's coupled to a phosphor screen, either via a fiber-optic link or a visible light lens system. Limited field-of-view CCD-based digital mammography systems manufactured by Fischer and Lorad received FDA approval in late 1992 for breast imaging during stereotactic core biopsy (5 x 5 cm field). Currently, however, these systems lack adequate spatial resolution for commercial full-field mammography. Other similar systems using linear photodiode arrays to scan image intensifier tubes have also been reported [39,40]. However, because of the intermediate step involved in these systems to convert x-ray energy to usable electrical signal, there is inherently a significant loss in the performance of these systems as compared to the systems based on primary x-ray sensors.

Another proposed x-ray area sensors is an amorphous selenium (a-Se) based primary sensor[41]; storage phosphor screens reusable flat plate fitted into a cassette [42-45] with limited spatial resolution (4-5 lp/mm); Systems using transparent phosphor [46]; photoconductive a-Se plate readout either with an electrometer array or a laser [47-49].

	PRIMARY SENSORS	SECONDARY SENSORS
AREA SENSORS	a-Se	a-Si Storage Phosphor
SCANNING SENSORS	PGI Sensors	CCD Photodiodes

PGI is building two primary x-ray, slot-scanned digital mammography (DXM-1) prototype units based up on high performance direct x-ray detection hybrid sensors. It is schematically shown in Figure 1. The heart of this system is the semiconductor x-radiation sensors. As shown in Figure 1, the transmission is similar to a conventional screen-film mammography system except for a moving aperture. It consists of a x-ray tube and a beam collimating aperture that rotates about the tube focal spot. The moving aperture protects the patient from 'unsensed' x-rays by providing a fan shaped beam synchronous in its motion to the sensor assembly on the receptor side.

The key system specifications and performance identified as critical are:

Field of View - the system must image an area of similar size to that of a conventional mammography system (180 x 240 mm) and must be able to record this image with sufficient pixels to maintain the desired resolution.

Exposure time - the image must be acquired in a time consistent with reasonable comfort for the patient and in a way that the susceptibility to patient motion is no worse than a conventional film-screen system.

Image Quality - the quality of the image produced (sharpness, contrast, SNR) should be significantly superior to conventional film-screen systems at moderate and high spatial frequencies, and at a minimum, equal to conventional systems at low spatial frequencies.

Dose Efficiency - system should have high DQE to reduce dose to the patient without sacrificing image quality.

An issue that has not been resolved for digital mammography is the subject of spatial resolution. Karssemeijer [50,51], using a specially developed contrast-detail phantom determined that the smallest detectable microcalcification with film/screen at the typical exposures of about 11 mR at a 19 KeV effective energy is about 130 micrometers. This is despite the fact that the MTF of the film goes out to 20 lp/mm. In addition, Karssemeijer digitized the film with a 100 m spot size and performed an ROC study comparing the performance of radiologists viewing film/screen with that of radiologists viewing the digitized data on a CRT. No differences in the area under the ROC-curves were noted implying that a spatial resolution of 100 m spot size is adequate in mammography. On the other hand, Chan et al [52] from the University of Chicago found that digitizing a mammogram to 100 micrometers is not sufficient to represent the information in a mammogram.

Roehrig et al [53] expanded on Karssemeijer's work using two digital imaging systems used for mammographically guided stereotactic breast biopsy. The conclusion was that the improved DQE of one of the digital imaging systems over the DQE of the conventional film/screen permitted an improved signal-to-noise ratio, and therefore the digital system was capable of resolving an object of about 100 m. Had the digital imaging system been "ideal" in terms of DQE, it would have been able to resolve an object ("microcalcification") of 70 m in diameter at the above mentioned x-ray fluence. Analysis of the system and extensive x-ray sensor test data demonstrate that the system design would meet the above goals. Image quality is projected to be much better than film-screen. The modulation transfer function for this system at 10 line-pairs/mm should be almost 3 times better than film-screen systems. Predicted detective quantum efficiency (DQE) at 15 line pairs/mm is about 15 times better than that of film-screen at 15 lp/mm. Image quality operating in normal contact mode should surpass that obtainable from conventional systems in magnification mode.

The high predicted DQE of the system allows x-ray exposure to be reduced by a factor of up to 5 from the typical film-screen exposures while maintaining the same signal to noise ratio at low spatial frequencies. Even at this reduced exposure, this system will have a better signal to noise ratio at 13 lp/mm than film-screen at 10 lp/mm.

Major design issues identified are related to x-ray tube loading, scan time and in-scan field of view. Only a small fraction (slot width/240 mm in-scan field of view) of the x-rays used in a conventional system can be employed in generating a slot scan image. The system design must, therefore, be optimized to minimize tube loading and keep the total scan time to about 4.0 seconds (an integrated tube output of about 3 times that of typical systems). The total heat loading on the tube can be reduced if, as seems likely, efforts to optimize the beam shape of a mammography x-ray tube for slot scanning are

successful. An x-ray tube suitable for our application is now available to us through Fischer Imaging Corporation, a collaborating partner in this project.

Figure (2) shows assembly of a direct x-ray sensing hybrid semiconductor sensor employed in the DXM-1. The solid-state sensor is based on proven technology developed by the defense industry for infrared and x-ray imaging. The sensor is a hybrid structure incorporating a detector and a readout/multiplexer. The detector is a silicon PiN diode array with a thickness of 1.5 mm. It is hybridized to a low noise readout IC (silicon) through indium metal interconnects. The hybrid sensor has a significant advantage that the detector IC and the readout IC can be designed optimized and fabricated separately.

Each sensor is about 6 mm wide and 23 mm in length. As shown in Figure 3, eight of these sensors are aligned to form a staggered array for a cross-scan dimension of about 180 mm. With an in-scan motion for four seconds, it provides a normal size mammogram (180 mm by 240 mm).

Prototype hybrid sensors designed specifically for applications in screening and diagnostic mammography were fabricated and tested by PGI. Some of the tests were conducted independently at the University of Arizona, Tucson by Prof. Hans Roehrig [54]. Figure (4) shows the predicted and measured values of quantum efficiency for 1.0 mm and 1.5 mm thick detectors with molybdenum and tungsten x-ray spectra. As shown in this figure, the measured DQE data are consistent with the predicted values. As shown in Figure (5), the PGI direct x-ray sensing system DQE is significantly better than the film-screen system. The measured quantum efficiency of a 1.5 mm thick detector is over 80%. On the other hand, scatter and grid effects reduce the film-screen system DQE to about 7% to 20%. Figure (6) shows that the MTF data approaches the predicted values. At 10-line pairs/mm, the system MTF is 20% when the sensor is operated in one sample per dwell mode and almost 40% when the sensor is operated in the two samples per dwell mode. This MTF performance is far superior to a film-screen system.

Initial testing of the prototype version of the DXM-1 has demonstrated a detective quantum efficiency greater than 80% and a Nyquist image resolution limit of greater than 17 line pairs per millimeter. Images of the ACR/RMI-156 quality assurance breast phantom acquired using these prototype sensors demonstrate image quality superior to film-screen even at exposure levels one-fifth to one-half the normal for film-screen. For instance, at one-fifth the exposure normal for film-screen, thirteen out of the sixteen targets in the breast phantom are clearly visible. At an exposure level of one-half the normal for screen film, all sixteen targets are discernible. In a typical film-screen image of the phantom, on the other hand, only thirteen out of the sixteen targets are visualized on the average. These results were exhibited and presented at the 1994 RSNA meeting in Chicago. The peer reviews received were gratifying [55].

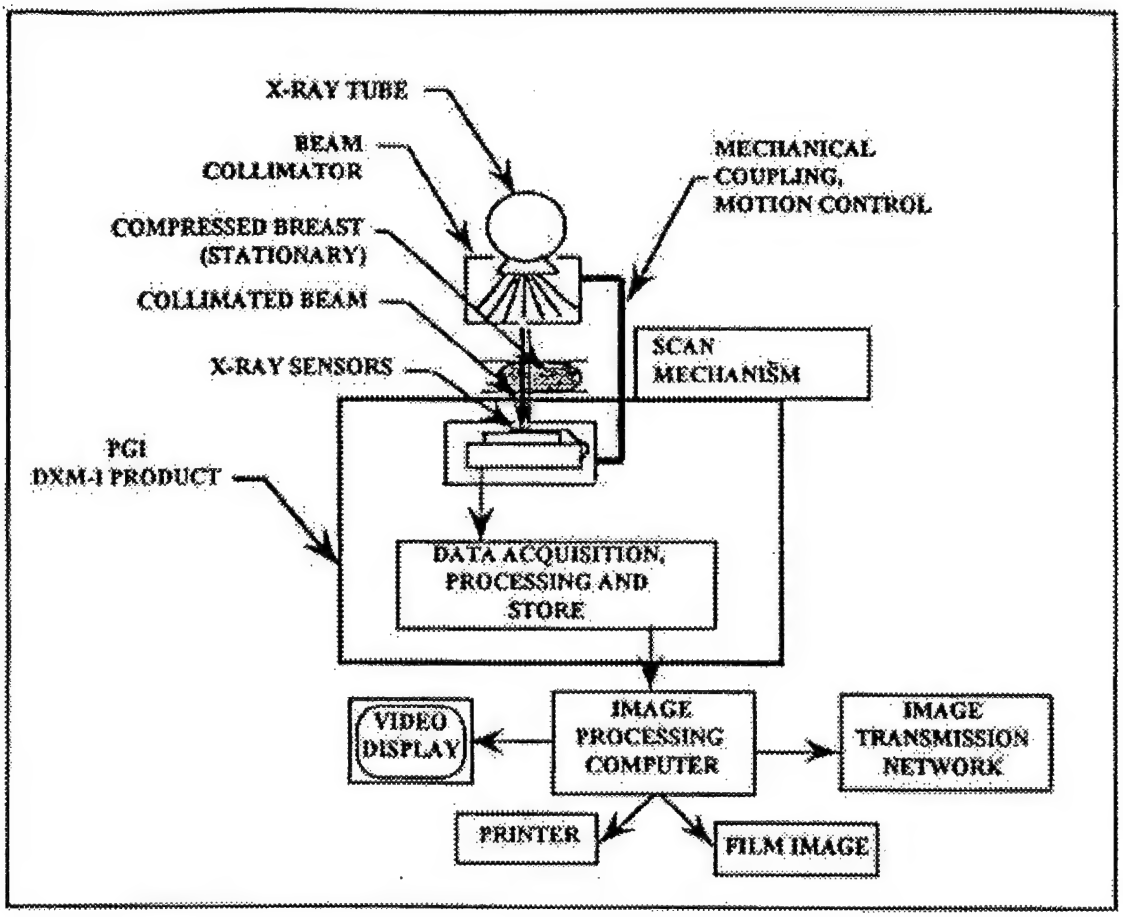

Figure 1: Schematic Representation of the DXM-1 Digital Mammography System

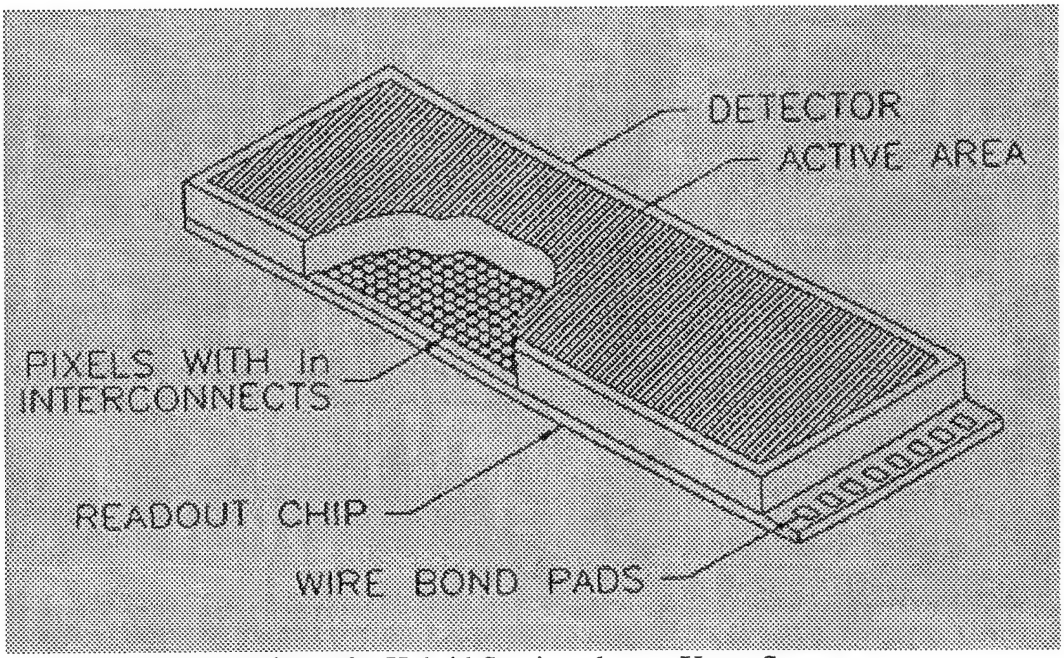

Figure 2: Hybrid Semiconductor X-ray Sensor

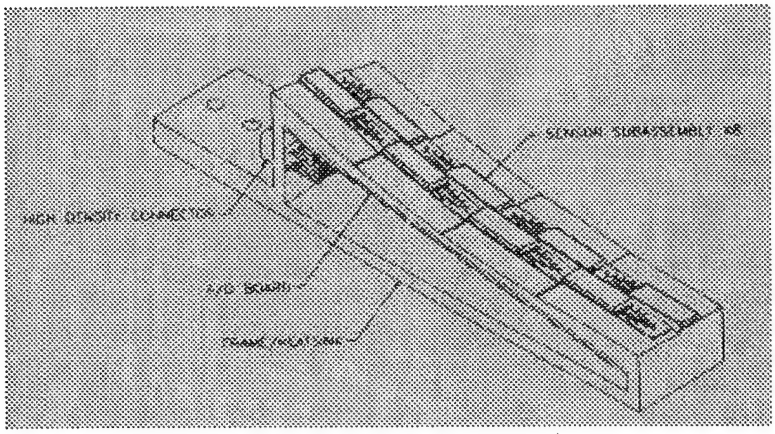

Figure 3: Slot-scanning Detector Array

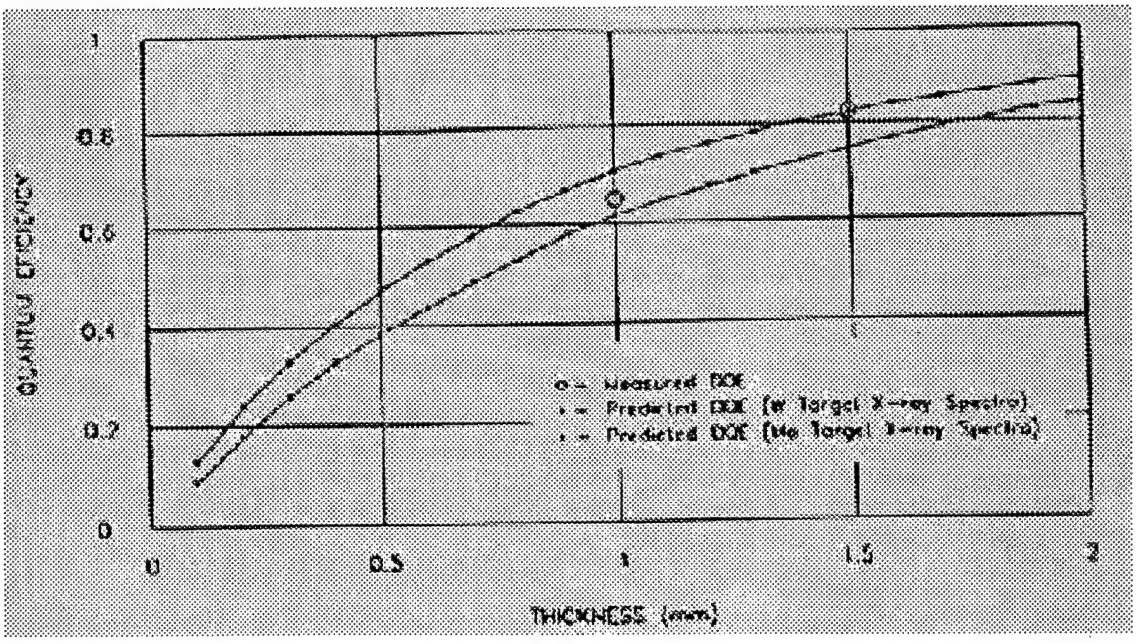

Figure 4: Predicted and Measured DQE Values for the Silicon PiN Diode Sensor

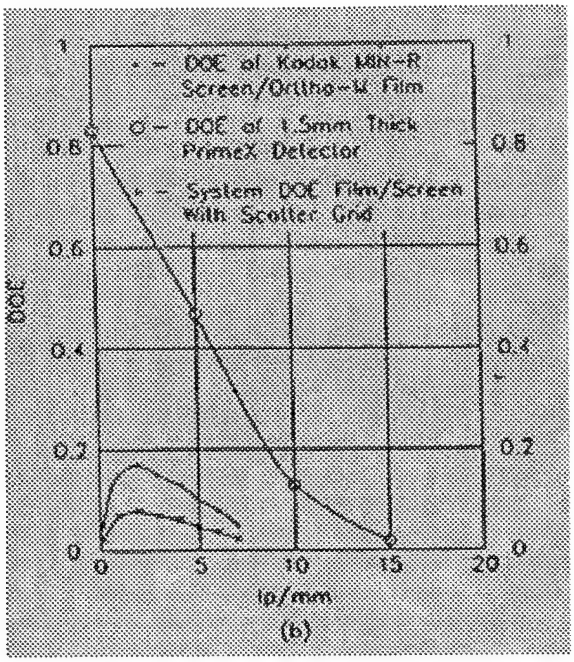

Figure 5: Comparison of DQE (film and DXM-1)

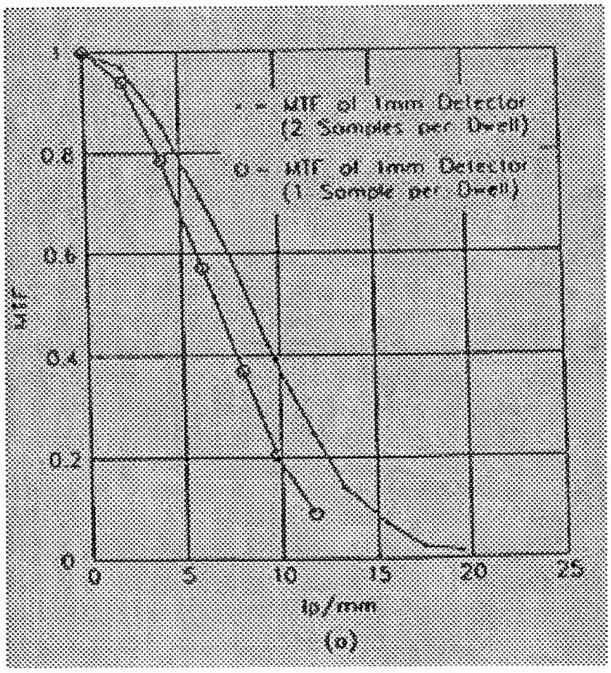

Figure 6: Comparison of MTF (film and DXM-1)

Appendix B

X-ray Absorption of the 1.53 mm thick Silicon of the Primex x-ray converter.

Primex Si-detector; absorption of x-rays, estimated from x-ray images of three detector pieces, placed on the input of a CCD-based x-ray camera, using a screen fiber-optically coupled to the 1024 x 1024 pixel CCD. The x-ray camera had a field of view of about 5 cm x 5 cm. The enclosed schematic describes the experimental set-up.

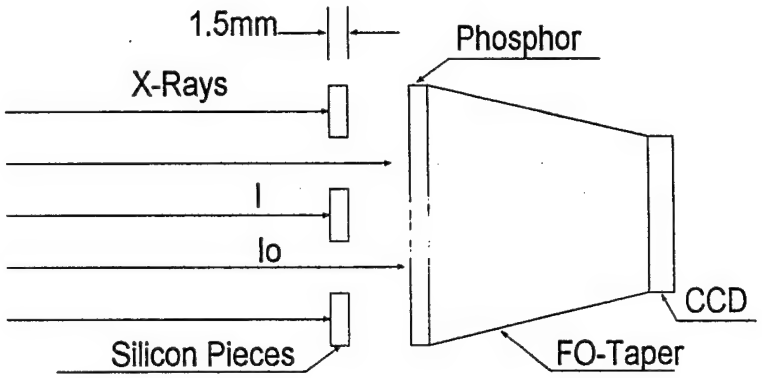

The idea was to determine the absorption A from the measurements of Signal (equivalent to I) and Background (equivalent to I_o) as

$A = (I_o - I)/I_o$ = (Background - Signal)/Background

The enclosed three figures are sample images for the three x-ray conditions A., B., and C. The profiles show how the digital values for Signal (= I) and Background (= I_o) were determined

The result of the measurements:

At 50.5 keV effective energy (HVL = 7.21 mm Al), using a CGR source at 80 kVp + 20 mm Al
Absorption : 12.3%

At 19 keV effective energy (HVL = 0.655 mm Al), using a Toshiba "Mammo-Source", at 30 kVp + 3.9 cm Plexiglass
Absorption overall: 73.3%

At 14.9keV effective energy (HVL = 0.339 mm Al), using a Toshiba "Mammo-Source", at 26 Kvp and Mo-Filter
Absorption : 86.9%

Figure B-1

Primex detector on CCD camera with optical fiber reducer
X-ray Source: 80Kvp, 2 cm Al(50Kev)

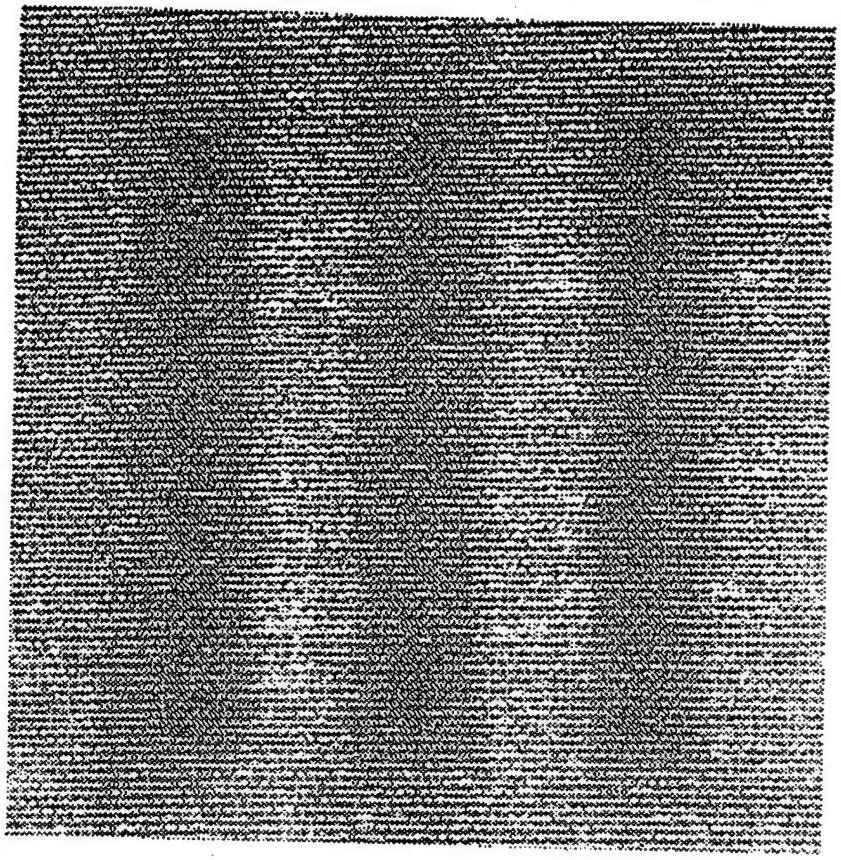

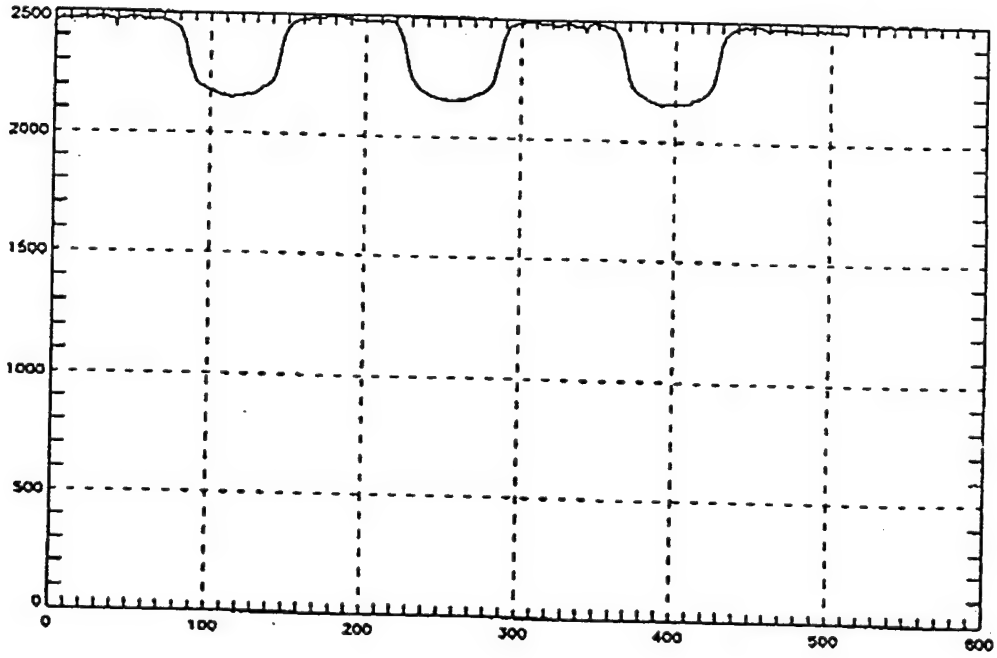

Figure B-2

Primex detector on CCD camera with optical fiber reducer
X-ray Source: 30 Kvp, Plus plexiglass filer(20Kev)

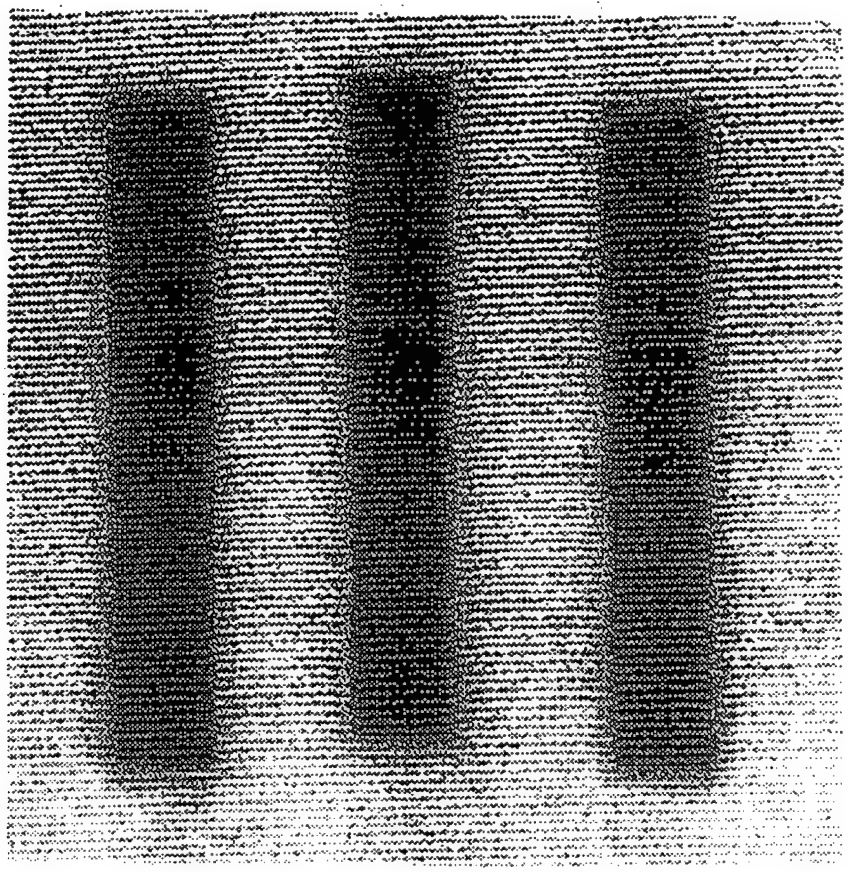

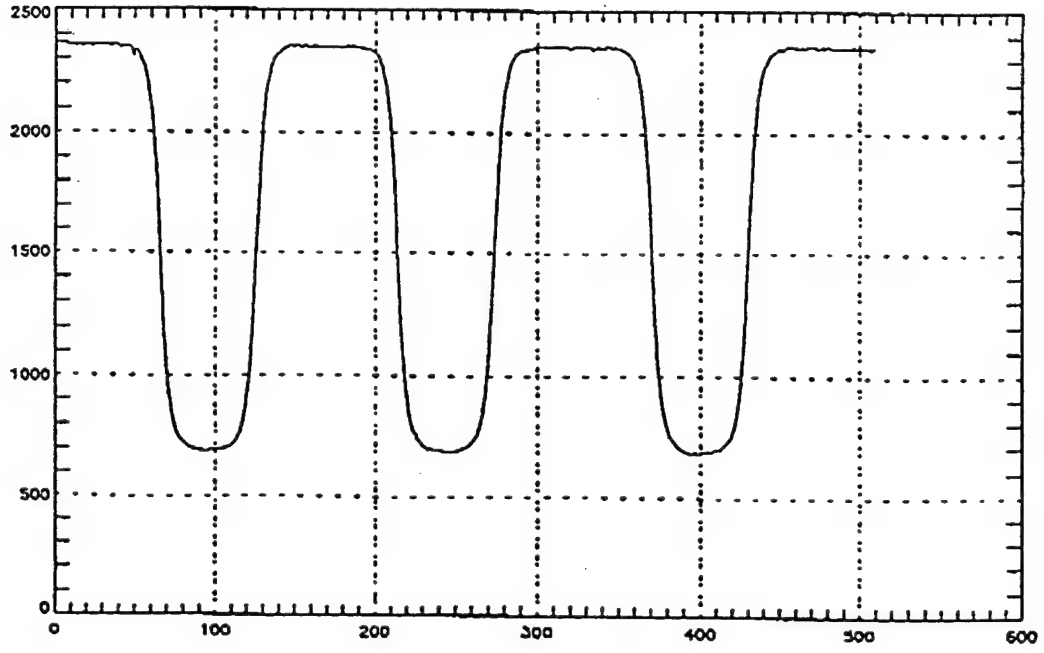

Figure B-3

Primex detector on CCD camera with optical fiber reducer
X-ray Source: 26 Kvp, no X-ray filter

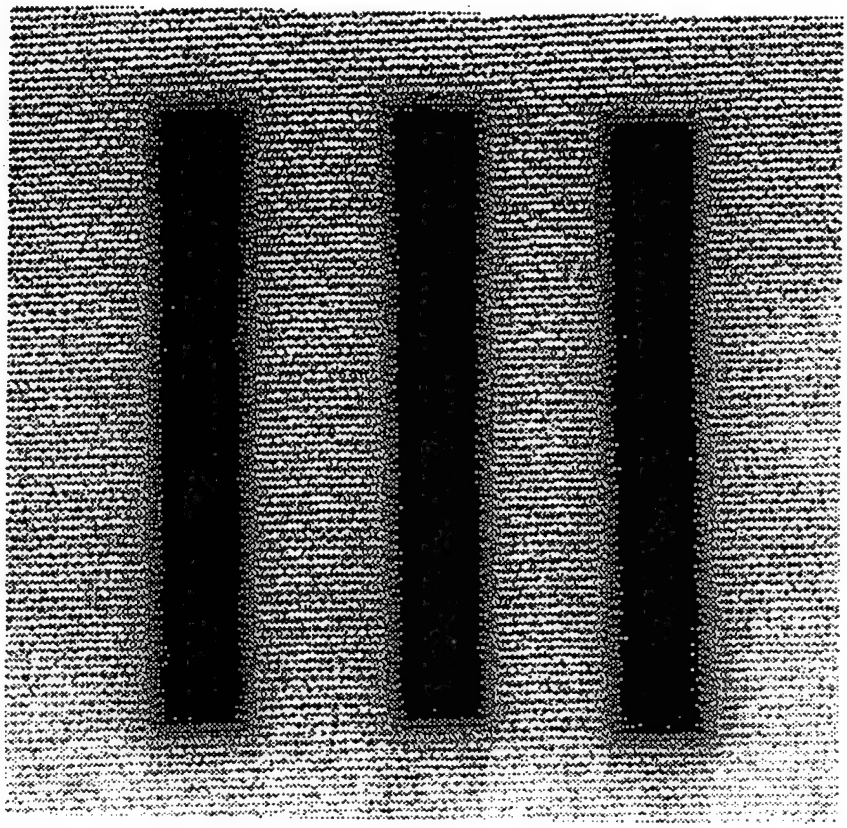

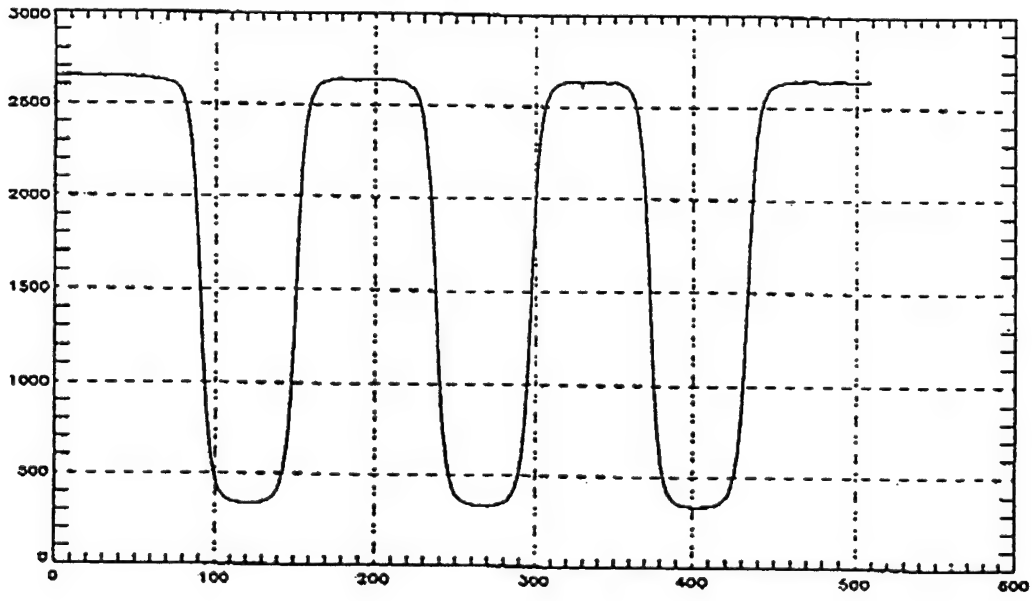

Figure B-4

The size of each of the three detector pieces was approximately

	Object 1	Object 2	Object 3
length [mm]:	18.84	18.88	18.84
width [mm]:	2.84	2.85	2.83
height [mm]:	1.53	1.52	1.52
Volume [cm^3]	.082	.082	.081
Weight [g]	.18865	.18865	.18815
Density [g/cm^3]	2.301	2.301	2.323
Density of Si from reference books [g/cm^3]	2.42	2.42	2.42

A.: Exposures at 50.5 keV effective energy (HVL = 7.21 mm Al),using CGR source at 80 kVp + 20 mm Al

Exposure	Pos.	Object 1				Object 2				Object 3			
		Signal	Back-ground	Diff.	Absorption	Signal	Back-ground	Diff.	Absorption	Signal	Back-ground	Diff.	Absorption
1.	1.	1011	1153	142	.123	1016	1157	141	.122	1009	1154	145	.126
	2.	1016	1155	139	.120	1015	1161	146	.126	1014	1159	145	.126
	3.	1011	1158	147	.127	1015	1159	144	.124	1011	1155	144	.124
Absorption, ave:					12.3%				12.4%				12.5%
2.	1.	2122	2430	308	.127	2128	2436	308	.126	2125	2423	298	.123
	2.	2129	2434	305	.125	2134	2444	310	.127	2139	2428	289	.119
	3.	2125	2427	302	.124	2129	2437	308	.126	2126	2433	307	.126
Absorption, ave:					12.5%				12.6%				12.3%
3.	1.	2903	3295	392	.119	2898	3303	405	.123	2898	3299	401	.122
	2.	2904	3298	394	.119	2911	3307	396	.120	2899	3308	409	.124
	3.	2898	3291	393	.119	2900	3306	406	.123	2901	3297	396	.120
Absorption, ave:					11.9%				12.2%				12.2%

Absorption overall: 12.3%

Figure B-5

B.: Exposures at 19 keV effective energy (HVL = 0.655 mm Al), using a Toshiba "Mammo-Source", at 30 kVp + 3.9 cm Plexiglass

Exposure	Pos.	Object 1 Signal	Back-ground	Diff.	Absorption	Object 2 Signal	Back-ground	Diff.	Absorption	Object 3 Signal	Back-ground	Diff.	Absorption
1.	1.	562	2142	1580	.738	562	2141	1579	.738	568	2139	1571	.734
	2.	557	2146	1589	.740	557	2141	1584	.740	566	2139	1573	.735
	3.	556	2144	1588	.741	561	2138	1577	.738	563	2144	1581	.737
Absorption, ave:					74.0%				73.9%				73.5%
2.	1.	940	3439	2499	.727	934	3432	2498	.728	946	3430	2484	.724
	2.	932	3445	2513	.729	932	3432	2500	.728	942	3428	2486	.725
	3.	931	3433	2502	.729	936	3434	2498	.727	939	3428	2489	.726
Absorption, ave:					72.8%				72.8%				72.5%

Absorption overall: 73.3%

C.: Exposures at 14.9keV effective energy (HVL = 0.339 mm Al), using a Toshiba "Mammo-Source", at 26 Kvp and Mo-Filter

Exposure	Pos.	Object 1 Signal	Back-ground	Diff.	Absorption	Object 2 Signal	Back-ground	Diff.	Absorption	Object 3 Signal	Back-ground	Diff.	Absorption
1.	1.	249	1927	1678	.870	247	1916	1669	.871	252	1926	1674	.869
	2.	245	1924	1679	.873	243	1916	1673	.873	246	1924	1678	.872
	3.	244	1924	1680	.873	245	1919	1674	.872	247	1923	1676	.872
Absorption ave:					87.2%				87.2%				87.1%
2.	1.	475	3540	3065	.866	471	3527	3056	.866	478	3540	3062	.865
	2.	465	3543	3078	.865	462	3532	3070	.869	468	3543	3075	.868
	3.	466	3550	3084	.869	471	3544	3073	.867	476	3541	3065	.866
Absorption ave:					86.7%				86.7%				86.6%

Absorption overall: 86.9%

Figure B-6

Half-Value layers of Primex Mammo-x-source

3.9 cm Plexiglass		3.9 cm Plexiglass	No Plexiglass	No Plexiglass
Al-Thickn [mm]	[30 kVp] Exposure [mr]	[26 kVp] Exposure [mr]	[30 kVp] Exposure [mr]	[26 kVp] Exposure [mR]
0	79.6	37.8	2790	1771
0.1	70.6	33.9	2220	1374
0.2	63.2	29.3	1826	1095
0.3	56.56	26	1523	899
0.4	50.5	22.6	1276	742
0.5	45	20.05	1094	621
0.6	40.75	17.9	920	519
0.7	36.4	15.65	779	
0.8	32.9	13.95		
0.9	29.8	12.5		
1	27	11.02		
	HVL: 0.626 mm Al	HVL 0.557 mm Al	HVL 0.363 mm Al	HVL 0.32 mm Al
	mu/rho (0.5) 4.101	mu/rho (0.5) 4.609	mu/rho (0.5) 7.0722	mu/rho (0.5) 8.0225
	E-eff [kev] 18.73	E-eff [keV] 17.99	E-eff [keV] 15.55	E-eff [keV] 14.89

Figure B-7

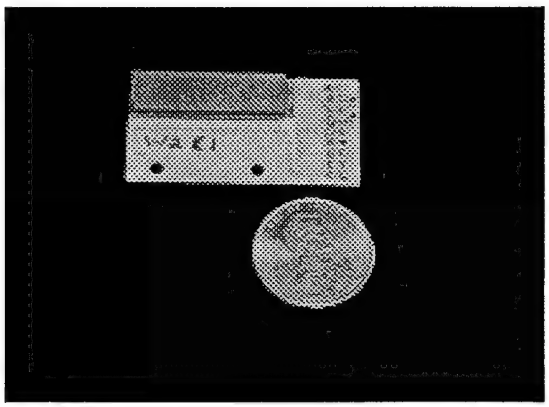

Figure B-8: Silicon-Based Hybrid PiN Diode Array

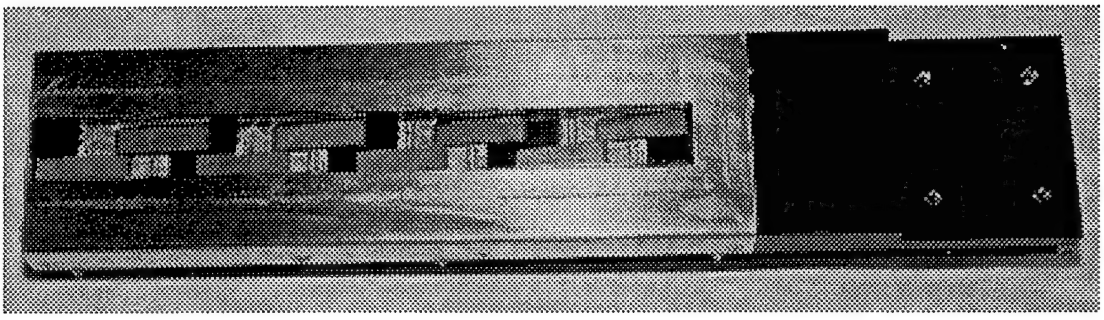

Figure B-9: DXM-1 Detector Module

Figure B-10: Fischer Imaging Corporation's Sensoscan
Digital Mammography Gantry – Side View
Tube Head Exposed

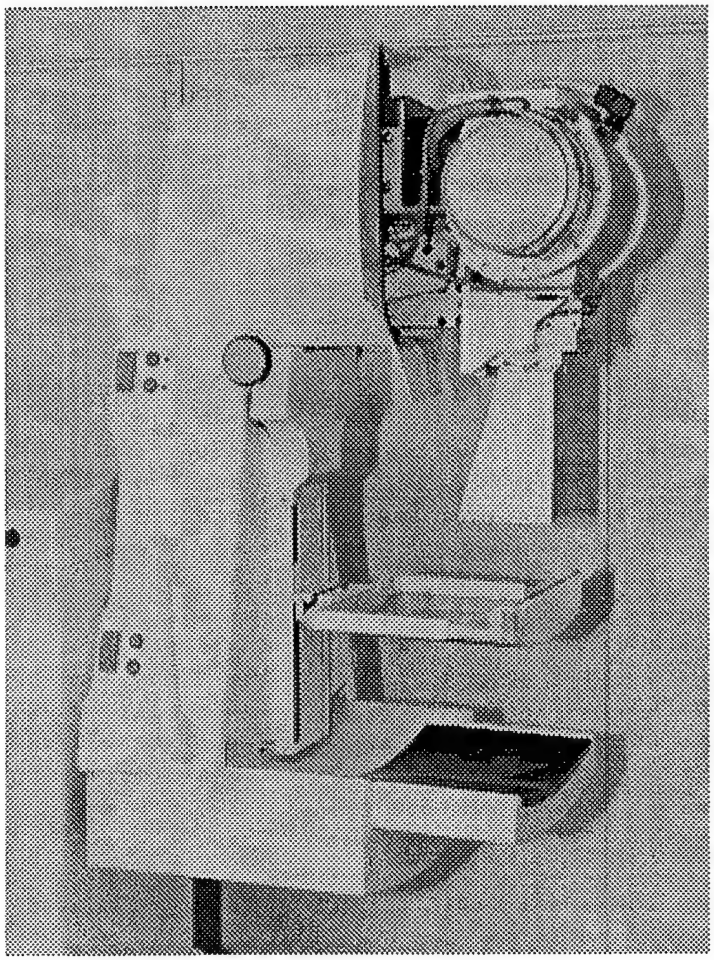

Figure B-11: Fischer Imaging Corporation's Sensoscan
Digital Mammography Gantry – Front View
Tube Head Exposed

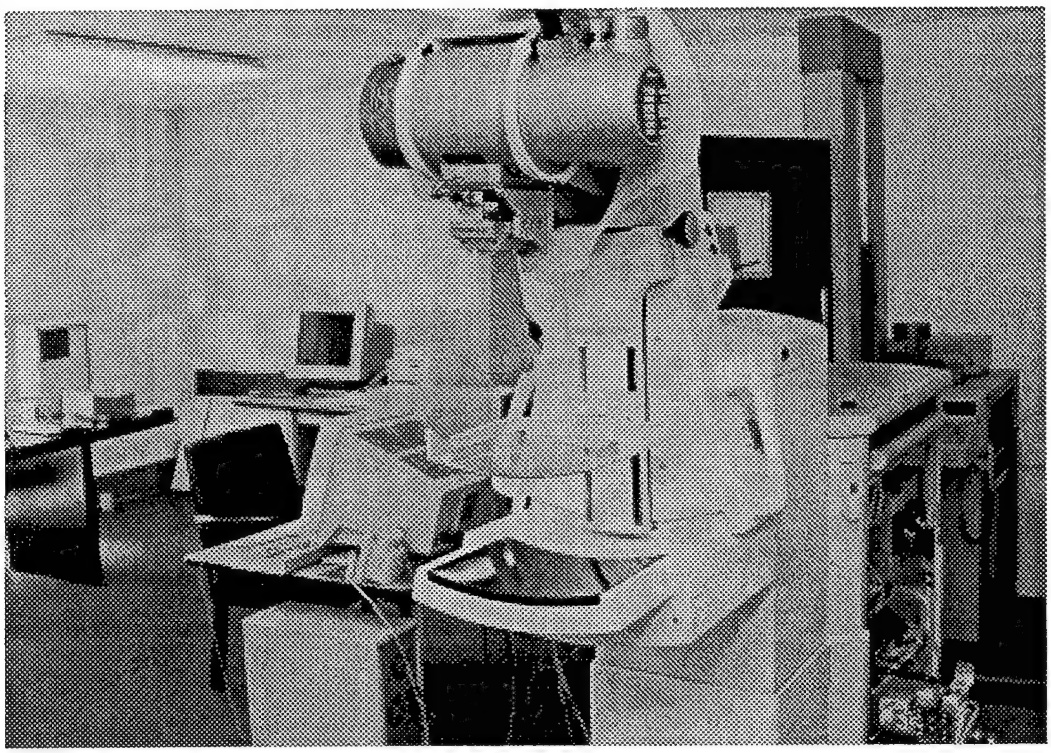

Figure B-12: Fischer Imaging Corporation's
Sensoscan Digital Mammography
Gantry – Front View

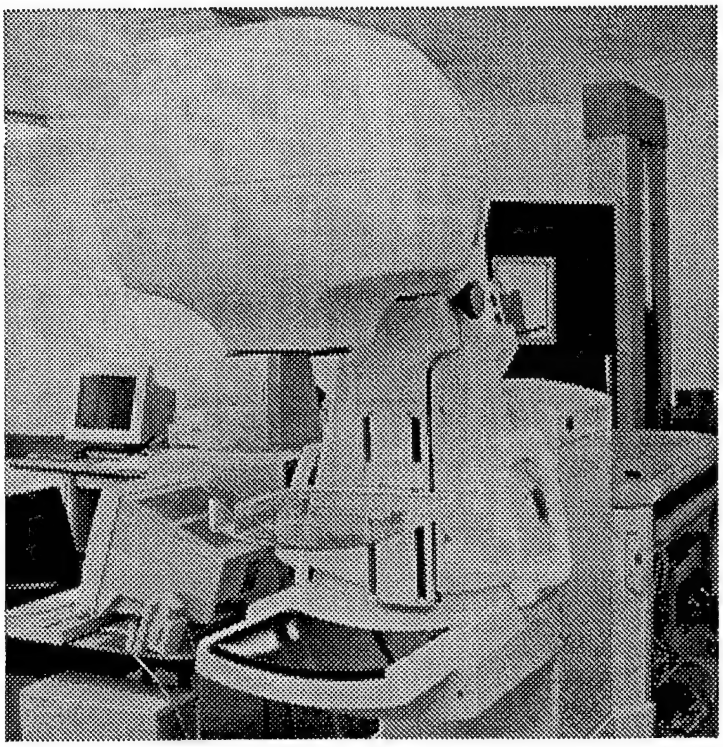

Figure B-13: Fischer Imaging Corporation's Sensoscan
Digital Mammography Gantry – Side View

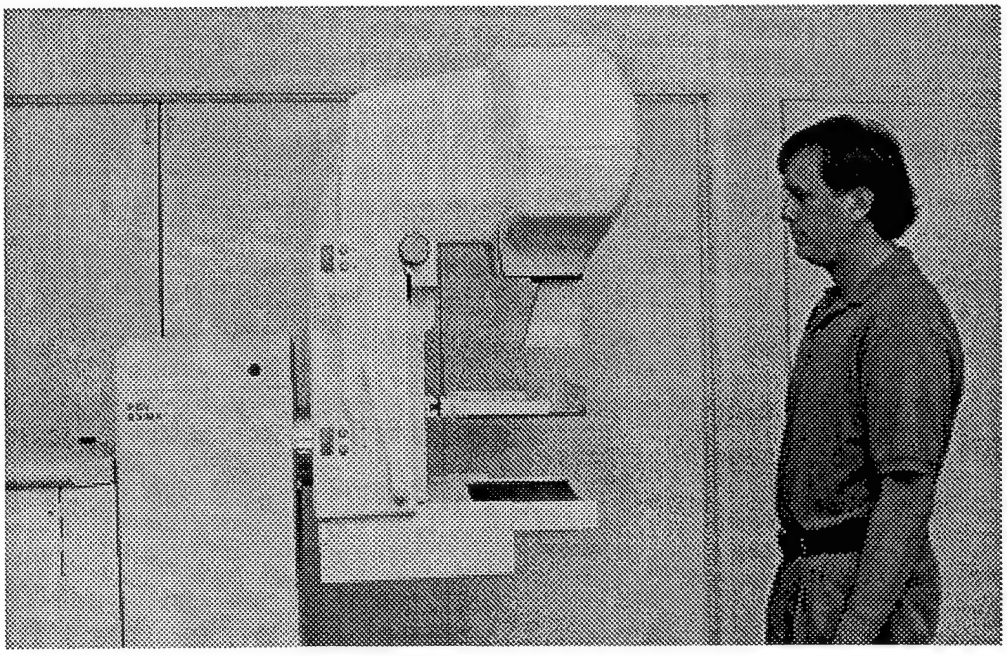

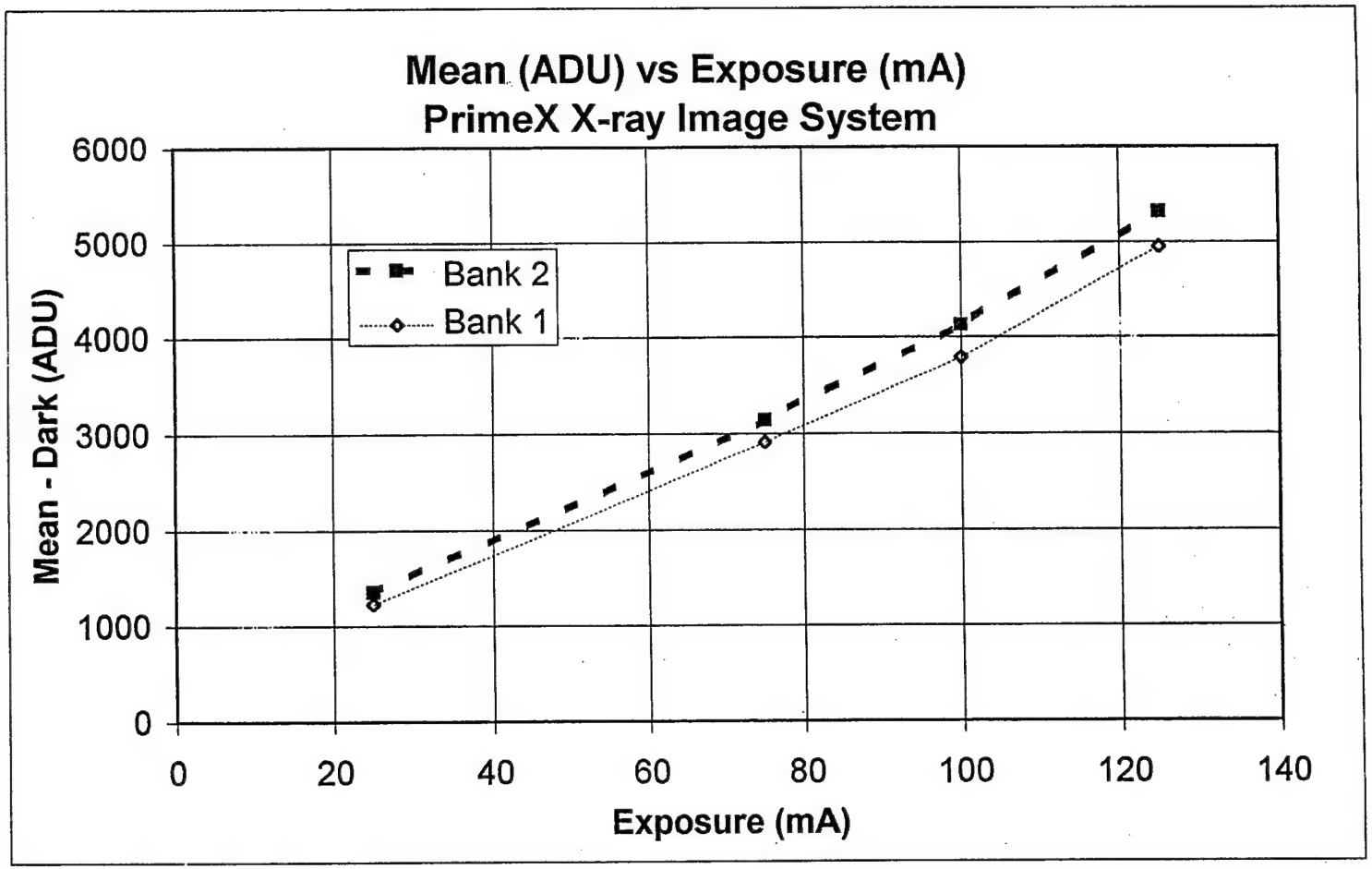
Mean (ADU) vs Exposure (mA)
PrimeX X-ray Image System
Mean - Dark (ADU)
6000
5000
4000
3000
2000
1000
0
Bank 2
Bank 1
0
20
40
60
80
100
120
140
Exposure (mA)

Figure B-14

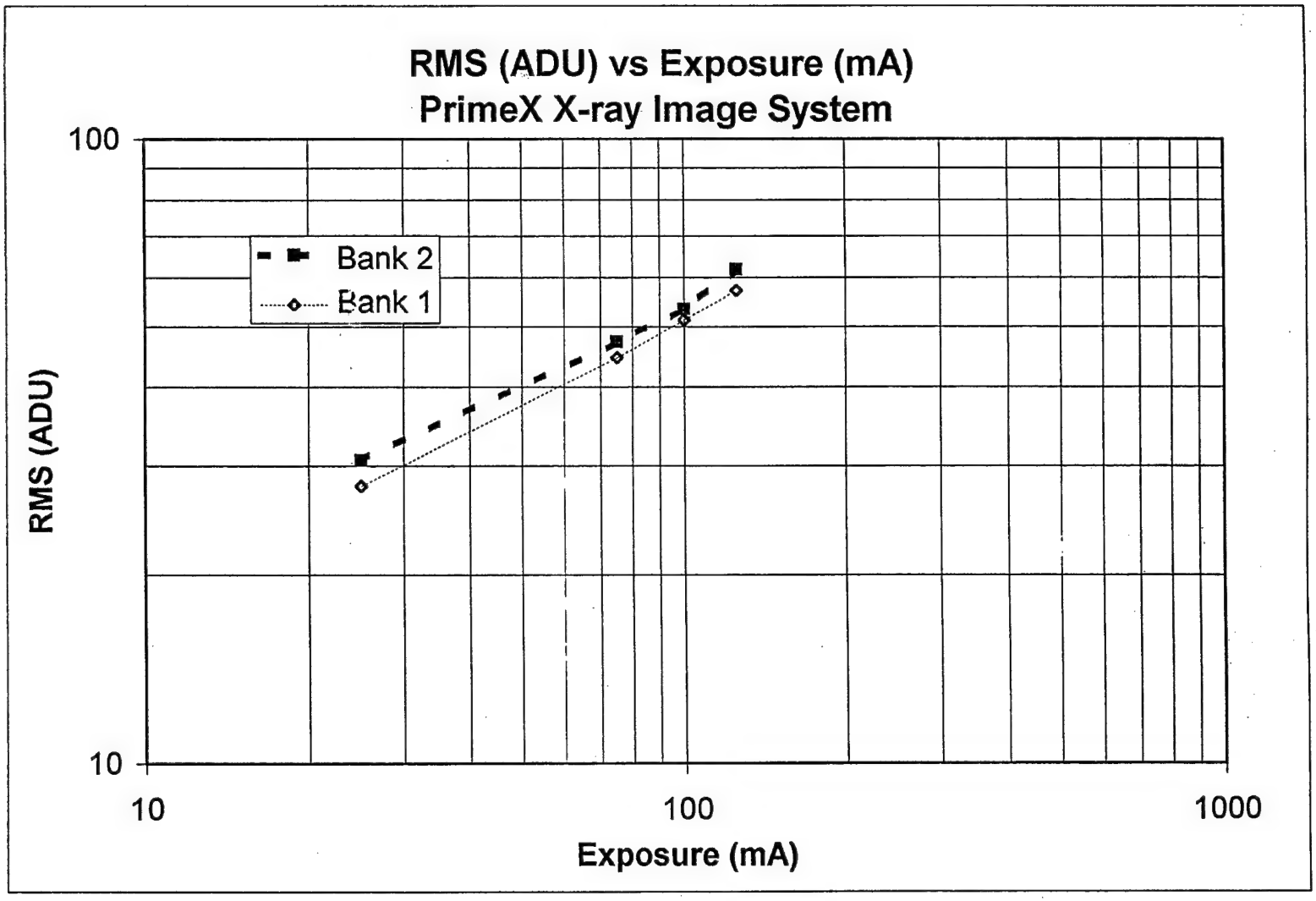
RMS (ADU) vs Exposure (mA)
PrimeX X-ray Image System
100
10
RMS (ADU)
Bank 2
Bank 1
10
100
1000
Exposure (mA)

Figure B-15

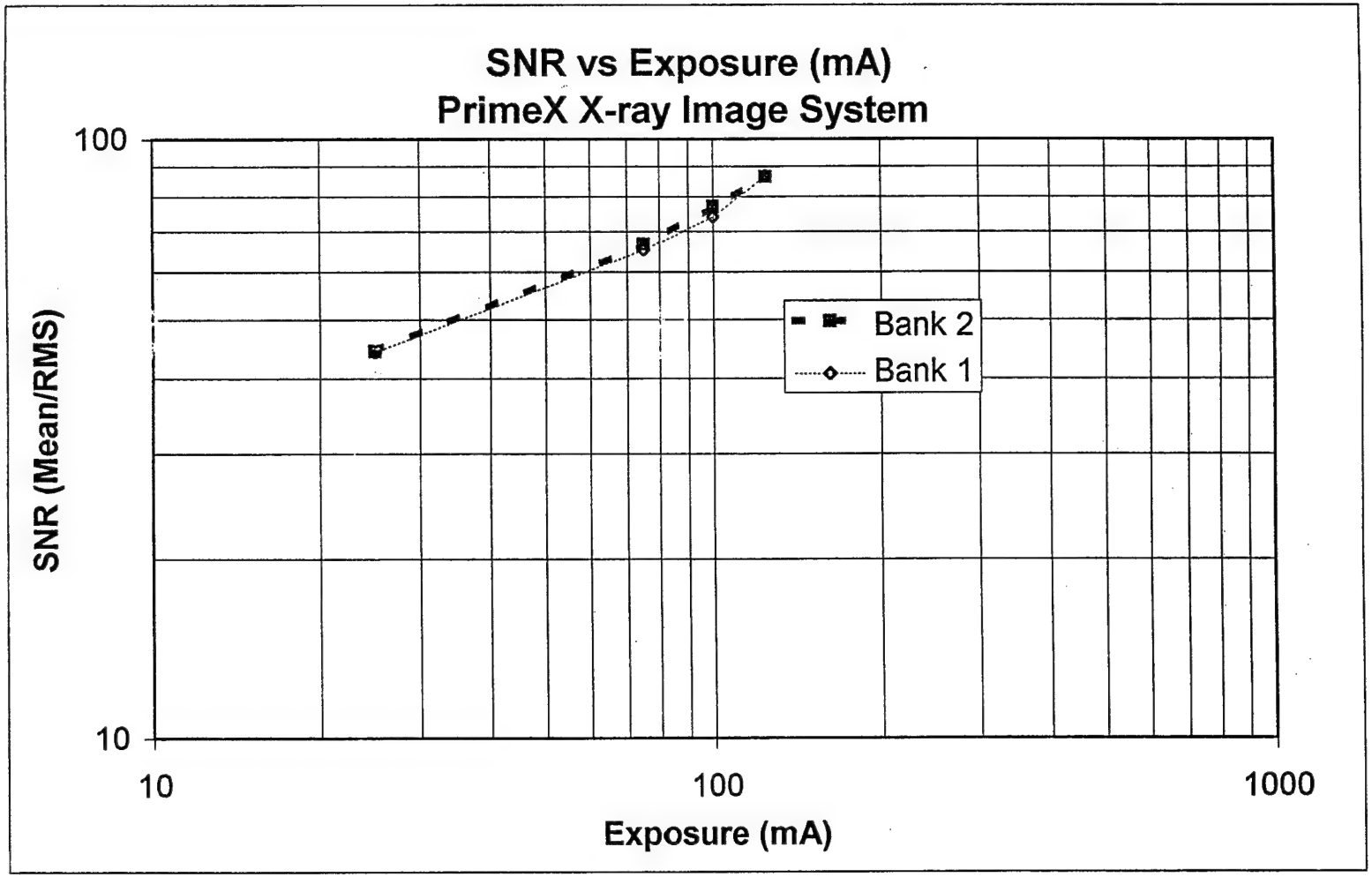
SNR vs Exposure (mA)
PrimeX X-ray Image System
100
10
SNR (Mean/RMS)
Bank 2
Bank 1
10
100
1000
Exposure (mA)

Figure B-16

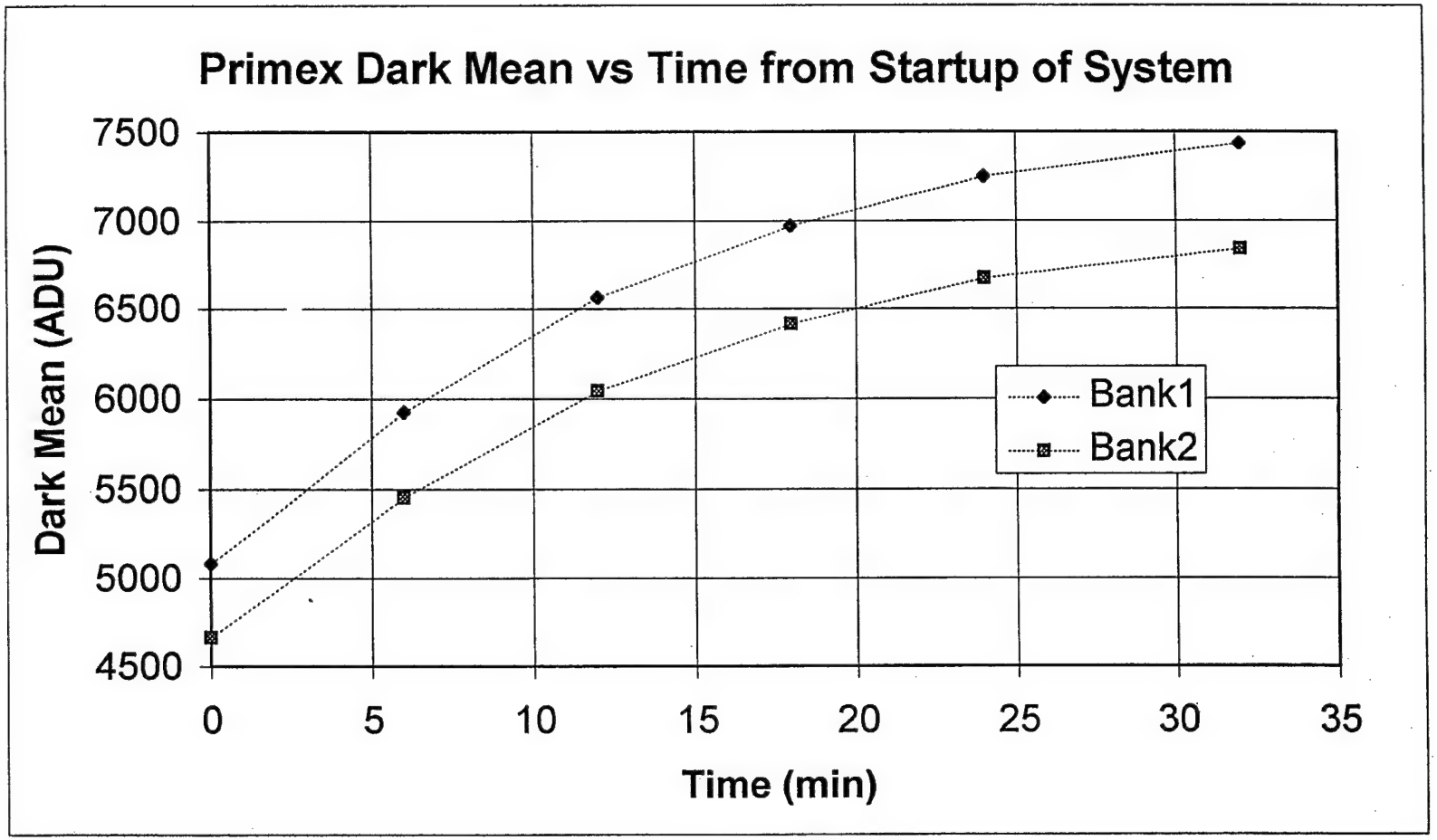
Primex Dark Mean vs Time from Startup of System
Dark Mean (ADU)
7500
7000
6500
6000
5500
5000
4500
0
5
10
15
20
25
30
35
Time (min)
Bank1
Bank2

Figure B-17

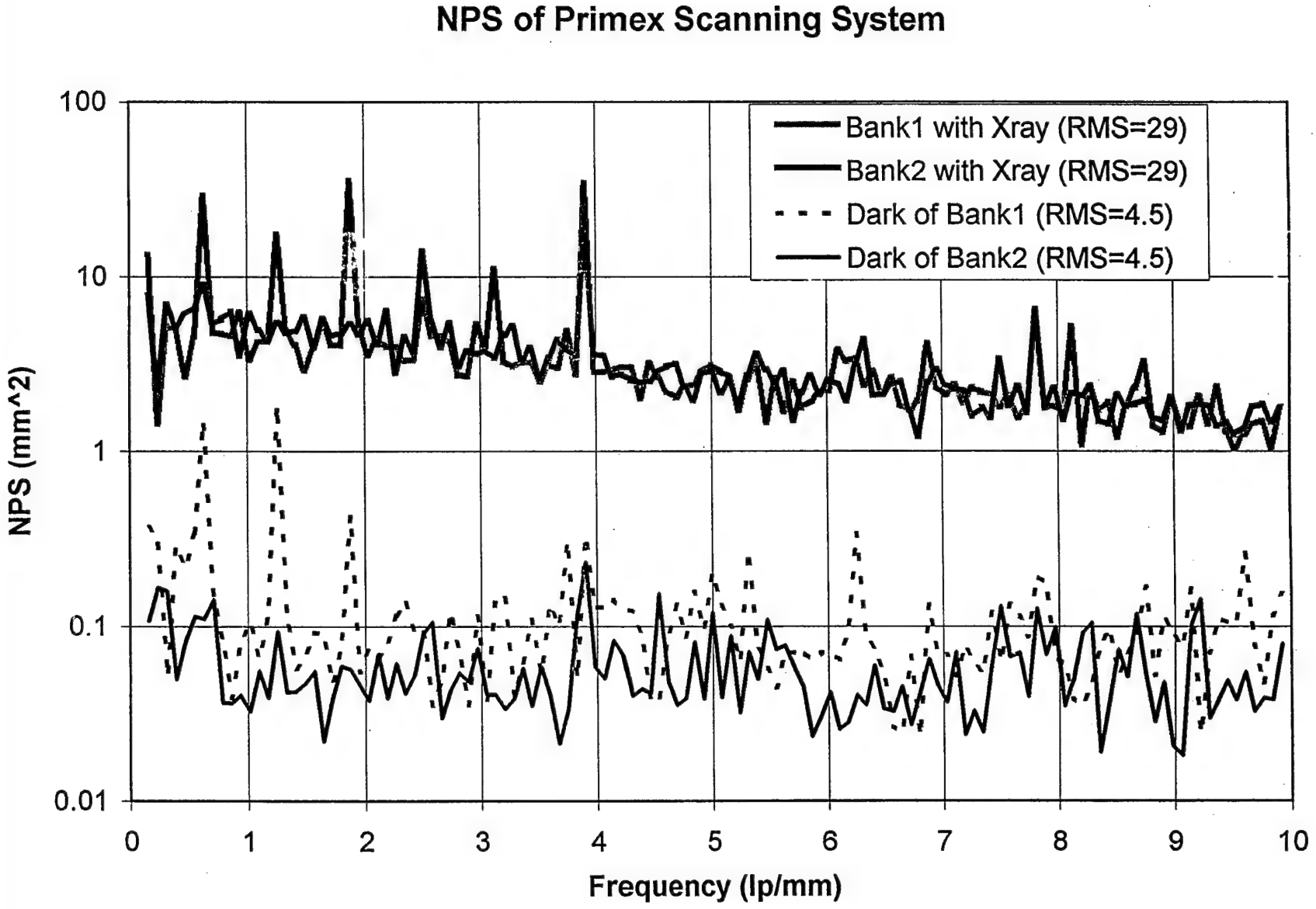
NPS of Primex Scanning System
Bank1 with Xray (RMS=29)
Bank2 with Xray (RMS=29)
Dark of Bank1 (RMS=4.5)
Dark of Bank2 (RMS=4.5)
NPS (mm^2)
100
10
1
0.1
0.01
0
1
2
3
4
5
6
7
8
9
10
Frequency (lp/mm)

Figure B-18

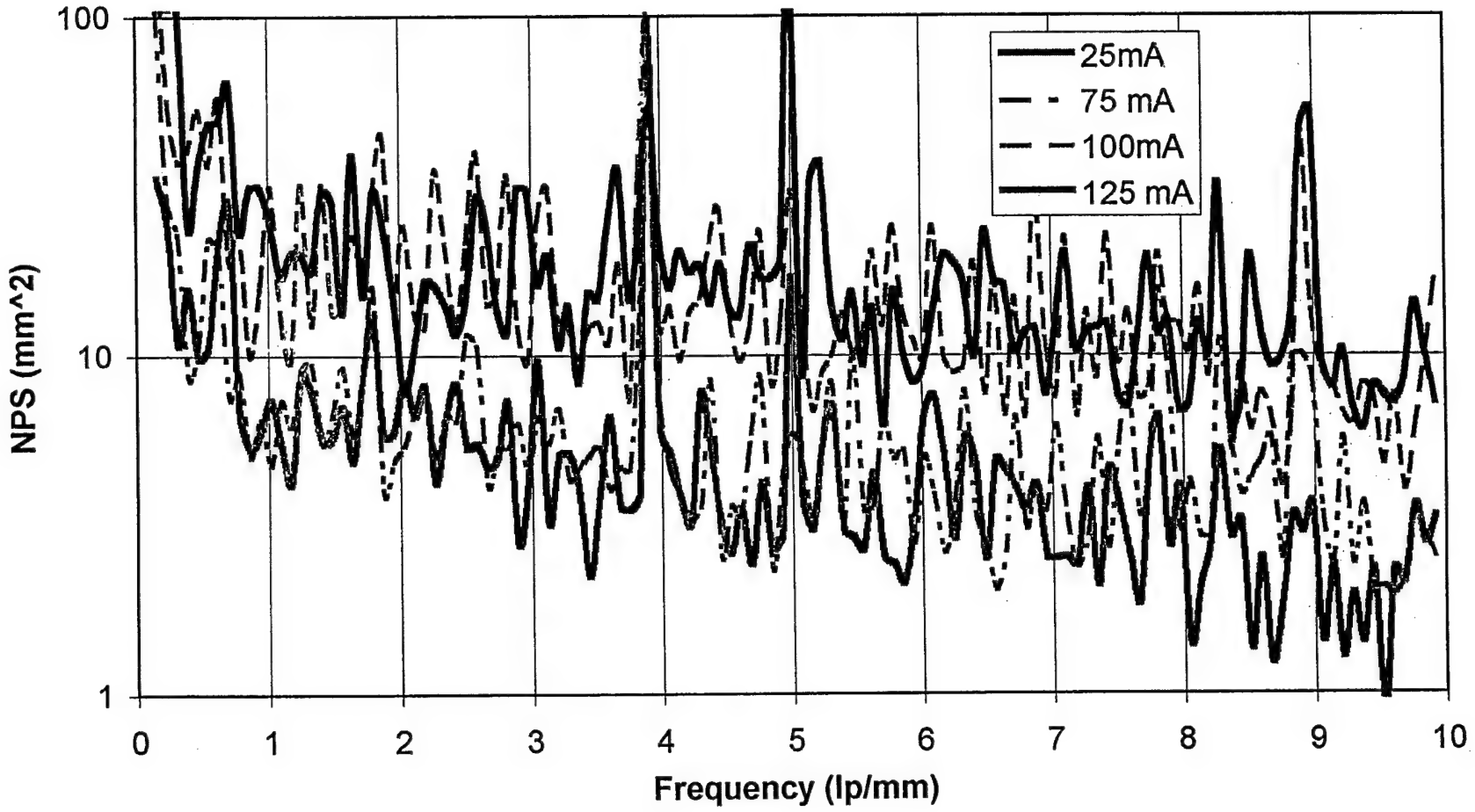
NPS of Primex System
100
10
1
NPS (mm^2)
0
1
2
3
4
5
6
7
8
9
10
Frequency (lp/mm)
25mA
75 mA
100mA
125 mA

Figure B-19

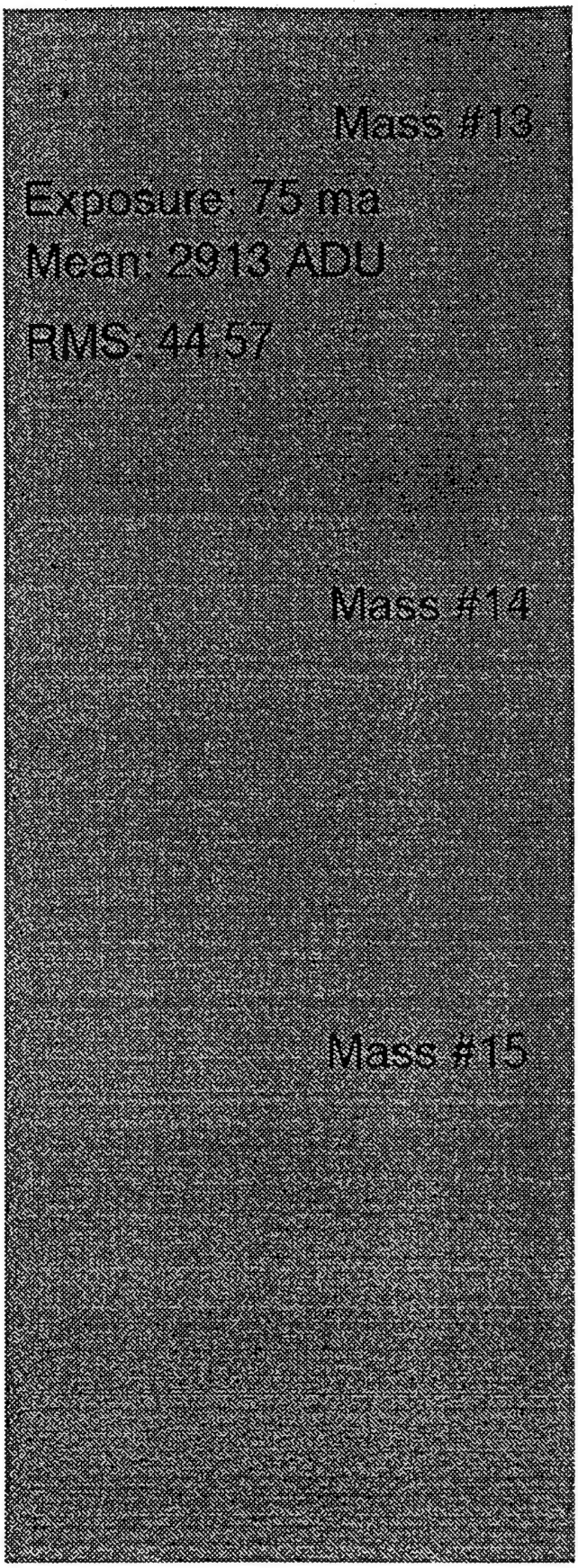

Figure B-20

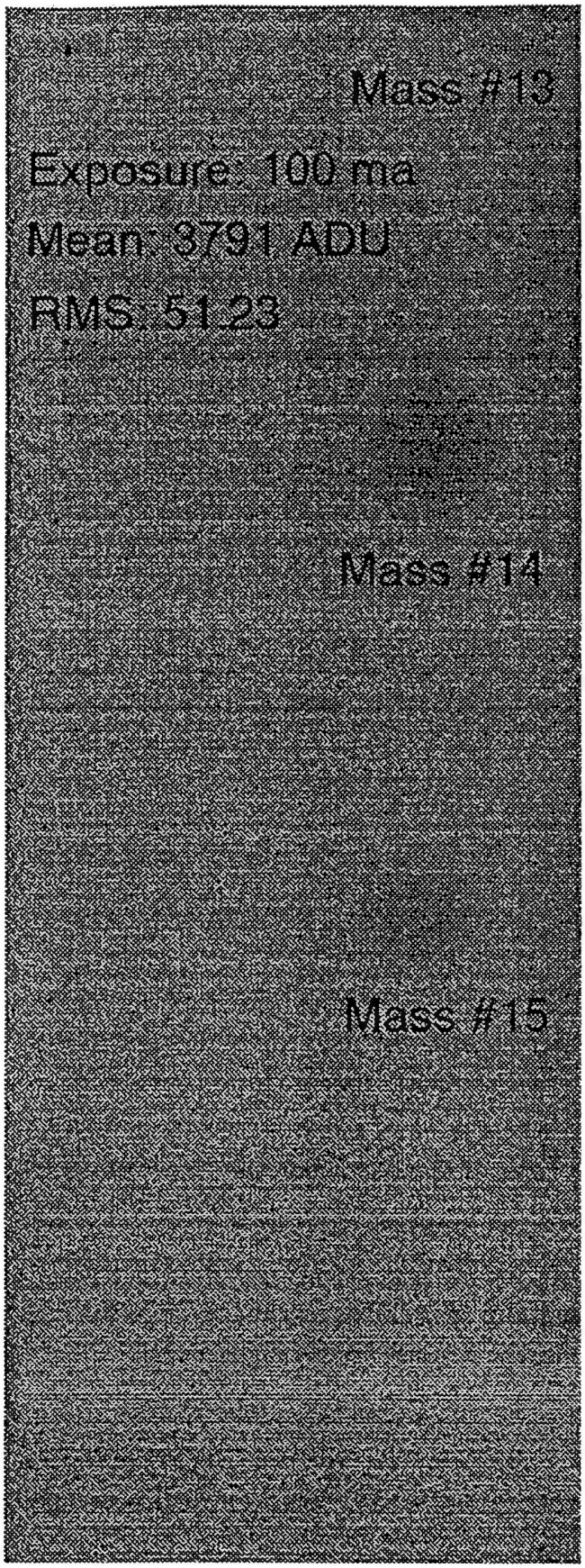

Figure B-21

2. DESCRIPTION

The Mammographic Phantom is made up of a wax block containing 16 various sets of test objects, a 3.3 cm (1.3 inch) thick acrylic base, a tray for placement of the wax block, and a .3 cm (.12 inch) thick cover. All of this together approximates a 4.0 to 4.5 cm compressed breast. Five simulated micro-calcifications, six different size nylon fibers simulate fibrous structures, and five different size tumor-like masses are included in the wax insert.

Figure 2 lists the sizes of the test objects and their position in relation to the notched corner of the wax block.

	Region Materials
1.	1.56 mm nylon fiber
2.	1.12 mm nylon fiber
3.	0.89 mm nylon fiber
4.	0.75 mm nylon fiber
5.	0.54 mm nylon fiber
6.	0.40 mm nylon fiber
7.	0.54 mm simulated micro-calcification
8.	0.40 mm simulated micro-calcification
9.	0.32 mm simulated micro-calcification
10.	0.24 mm simulated micro-calcification
11.	0.16 mm simulated micro-calcification
12.	2.00 mm tumor-like mass
13.	1.00 mm tumor-like mass
14.	0.75 mm tumor-like mass
15.	0.50 mm tumor-like mass
16.	0.25 mm tumor-like mass

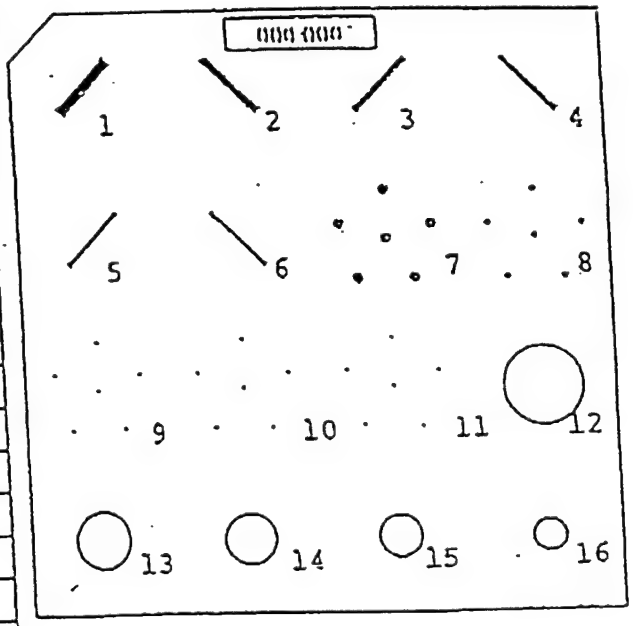

Figure 2. A schematic view of the Mammographic Phantom giving the test object sizes and position numbers used for reference.

Note: Numbers are for reference only. The wax block can be removed (carefully) and placed in different orientations (even upside down) for a randomized effect if desired.

Figure B-22: ACR Accreditation Phantom Image Schematic

Figure B-23: Prototype 2-channel DXM-1 DSP

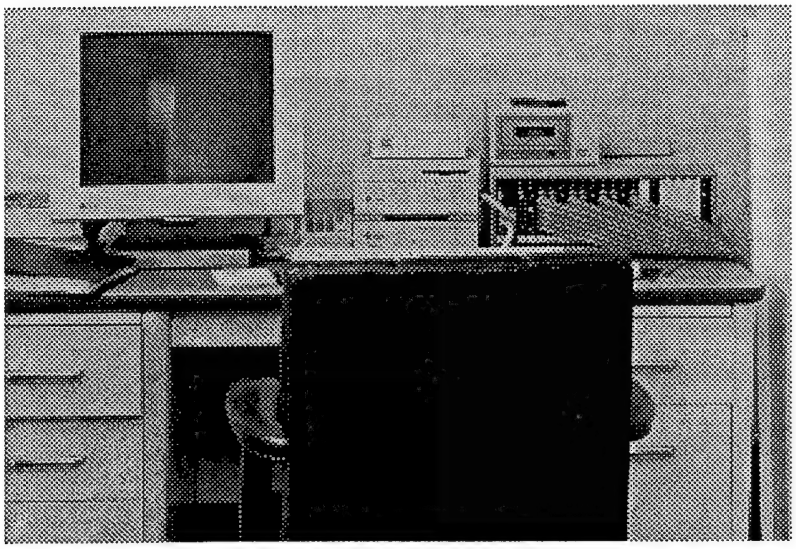

Figure B-24: Prototype 2-channel DXM-1 Gantry

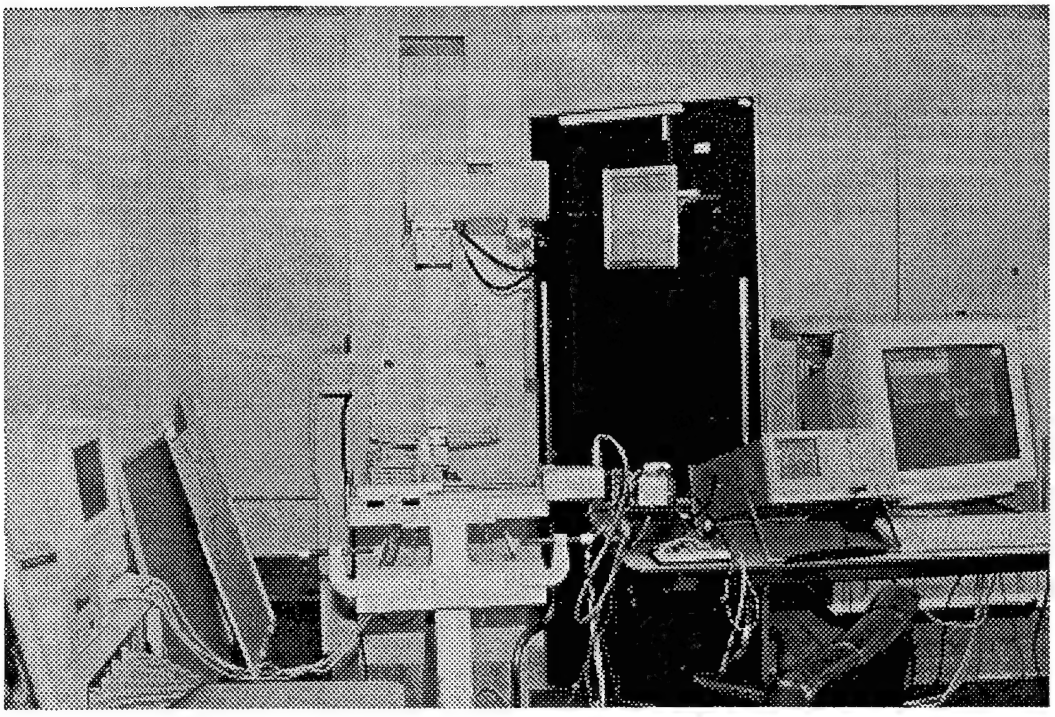

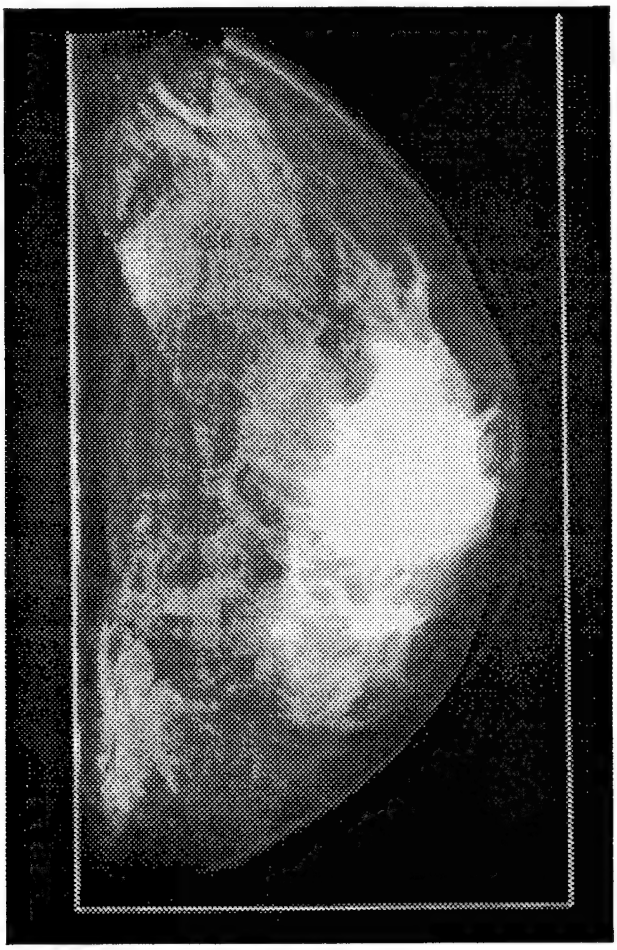

Figure B-25: Cadaver Breast Image Acquired with the DXM-1

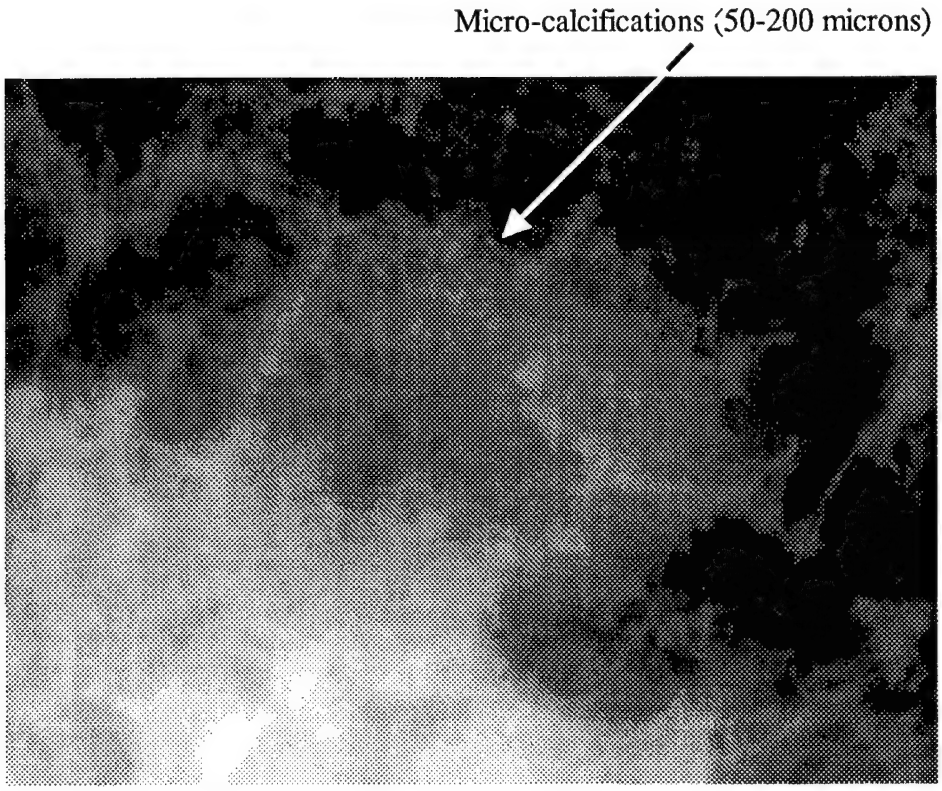

Figure B-26: Cadaver Breast Image Acquired with the DXM-1
Area of Interest Showing Microcalcifications

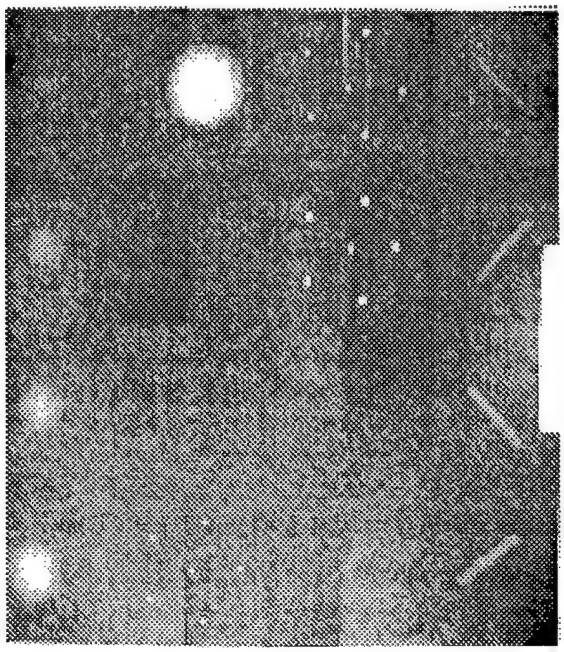

Figure B-27: ACR Accreditation Phantom Image Acquired with the DXM-1
15 of 16 spec groups visible

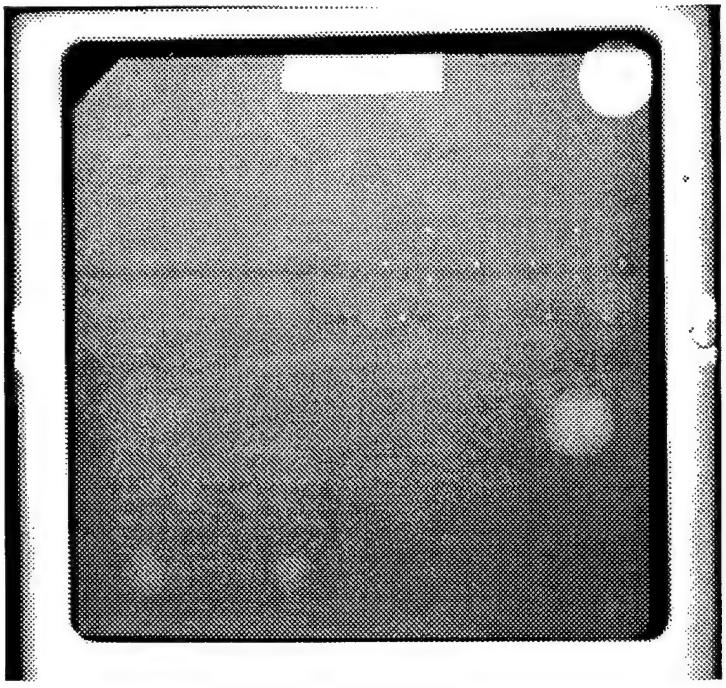

Figure B-28: ACR Accreditation Phantom Image Acquired with Film/Screen

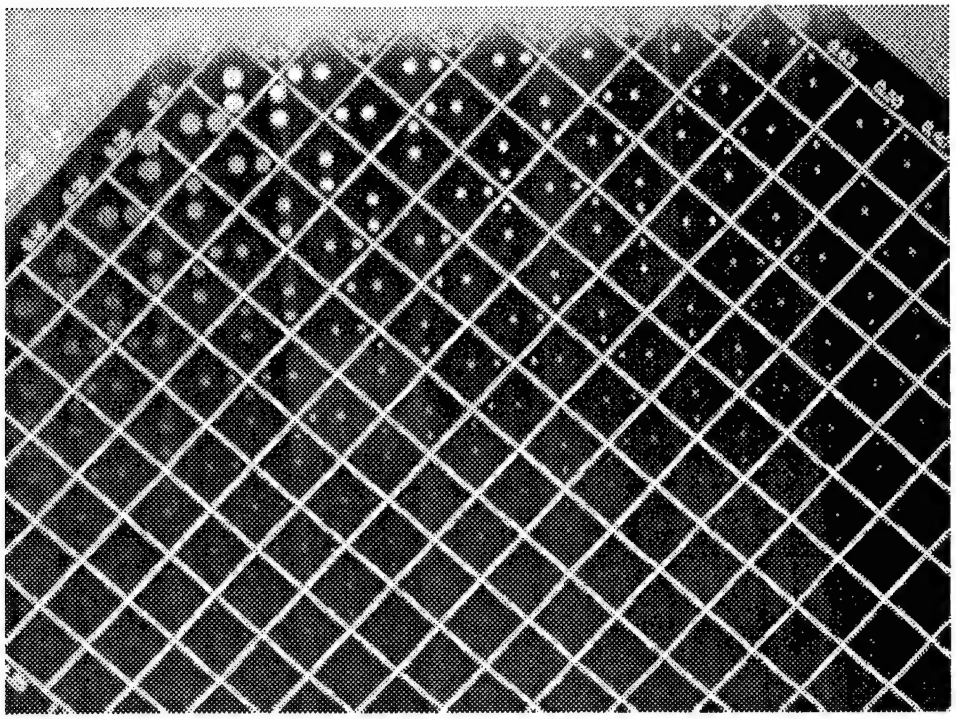

Figure B-29: CDMAM Phantom Image Acquired with the DXM-1

Figure B-30: Full-Field Mammographic Image of a Patient with the DXM-1

Appendix C

Black Forest ENGINEERING, INC.
719-495-0735 fax: 719-495-4658 email: gaalema@bfe.com
12930 Morris Trail, Colorado Springs, CO 80908
www.sni.net/BFE/

BFE 124
On-chip TDI Error Investigation

Executive Summary

A careful analysis of the BFE124B circuitry, as implemented, has revealed two obviously serious design errors in the digital control logic. Two additional issues have been identified that may cause problems in certain (high) signal conditions.

The first major error (**read order**) is an error in the order of the pixel readout within a row, and the second (**o/n timing**) involves the timing of the state machine increment.

1. The logic that selects which capacitor to read out is not in the proper phase relative to the advance of the image across the detectors. The net result is that a capacitor gets part of it's charge due to one image pixel and the rest due to an image pixel four pixels away creating a ghost image.

2. The state machine that steers charge from each detector to the appropriate integration capacitor for a given row is supposed to advance as soon as that row is read out. An error in the logic results in all rows advancing simultaneously when the last row is reached. For rows near the far end of the chip the effect is minimal, since the actual advance is occurring close to where it is supposed to. But as the addressed row moves away from the end of the chip, the capacitor that was just read out continues to view the wrong image pixel (one located four pixels away from where it should be looking) until the end of the sub-frame. Similarly, the capacitors that were not read out continue to view the wrong image pixel, but in these cases it is the adjacent pixel. The net effect is a blurring of the image with a ghost image.

The read order error can be corrected on the present die using Focussed Ion Beam Milling/Epitaxy to cut and bridge 4 traces. However, the o/n timing error involving the state machine timing can only be corrected by modifying several of the layout masks and refabricating the entire chip. For evaluation purposes, the imaging capabilities of the BFE124B may be demonstrable using a FIB modified die provided only rows near the end of the chip are viewed.

General Summary

Note: The schematics that apply to this part of the circuit are structured in a way that makes them unhelpful to understanding the problem, so are not included.

The BFE124 is a 480 row Read-Out IC with two banks and 64 detector channels in each row of each bank. The two banks are located side-by-side and are offset vertically by one half the height of a pixel. The effect of the two banks thus oriented is to create a virtual 960 row array.

While it is technically a 2D area array, it is designed to function as a 1D scanning-mode linear array. The purpose of the 64 detector channels is to improve the signal-to-noise ratio without sacrificing image scan-time. This is done using Time Delayed Integration (TDI) where the signal from adjacent detector channels are added together with the appropriate time delay so that the signal from each detector channel corresponds to the same picture element (pixel) for all 64 channels. Appropriate post processing can also create the effect of having a 480-row linear array with 128 channels combined via TDI.

The TDI is performed in two stages. First, 4-channel TDI is performed on chip. Second, the output data is post-processed to perform another sixteen stages of TDI resulting in the final 64-channel TDI output.

The 4-channel on-chip TDI is performed within each unit cell where there are four detectors and four signal-integration capacitors. At any moment in time, each detector is mapped to one of the four capacitors. As the image scans across the chip, and hence moves from one detector to the next, this mapping is altered so that the detector that is viewing a particular region in the image is always mapped to the same capacitor until the image moves beyond that family of four detectors.

In order to maximize the amount of time that a given signal is integrated while allowing continuous scanning and readout, each row of pixels works independently. As the row counter reaches a particular row, one of the four pixels is sampled for readout. The corresponding capacitor is then reset and, when the row counter advances to the next row, the detector/capacitor mapping is advanced. Each complete cycle of the row counter thus reads out one-fourth of the pixels in the array and is referred to as a sub-frame. It therefore takes four sub-frames to read out all pixels and complete an entire image frame. The partial image read out with each sub-frame consists of every fourth pixel in the image. Subsequent sub-frames also read out every fourth pixel, offset by one from the prior sub-frame, such that the four sub-frames that make up a complete image are interleaved.

Conceptual Event Pipeline (implementation details ignored):

When the row counter reaches a particular pixel's row:

- Route the signal on the terminal capacitor (the capacitor connected to the trailing detector) to the column sample and hold circuitry.
- Capture the signal.
- Reset the charge on the terminal capacitor.

When the row counter advances to the next row:

- Shift the detector/capacitor mapping so that the just-reset capacitor becomes the initial capacitor (the capacitor connected to the lead detector). All other capacitors shift to match the motion of the image across the detectors.

Detector/Capacitor Mapping:

The on-chip TDI is capable of integrating either an image traveling left-to-right across the chip or right-to-left. However, since the detector to capacitor mapping is sensitive to the scan direction, the chip must be aware of the direction. This is accomplished through the Pleft input signal. If Pleft is HI, then the image scans across the chip from left-to-right.

In the following tables, the alphabetic entries denote image pixels. Imagine an image that consists of the letters of the alphabet in ascending order that is scanned across the chip: (XYZABCDEFGH)
The table indicates which letter is being viewed during a given Time Step by each detector.

Pleft = HI: Pixel seen by each detector as the image scans left-to-right:

Detector	D1	D2	D3	D4	
Time Step 1	A	Z	Y	X	
Time Step 2	B	A	Z	Y	
Time Step 3	C	B	A	Z	
Time Step 4	D	C	B	A	Read out pixel A and reset capacitor
Time Step 5	E	D	C	B	Read out pixel B and reset capacitor
Time Step 6	F	E	D	C	Read out pixel C and reset capacitor
Time Step 7	G	F	E	D	Read out pixel D and reset capacitor
Time Step 8	H	G	F	E	

In order to integrate the appropriate signal, the following detector to capacitor mapping must be implemented (based on pixels A-D and extending forward and backward for all others):

Detector	D1	D2	D3	D4	State
Time Step 1	**C1**	C4	C3	C2	S1
Time Step 2	**C2**	**C1**	C4	C3	S2
Time Step 3	**C3**	**C2**	**C1**	C2	S3
Time Step 4	**C4**	**C3**	**C2**	**C1**	S4
Time Step 5	C1	**C4**	**C3**	**C2**	S1
Time Step 6	C2	C1	**C4**	**C3**	S2
Time Step 7	C3	C2	C1	**C4**	S3
Time Step 8	C4	C3	C2	C1	S4

Pleft = LO: Pixel seen by each detector as the image scans right-to-left:

Detector	D1	D2	D3	D4

Time Step 1	X	Y	Z	A	
Time Step 2	Y	Z	A	B	
Time Step 3	Z	A	B	C	
Time Step 4	A	B	C	D	Read out pixel A and reset capacitor
Time Step 5	B	C	D	E	Read out pixel B and reset capacitor
Time Step 6	C	D	E	F	Read out pixel C and reset capacitor
Time Step 7	D	E	F	G	Read out pixel D and reset capacitor
Time Step 8	E	F	G	H	

Detector	D1	D2	D3	D4	State
Time Step 1	C4	C3	C2	**C1**	S4
Time Step 2	C3	C2	**C1**	**C2**	S3
Time Step 3	C2	**C1**	**C4**	**C3**	S2
Time Step 4	**C1**	**C4**	**C3**	**C2**	S1
Time Step 5	**C4**	**C3**	**C2**	C1	S4
Time Step 6	**C3**	**C2**	C1	C4	S3
Time Step 7	**C2**	C1	C4	C3	S2
Time Step 8	C1	C4	C3	C2	S1

If the Read and Reset capacitor mapping is ignored for now, there are four Detector/Capacitor Mapping States:

State	D1	D2	D3	D4
S1	C1	C4	C3	C2
S2	C2	C1	C4	C3
S2	C3	C2	C1	C2
S4	C4	C3	C2	C1

Since each row is independent, each row needs two Finite State Machines (FSM). The choice of which state machine to use is determined by the status of the Pleft signal. Each row's state machine is advanced as soon as a capacitor is read out and reset. This occurs once per Sub-frame, when the row counter points to that particular row (actually, the next row).

Pleft = HI:	FSM#1:	S1►S2►S3►S4►repeat
Pleft=LO:	FSM#2:	S4►S3►S2►S1►repeat

Physically implementing two FSM's in each row is not desirable and can be avoided by operating four global state machines that are clocked once per Sub-frame:

Pleft = HI:	FSM#1A:	S1►S2►S3►S4►repeat
Pleft = HI:	FSM#1B:	S2►S3►S4►S1►repeat
Pleft=LO:	FSM#2A:	S4►S3►S2►S1►repeat
Pleft=LO:	FSM#2B:	S3►S2►S1►S4►repeat

As can be seen, the only difference between the A and B state machines is that the B state machine leads the A state machine by one state. In fact, the A and B state machines can be (and are) implemented as a single FSM with twice as many output signals.

To see how these are used to create the virtual state machines in each row, consider a row R such that 0<R<(N-1) where N is the total number of rows (i.e., N=480). If x is the row currently pointed to by the row counter, then (as an example) we want the following behavior:

Upon each row clock: If x<(N-1) then x►x+1 else x►0

x=R:	Read out and reset the terminal capacitor.
x=R+1:	Advance FSM from S1 to S2

This behavior can be synthesized as follows:

x=R:	Read out and reset the terminal capacitor.
x=R+1:	Switch from FSM#1A (S1) to FSM#1B (S2).
x=0:	Advance FSM#1A (to S2) and FSM#1B (to S3)
	Switch from FSM#1B (S3) to FSM#1A (S2)

The effect of the two events that occur at x=0 is to keep the row in S2.

To implement this behavior, generate the proper state signals and route them globally to each row. Since only one state machine (FSM#1 or FSM#2) is used at a time, their outputs can be multiplexed onto a bus according to the Pleft signal. This serves to minimize the routing and logic.

Since the bus contains both the A and the B families of signals, a simple latch in each row can use the row decoder (which must already be present) to select between the two families. When the row decoder advances to the next row, the B family is selected. When the row counter wraps around to row zero, the A family is selected.

Synchronization of the Finite State Machines to the Pixel Readout and Reset Logic

As mentioned previously, it takes four sub-frames to read out and to reset all four capacitors in each unit cell, one capacitor per sub-frame. Since the FSM's that determine the detector to capacitor mapping also have a period of four sub-frames, it is only natural to use the same FSM for all three purposes. But care must be taken to properly establish the relative phases between the three operations, otherwise pixel mixing (resulting in ghost images) will occur.

To establish the necessary relationships, the event sequences used to establish the detector to capacitor mappings for both scan directions are reproduced below, along with the additional mapping information necessary for the Read & Reset (R&R) event. It must be kept in mind that each Time Step listed below is a sub-frame and lasts for one complete cycle of the row counter. In each Time Step, the capacitors are integrating the signal from their respective detectors for the entire sub-frame. At the end of the sub-frame, one of the capacitors is selected for read out. It is

sampled and then reset just prior to advancing the detector mapping. The state machine only needs to select which capacitor will be read out at the end of the sub-frame. The row and column decoders control the fine timing of the actual sample and reset events.

Pleft = HI:

Detector	D1	D2	D3	D4	State	R&R
Time Step 1	**C1**	C4	C3	C2	S1	C2
Time Step 2	**C2**	**C1**	C4	C3	S2	C3
Time Step 3	**C3**	**C2**	**C1**	C2	S3	C4
Time Step 4	**C4**	**C3**	**C2**	**C1**	**S4**	**C1**
Time Step 5	C1	**C4**	**C3**	**C2**	**S1**	**C2**
Time Step 6	C2	C1	**C4**	**C3**	**S2**	**C3**
Time Step 7	C3	C2	C1	**C4**	**S3**	**C4**
Time Step 8	C4	C3	C2	C1	S4	C1

Pleft = LO:

Detector	D1	D2	D3	D4	State	R&R
Time Step 1	C4	C3	C2	**C1**	S4	C4
Time Step 2	C3	C2	**C1**	**C2**	S3	C3
Time Step 3	C2	**C1**	**C4**	**C3**	S2	C2
Time Step 4	**C1**	**C4**	**C3**	**C2**	**S1**	**C1**
Time Step 5	**C4**	**C3**	**C2**	C1	**S4**	**C4**
Time Step 6	**C3**	**C2**	C1	C4	**S3**	**C3**
Time Step 7	**C2**	C1	C4	C3	**S2**	**C2**
Time Step 8	C1	C4	C3	C2	S1	C1

As can be seen, which capacitor is read and reset is dependent not only on the state, but on the scan direction as well.

				Pleft: HI	LO
State	D1	D2	D3	D4	R&R
S1	C1	C4	C3	C2	C2	C1
S2	C2	C1	C4	C3	C3	C2
S3	C3	C2	C1	C2	C4	C3
S4	C4	C3	C2	C1	C1	C4

Signal Polarities

In order to simplify the decode logic located in each row, the state machines are One-Hot encoded. Furthermore, the outputs must be conditioned to ensure that they are non-overlapping in order to prevent unwanted transfers between the signal integration capacitors.

PoX/PnX: These are two families of signals with four signals in each family (the X is a wildcard which stands for {A,B,C,D}). These state signals determine the detector/capacitor mapping and

are Active-LO One-Hot encoded. PoX is the old state (the A state machine) and PnX is the new state (the B state machine).

PselX: This family of four signals selects which capacitor is routed to the sample and hold circuitry and then reset. They are Active-HI One Hot encoded.

ModeS/ModeR: These two signals control the set and reset of the SR latch that determines which family of signals (PoX or PnX) is routed to the unit cells in that row. Both inputs are Active-HI. When reset (ModeR taken HI) then PoX is routed out. When set (ModeS taken HI) then PnX is routed out.

Active Signals

The PnX family needs to always precede the PoX family, but the relationship of the PselX family is scan direction dependent. For Pleft=HI, PselX must lead PoX while for Pleft=LO is must equal PoX. The reason is that the terminal detector is located on the opposite side of the unit cell.

Pleft = HI

State	PoX	PnX	PselX
S1	A	B	B
S2	B	C	C
S3	C	D	D
S4	D	A	A

Pleft = LO

State	PoX	PnX	PselX
S4	D	C	D
S3	C	B	C
S2	B	A	B
S1	A	D	A

Known Design Errors/Issues:

(1) The signal that asserts the ModeR lines is not generated on chip. It is the logical OR of the MRST and ROWRST signals which are externally supplied. The intent was for the chip not to require either of these signal and they have default pulldown resistors on them. But, as implemented, the ROWRST signal must.

Corrective Action:

Short term - externally apply the necessary reset signals.
Long term - internally generate a reset signal.

(2) The signal that is routed to the ModeS lines of the mode latches is of the wrong polarity. The signal is supposed to be active-HI and the signal that is actually routed to this circuitry is the Qb output of the row-enable shift register (the rowenb signals). The result is that the Mode Latches are continuously held in a SET state except during the brief time that they are supposed to actually be set. The RESET signal is therefore basically ignored - except during the brief time that it is being asserted in which case both the ModeS and the ModeR are HI which is an undefined state - the consequence is that the PFET in all eight transmission gates are turned ON. As soon as the reset is relaxed, the latch is immediately SET.

Corrective Action:

Short term: None possible.

Long term: Requires an inversion in the ModeS line, either explicitly or by changing the polarity of the RS Latch.

(3) When the Mode Latch changes state, there is approximately a 2ns overlap between the state signals going to the unit cells - both the old and the new signals are asserted simultaneously permitting charge transfer between the signal integration capacitors under high signal conditions.

Corrective Action:

Short term: None possible.

Long term: Requires modification of the Mode Logic to suppress one family until the other family is removed completely. Perhaps the buffers can be modified to take all of the outputs high until during the transition.

(4) The derivations of the PoX and PnX families are basically reversed. As implemented, the PnX signals lead the PoX signals. In addition, the PselX signals equal the PoX signals when Pleft=HI and precede the PoX signals when Pleft is LO. It is the error in the PselX signal that is causing the ghost images.

Corrective Action:

Short term: These can be modified using IBE. Due to Issue #2 above, there is little point in correcting the PoX/PnX relationships. But by correcting the PselX derivation relative to the PoX, it should be possible to eliminate the ghost image (due to this error). Given Issue #2, the PnX family must be treated as being the PoX family for the purpose of establishing the PselX family, since the PselX signal is acted upon just prior to switching from PoX to PnX and the PnX family is (incorrectly) asserted at that time.

Long term: Derive the signals correctly.

Appendix D

Grant Number DAMD17-1-7016

TITLE: Novel High Resolution, Lowdose Flat Panel Mammography Detector Technology

PRINCIPAL INVESTIGATOR: Robert M. Iodice

CONTRACTING ORGANIZATION: InfiMed, Inc.
121 Metropolitan Drive
Liverpool, NY 13088

REPORT DATE: March 1999

TYPE OF REPORT: Alternative Approach Proposal

PREPARED FOR: U.S. Army Medical Research and Materiel Command
Fort Detrick, Maryland 21702-5012

DISTRIBUTION STATEMENT: Approved for public release;
Distribution unlimited

The views, opinions and/or findings contained in this report are those of the author(s) and should not be construed as an official Department of the Army position, policy or decision unless so designated by other documentation.

Introduction

Over the preceding period of this grant, we have explored the feasibility of making a mammographic imaging sensor by combining a Thallium Bromide (TlBr) photoconductor with an addressable array of cold cathode field emitters in a novel Field Emission X-ray Imaging System (FEXIS). As described in our annual report of September 1998, we were able to make significant progress on the photoconductor, but we experienced difficulties in acquiring suitable field emitter arrays to enable the proof of concept.

The development of TlBr has proceeded on plan throughout this period. We have been able to produce X-ray sensitive TlBr films of good quality up to 9" in diameter. The high DQE, superior spatial resolution, wide dynamic range, and unprecedented contrast resolution that were predicted have been verified in tube configurations with a single scanned electron beam readout. Unfortunately, the field emitter array readout technology has not progressed adequately during this period.

It was hoped that the mammography FEXIS could leverage off existing FED designs, and a suitable emitter array could be produced with only simple process modifications. However there are two special requirements for the field emitter array which make this tasks more difficult. One is the requirement of small pixels size required for mammography of approximately 50 microns. Filed emitter displays have faced problems with keeping a small electron spot size, and many suppliers are investigating the addition of gates or structures to provide additional focussing. The second issue is the requirement for higher beam current in order to discharge the target pixel within a pixel time. In the display industry, demands for brighter displays are pushing vendors to increase beam current.

At the time of the annual report, it had become evident that the field emitter array technology for the display industry was not progressing as quickly as had been advertised. Field emitter displays are still limited in performance by focussing issue, as well as manufacture issues including the challenges of maintaining a high vacuum in a flat panel configuration. This has led to arcing issues which limit the applied voltage, and cause short product lifetimes. Due to these issues, our field emitter sub-contractor, FED Corporation, which had demonstrated difficulties meeting scheduled

delivery dates, and supporting this program, has chosen to exit the field emitter technology arena, and focus on other display technologies.

Alternative Plan

As a result of the difficulties with the field emitter arrays, we have investigated several alternative readout mechanisms that take advantage of the superior properties of the Thallium Bromide photoconductor. Initially we investigated alternative field emitter suppliers to see if there were other suppliers, or other field emitter array technologies that would be more suited to the needs of a flat panel detector. The results, as reported in the annual report, showed that maturity of the technology is not sufficient for this product at this time, although it is likely to progress significantly over the next 2-3 years. In addition, many of the companies remaining in the field emitter display business are even more focussed on developing high volume displays and overcoming the development problems there, and are unwilling to invest effort in alternative applications.

A second alternative readout mechanism that we have investigated since the delivery of the annual report appears to offer much more promise, and appears to be feasible more near term. This approach uses a slot scan imaging techniques rather than an area imaging technique. The slot scan techniques has been under investigation by several companies including PrimeX General Imaging (PGI), and the performance advantages of such an approach have been demonstrated. This approach is summarized in the "Background" section below. The approach taken by PGI, which has been partially supported by US Army medical Research and Materiel Command funding uses silicon as the detector material. The replacement of the silicon detector by Thallium Bromide would provide higher performance and simultaneously lower the cost.

At this point in the grant, due to the lack of performance by FED Corporation and subsequent reduction of payment to the sub-contractor, much of the allocated funding remains in the grant. We hereby propose reallocating the remaining funding of approximately $220k towards the investigation of our alternative approach to a High Resolution, Low Dose Flat Panel Mammography Detector. This proposal describes the slot scan approach using silicon detectors, the advantages of combining the slot scan approach with the TlBr photoconductor, the challenges to be overcome, and the program plan to address these challenges.

Background

PrimeX General Imaging Corp (PGI) has developed a hybrid silicon-PIN photo diode detector for use in a slot-scanning digital imaging system for mammography funded in part by a 3-year, $1.6 million grant from the U.S. Army Medical Research and Material Command (Grant No. DAMD17-96-1-6239).

The advantages of a slot-scanning radiography system are lower cost and inherent scatter rejection. These advantages can only be realized if no motion artifacts are introduced into the acquired image. In order to eliminate motion artifacts the object to be imaged must not move during image scan and there can be no jitter introduced from the mechanical scanning mechanism. In mammography, the breast is immobilized during the exam even though a film image is acquired in a fraction of a second. The resolution required for mammography (10 – 20 lp/mm) implies that motion artifacts be less than 25 microns. This translates to a scanning precision of 1,000 dots per inch. This feat is easily achievable with many existing scanning systems including photocopiers and desktop scanners. Moreover, many types of motion induced artifacts can be corrected with software programs.

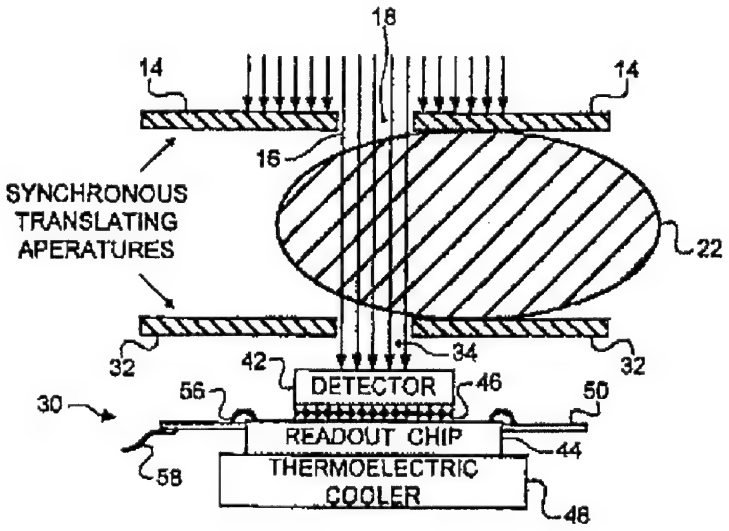

The ideal scanning aperture is a slit that is one pixel wide. Such a slit would provide the maximum scatter rejection. This approach is not practical for mammography since doing this would require an enormous amount of x- ray power to scan an 8 in x 10 in image in a reasonable amount of time (i.e., a few seconds). By increasing the slit width to a "slot" opens up the slit aperture, reducing the required tube power and provides a good compromise between scanning time, image quality and the required detector

surface area. Increasing the slot width increases the required detector surface area and its cost. A slot width of 6 mm has been determined to be optimum as it provides an ideal balance between imaging performance and detector cost.

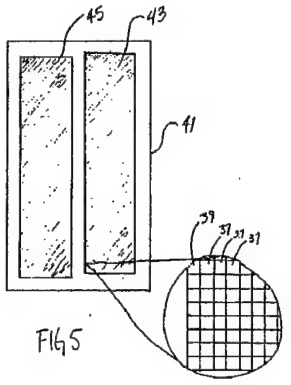

PGI's slot-scan sensor consists of a CMOS readout array that is bump bonded to a silicon-PIN photo diode. The detector contains a bifurcated array of diodes. Each array contains 61 columns and 480 rows of diodes, each diode is 50 microns square. The two arrays are offset from each other by half a pixel dimension (i.e., 25 microns in both the x and y directions).

Each sensor has an active area of 6 mm x 24 mm. The silicon diode substrate is 1 mm thick (1.5 mm thick substrates have been used as well). The diode array is connected to the CMOS readout array with an array of indium bump bonds such that each pixel is connected in parallel to the readout array. This technique is used in infrared focal plane array technology.

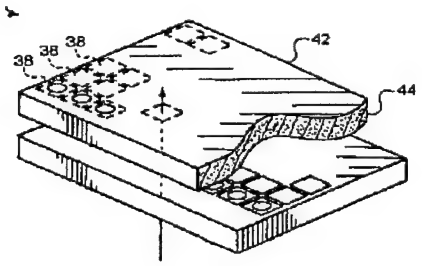

The CMOS readout array contains an integrating capacitor for each photo diode, a 4-pixel TDI register and the read out circuitry to address and clock out data. The advantage of the 4-pixel on-chip TDI register is that the overall data rate required to read out the array is reduced by a factor of four.

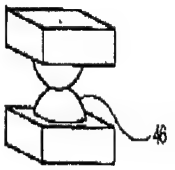

The advantage of using a silicon-based photo diode is that the incident radiation absorbed in the sensor medium is directly converted into electric charge that can be collected and integrated by the CMOS readout array. In contrast, a sensor using a scintillator to absorb incident radiation has an intrinsically lower performance since there are several energy conversion steps required before an electrical charge is produced. One of these steps involves the production of visible light that is emitted isotropically, scatters and is absorbed before it can be detected.

The slot-scanning detector consists of 8 discrete sensor arrays that are positioned in two parallel rows of 4 sensors. This design allows for contiguous pixel coverage in both the in-scan and cross-scan direction yet permits easy access to the bond pads for each sensor. However, this slot configuration requires a collimator that resembles a staggered brick pattern. Such a collimator is more difficult to manufacture than a traditional rectangle but is not a significant issue.

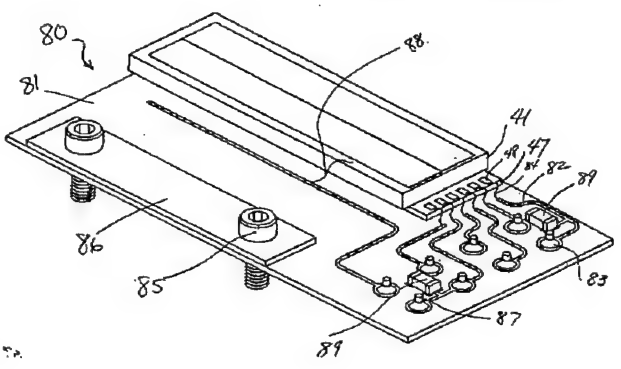

The slot-scanning detector with its 8 sensor arrays is connected to an analog signal processor located directly underneath the detector plane. Each sensor is connected to its own digitizer and all eight sensors are read out in parallel. The digitized output signals are sent to a remote Digital Signal Processor (DSP) where the pixel data is processed. The processing functions include additional TDI, off-set and gain correction and flat fielding. An image in bitmap form is produced and stored in memory and is made available to a workstation for review, archiving and further processing.

This entire assembly including the detector, analog signal processor and DSP is designed to be sold to OEMs as a digital camera to be integrated with a mammography gantry system. Since the gantry will have to scan the image there are no retrofit options at this time. PGI has designed the digital mammography camera to interface with a scanning mammography gantry manufactured by Fischer Imaging Corporation. Fischer is currently developing a slot-scanning mammography system called Senoscan that utilizes an array of fiberoptically coupled CCD arrays. The Senoscan

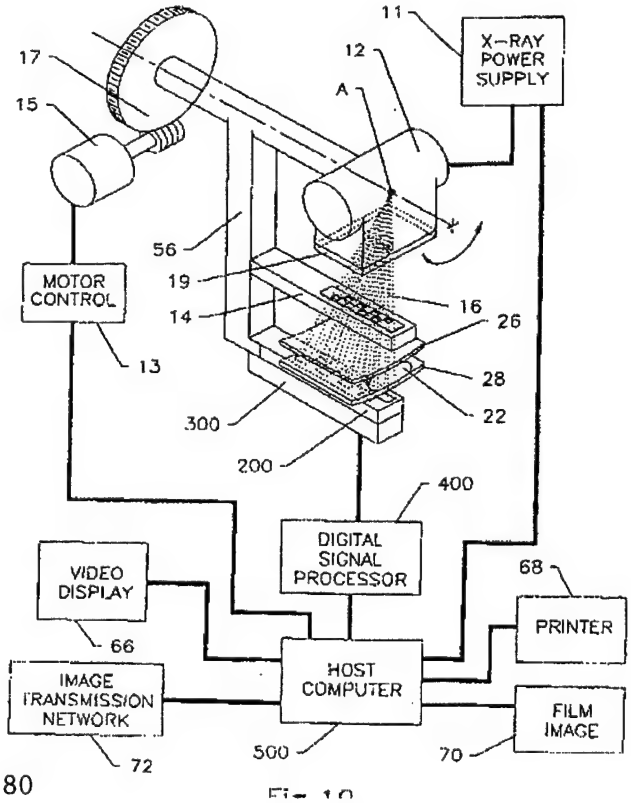

Fig. 10

gantry utilizes a radial scan technique where the x-ray generator is pivoted about its focal spot. The detector array is translated along the circumference of a circle with a radius of approximately 50 cm.

Program Concept – Combine the Best of Both TlBr and Slot Scan

The silicon-based hybrid PIN diode sensor has a quantum efficiency of approximately 67% for the x-ray energies used for mammography. While this compares favorably to the quantum efficiency for screened-film (approximately 10-20%) the increased quantum efficiency achievable with alternate detectors directly improves DQE giving higher sensitivity and/or reduced dose. Moreover, the cost of hybrid sensors is determined by the need to fabricate both a diode array and a readout array, have indium bumps applied and then bond the arrays together. The performance of the sensor and the cost to produce the sensor could be dramatically improved by applying a suitable photoconductor directly on the surface of the readout IC.

Thallium Bromide is an ideal photoconductor for use in x-ray imaging applications from the standpoint of absorption properties (>90% at mammographic energies) and photoconductive gain. A plot of the linear attenuation coefficients for Silicon and Thallium Bromide is shown below.

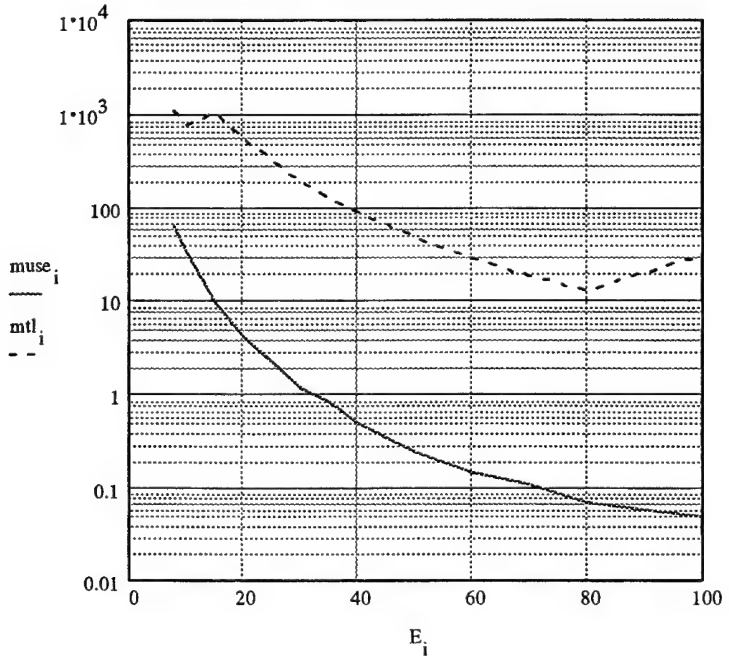

Linear Attenuation Coefficients (cm^{-1}) for Thallium Bromide (dotted) and Silicon as a function of X-ray Energy from 10 to 100 keV

For silicon an electron-hole pair can be liberated with 3.65 eV and for Thallium Bromide it requires about 6.5 eV. Accordingly, a 50-micron thick layer of Thallium Bromide can produce an equivalent signal as a 1-millimeter thick layer of silicon from the absorption of a 20-keV x ray.

Challenges to be Addressed

However, Thallium Bromide does have some shortcomings that must be overcome if it is to become a suitable photoconductor for x-ray imaging applications. The primary shortcomings are high dark current and aggressive chemical properties. The high levels of dark current are being addressed through a materials technology program funded by Xicon. The use of a slot scan system reduce the dark current challenges since the dwell time (approximately 1 msec) is only a small portion of the frame time (several seconds).

During the past few months a review of the challenges and possible approaches to developing a process to apply a coating of Thallium Bromide to the surface of an Integrated Circuit (IC) has been undertaken. As a result of this review a number of application methods have been identified and an approach to determine the feasibility of this concept has been developed.

For the sensor design employed by the slot-scan mammography system, applying a thin coating of Thallium Bromide to the surface of the readout IC would provide a near-50% increase in quantum efficiency compared to silicon. It would also reduce the cost of the sensor by eliminating the need to fabricate a PIN diode array and the hybridization process required to attach the diode array to the readout array. The main goal of this program is therefore to determine appropriate materials and develop a deposition process for coating TlBr on silicon integrated circuits.

If such a process can be developed it would have applications to amorphous silicon flat-panel x-ray detectors as well. Several x-ray imaging equipment manufacturers are currently developing amorphous silicon-flat panel x-ray detectors. For mammography applications it is likely that a 50-micron pixel will be required. Amorphous silicon flat panel detectors have a very small fill factor (about 15%) when utilizing 50-micron pixels. This

makes the use of scintillators impractical due to the fact that the light emitted by the scintillator spreads out and only 15% of the light would be collected. The use of a photoconductor eliminates this problem. X rays are absorbed in the photoconductor liberating electrons and holes which are collected at the electrodes. Shown below is a figure depicting the two processes. As shown, the signal (i.e., electrons) produced by the photoconductor is actually concentrated at the electrode whereas the signal (i.e., photons) produced by the scintillator spreads out and is diluted requiring a large fill factor to collect it efficiently.

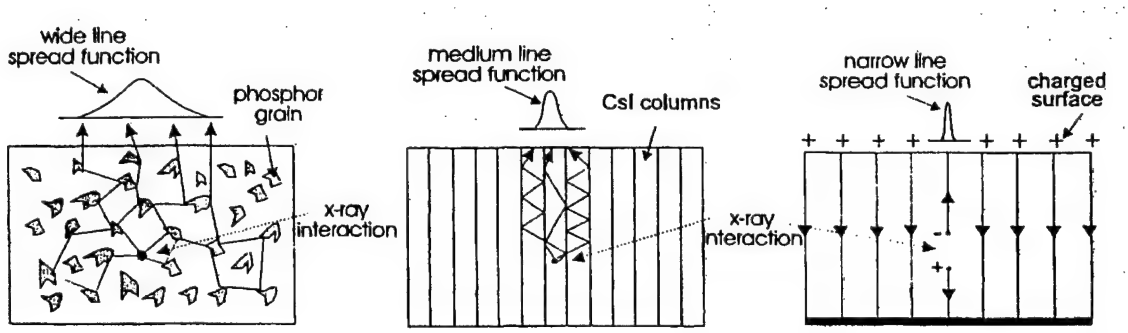

Based on the foregoing discussion, there is a great potential to improve the performance of both scanning and area detectors for mammography applications through the use of a photoconductor. Thallium Bromide as the potential to provide superior imaging capabilities than existing photoconductors such as amorphous selenium. This potential can only be realized if the chemical compatibility issues have been resolved. It is the goal of the proposed effort to establish the feasibility of applying Thallium Bromide to integrated circuits and thus capitalize on its superior x-ray imaging performance characteristics.

Research Plan

The goal of the proposed research effort is to establish the feasibility of applying a coating of Thallium Bromide to the surface of an integrated circuit for the purpose of producing an x-ray imaging detector. Several key issues have been identified that will have to be addressed in order to determine the feasibility of this concept. A 12-month effort is proposed to address these issues and a protocol has been developed to establish methods and materials that could be used to make the concept work.

The most important issue to be addressed is determining a suitable deposition process to apply a coating of Thallium Bromide to the integrated circuit. Five deposition methods have been identified that could accomplish this task, the most promising technique is straight-line evaporation as it has the potential to be the most effective and has the fewest disadvantages. Perhaps the most compelling reason to utilize this method is that it can be easily accomplished with the limited resources available for this project.

There are three material compatibility issues that must be resolved before this process can be made to work.

1) adhesion of the photoconductor to the integrated circuit,
2) chemical compatibility with the passivation layer of the integrated circuit
3) identifying a suitable intermetallic contact material that is compatible with the photoconductor and the metallization on the integrated circuit.

In addition, a material must be found that can act as a bond pad material for the bond wire required on the top surface of the photoconductor to apply a bias voltage. A number of materials have been identified that show promise as being suitable for both the intermetallic contact and bond pad material. These materials will be studied in connection with the proposed effort to determine optimum performance.

The proposed research effort will be carried out in three tasks. Task 1 will be devoted to establishing the viability of the straight-line evaporation technique and will address the most fundamental materials compatibility issues. Task 2 will be devoted to determining the best materials to use for intermetallic contacts between the photoconductor and the bond pads on the IC and for making a bond pad on the top surface of the photoconductor. Task 3 will be devoted to testing coated ICs in a prototype slot-scanning mammography system developed by PGI and described in further detail in the attached appendix.

Task I

In this task of the proposed effort, a straight-line evaporator system will be assembled with the capability of depositing Thallium Bromide films

on the readout IC. The readout IC is 26 mm x 8 mm and has a row of bond pads on one end that must be masked off. Initially, ICs will coated that are not functional to prove out the process of applying a uniform coating with a thickness of about 50 microns. ICs coated in this manner will have the photoconductor stripped off and a visual inspection will be made to determine if the passivation layer of the IC has been compromised by the Thallium Bromide. Another concern to be addressed here is the mismatch of the thermal coefficients of expansion of the thallium bromide and the integrated circuit. Thermal stress testing will be performed to determine under what conditions the thallium bromide coating will de-laminate from the IC.

Task II

In this task, the bond pads of the readout ICs will be coated with conductor materials that will prevent the thallium bromide from attacking the aluminum bond pads on the IC. This will be accomplished by sputtering the material on to the IC using a shadow mask previously developed by PGI. At this time materials such as copper oxide and indium-tin-oxide (ITO) are being considered for this purpose. An RF adaptor kit will be purchased to upgrade a DC sputtering system presently owned by Xicon to accomplish this task.

Once the materials have been properly deposited on the IC, they will be put into the straight-line evaporator to have the thallium bromide coated. A bond pad probably made from ITO will be applied to the top layer of the photoconductor as well. Several tests will be conducted including visual inspection, electrical continuity and circuit function on the IC.

Task III

In this task, successfully coated ICs will be packaged and inserted into the slot-scanning camera developed by PGI and exposed to light and x rays. Images and data can be accumulated in this way. Images will be acquired of the ACR Accreditation phantom and the image quality parameters of the coated IC will be obtained.

This task is facilitated due to the fact that PGI has already developed this equipment and has recently characterized its silicon-based diode sensors to provide a benchmark of performance. Image quality parameters will be

obtained and analyzed by Dr. Hans Roehrig, a consultant to this project. Dr. Roehrig has previously taken these measurements for the silicon-based diode sensors and will provide good continuity to the previous body of work.

Schedule

The program schedule will be revised to permit the completion of the analysis and demonstration of this alternative. A schedule summary is presented below, with the months from project restart indicated across the top:

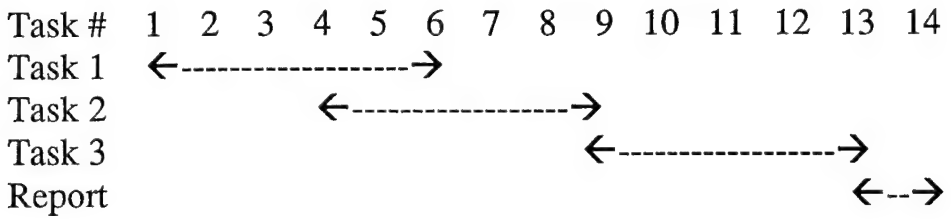

The research effort proposed above represents a best-case scenario to produce an effective coating process. There are a number of alternative approaches that could be implemented in the event that one or more of the individual process steps prove to be unfeasible. For example, if there is excessive corrosion of the passivation layer on the IC by the thallium bromide, an additional passivation layer could be applied to protect the IC. In a worst case scenario, the thallium bromide could be deposited on a ceramic layer that has a patterned metallization layer to act as a barrier and provide electrical contact to the IC.

If any of these approaches is required during the proposed effort, resources will be taken from task III, to devote more effort to the coating process. In this event, a less elegant process will evolve and a smaller testing and evaluation effort will ensue.

BUDGET

Detailed Cost Estimate

A budget summary chart for the proposed modification to this IDEA project is shown below. It includes a roll-up of the proposed costs for each cost element. It should be noted that a significant cost share is being contributed to the project by the participants due to the team's intense desire to see the program achieve commercialization success and to stay within the budget constraints suggested by this proposal. In particular,

Xicon, has developed the technology of producing a high-quality Thallium Bromide photoconductor layer. Xicon has contributed over $1M of effort in related work which will serve to accelerate this program, reduce the risk and lead to faster commercialization. Xicon will contribute all indirect costs as a cost share element of the program. This includes the cost to administrate the sub-contracts to the other organizations.

PGI Corporation has developed its CMOS-based slot-scanning mammography detectors in connection with an existing army grant. The CMOS readout integrated circuits are fully developed and require no further development to accomplish the tasks set forth in the proposed effort. Moreover, the x-ray generator, camera electronics and software required to test and evaluate the sensors for mammographic applications has already been developed. Approximately, $2M of private and government sponsored development effort has been previously spent in connection with the development of these components.

Total Budget:

Category	Total
Direct Labor	56,800
Fringe Benefits	14,200
Labor Costs, Total	71,000
Major Equipment	44,000
Materials, Supplies, Consumables	12,000
Subcontracts – PGI	59,000
Travel	4,000
Publications and Reports	1,000
Consultants	30,000
Other Direct Costs	0
Indirect Costs	0
Total Costs	219,114

Explanation:

Labor Budget:

Name	Project Role	Salary (annual)	Fringe %
Robert Iodice	PI, Project Manager, Engineer	$84,000	25%
Electronics Tech.	Electronics Technician	$40,000	25%

Name	% time applied	Project Cost	Fringe
Robert Iodice	20%	$16,800	$4,200
Electronics Technician	100%	$40,000	$10,000

Notes:
-. This assumes a standard year of 2080 hours
-. They $/year are based on actual salaries and estimates of Technicians Salary
-. The % allocation is based on level of effort required

Material Cost Includes:
-. Materials used in the fabrication of the photoconductor coatings
-. Supplies used in testing and characterization of the devices

Major Equipment Cost Includes:
-. A Thermal Evaporation System ($30,000) to deposit the Thallium Bromide on the CMOS IC.
-. A RF Sputtering Upgrade Kit to modify an existing DC sputtering system so that it can sputter Indium Tin Oxide films on the Thallium Bromide. ($13,800)

Subcontractor Costs – PGI Corporation

PGI corporation will provide under this fixed price contract, all of the CMOS packaging and testing materials and labor. They will also provide the camera electronics, x-ray generators and other support equipment required to test and evaluate the Thallium Bromide coated ICs. (The $54k in the budget includes $5k for Dev Sharma, $40k for Bill Yorke and $14k for John Cox).

Consultants:

Donald Ouimette is an electrical engineer with the University of Connecticut. He has been involved in the development of Thallium Bromide materials and materials characterization. Donald will provide the expertise to evaluate the materials compatibility issues and optimize the deposition process. The budget for this item would be $25k.

Hans Roehrig is a professor at the University of Arizona's Department of Radiology. He will provide the expertise to carry out the experimental protocol required to test and evaluate the Thallium Bromide coated ICs. X-ray image parameters including resolution, sensitivity and modulation transfer function (MTF) will be measured and compared with the existing hybrid silicon-based PiN photodiode sensors now under development. The budget for this item is $5k.

Appendix E

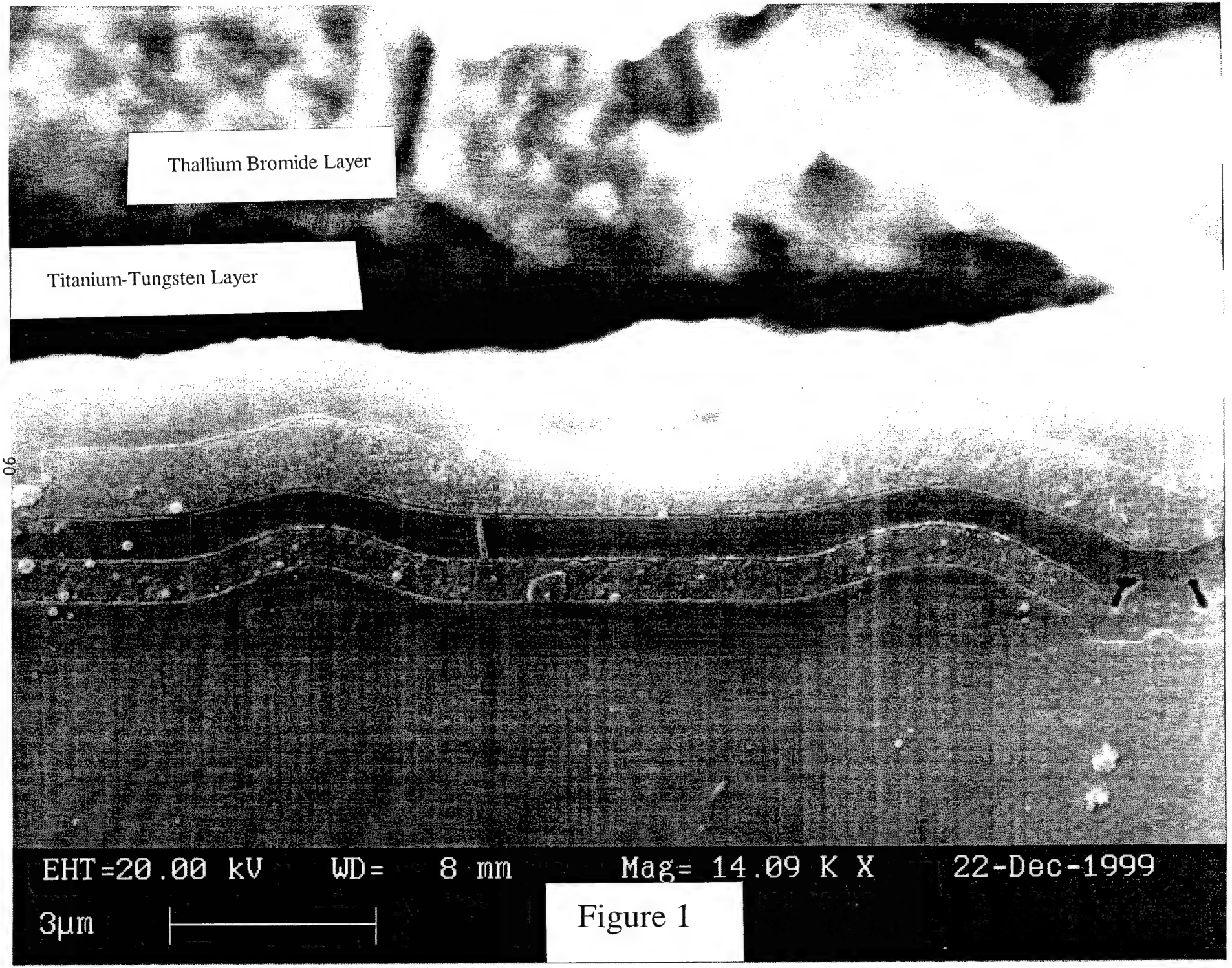
Thallium Bromide Layer
Titanium-Tungsten Layer
EHT=20.00 kV
WD= 8 mm
Mag= 14.09 K X
22-Dec-1999
3µm

Figure 1

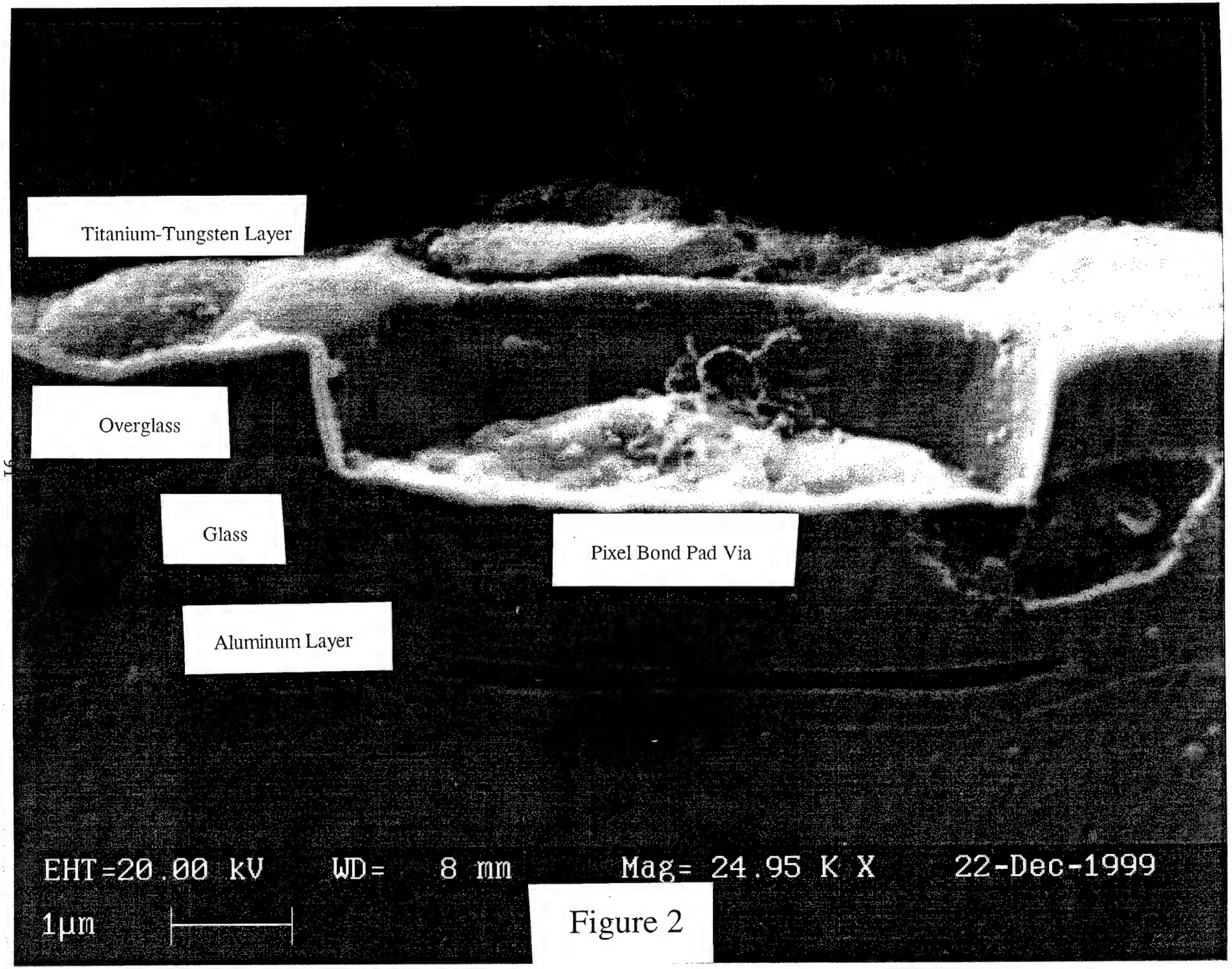
Titanium-Tungsten Layer
Overglass
Glass
Pixel Bond Pad Via
Aluminum Layer
EHT=20.00 kV
WD= 8 mm
Mag= 24.95 K X
22-Dec-1999
1µm

Figure 2

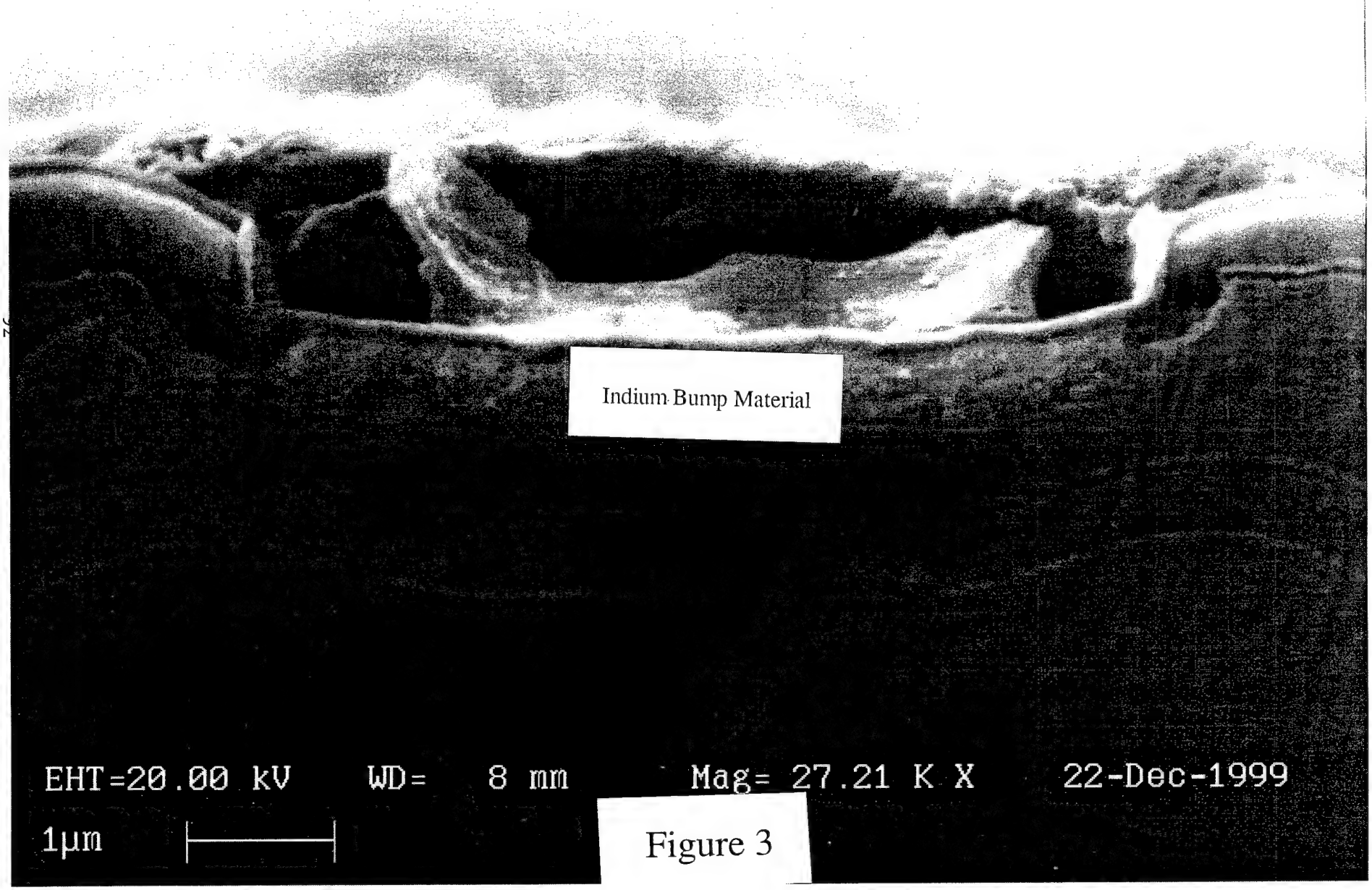
Indium Bump Material
EHT=20.00 kV
WD= 8 mm
Mag= 27.21 K X
22-Dec-1999
1µm

Figure 3

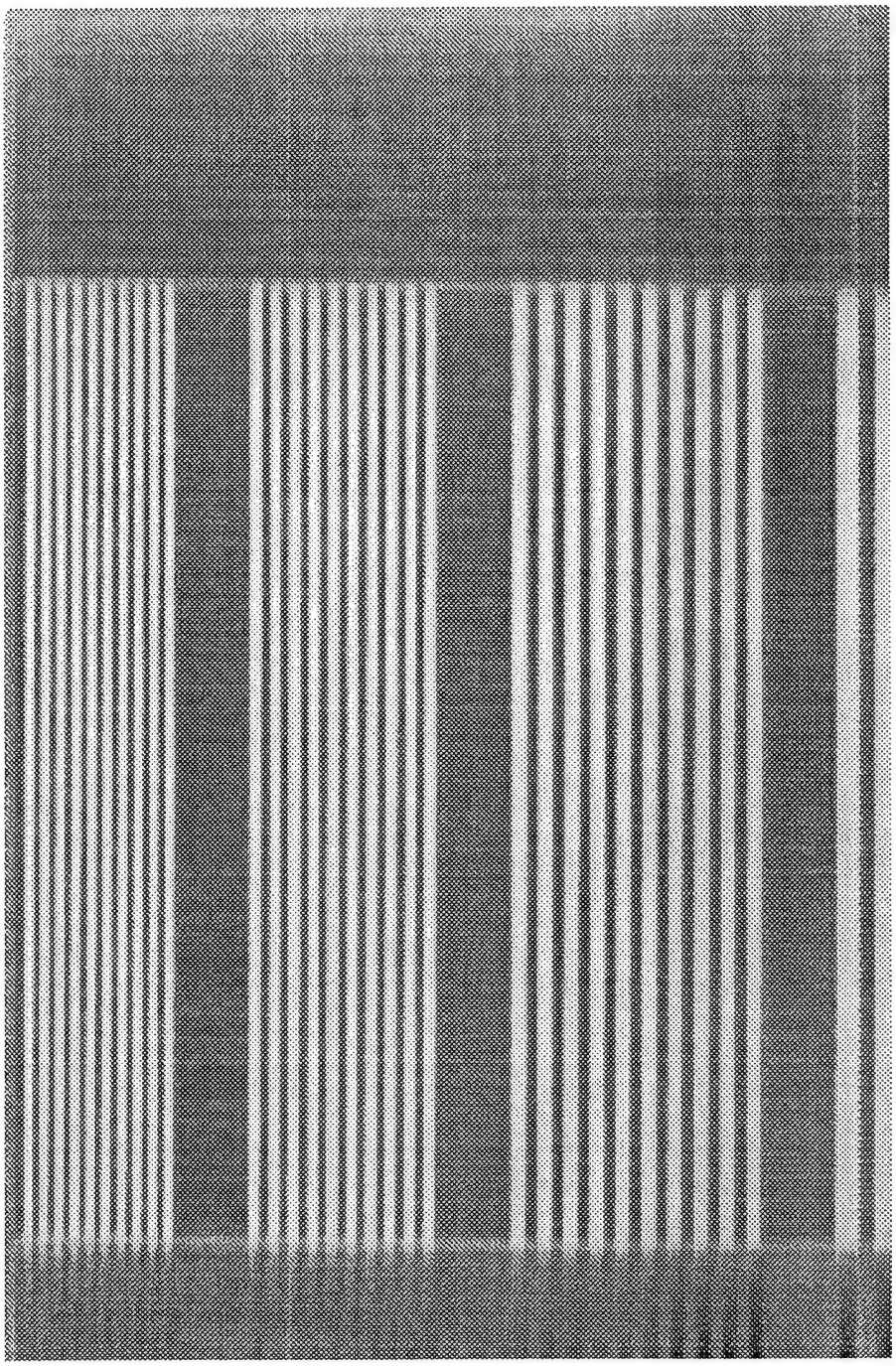

Figure E4: Lead-foil Penetrameter Image Acquired with a Thallium Bromide Coated Semiconductor Sensor Array (3.0, 2.5 and 2.0 lp/mm)

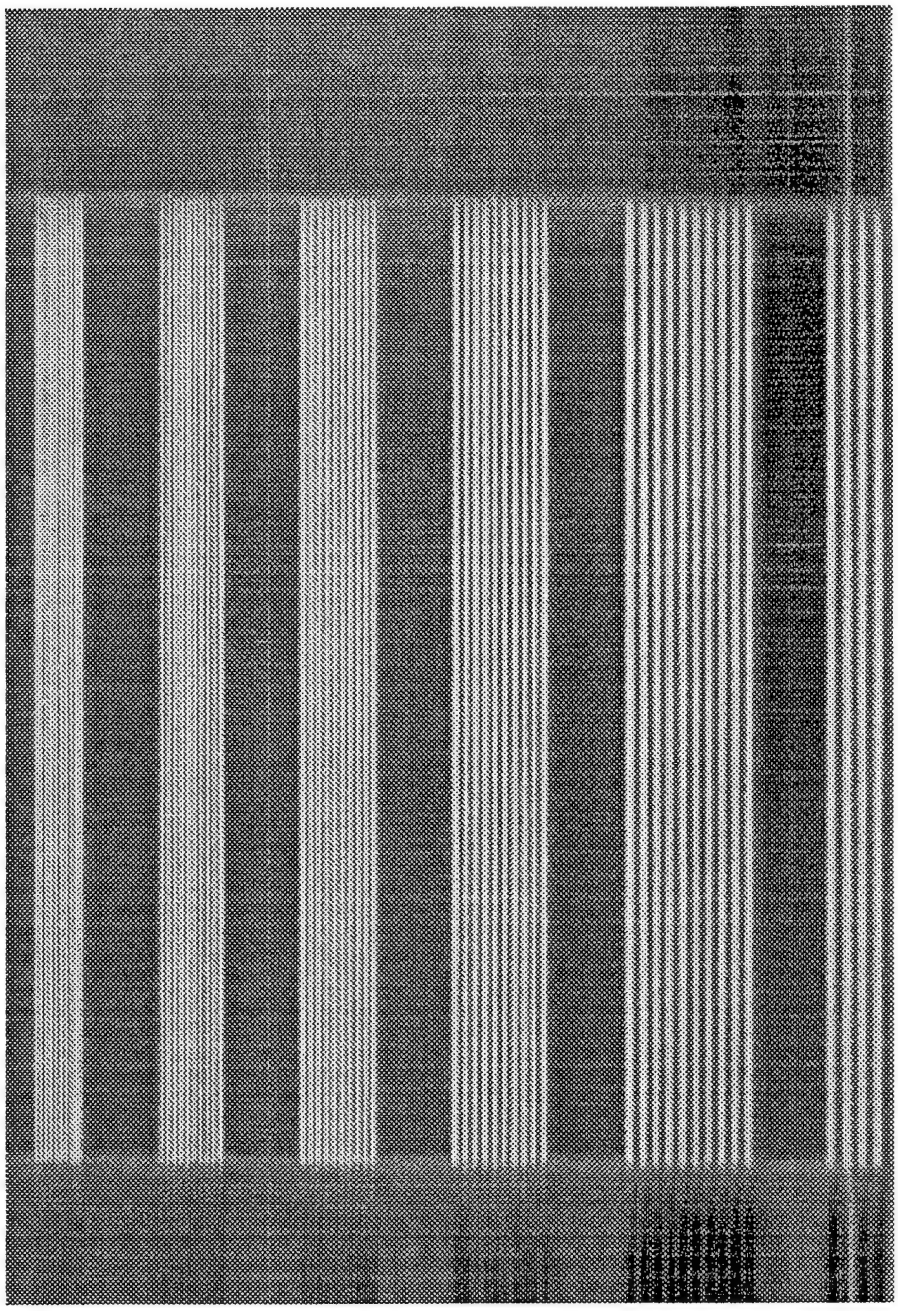

Figure E5: Lead-foil Penetrameter Image Acquired with a Thallium Bromide Coated Semiconductor Sensor Array (10.0, 8.0, 6.0, 5.0, and 4.0 lp/mm)

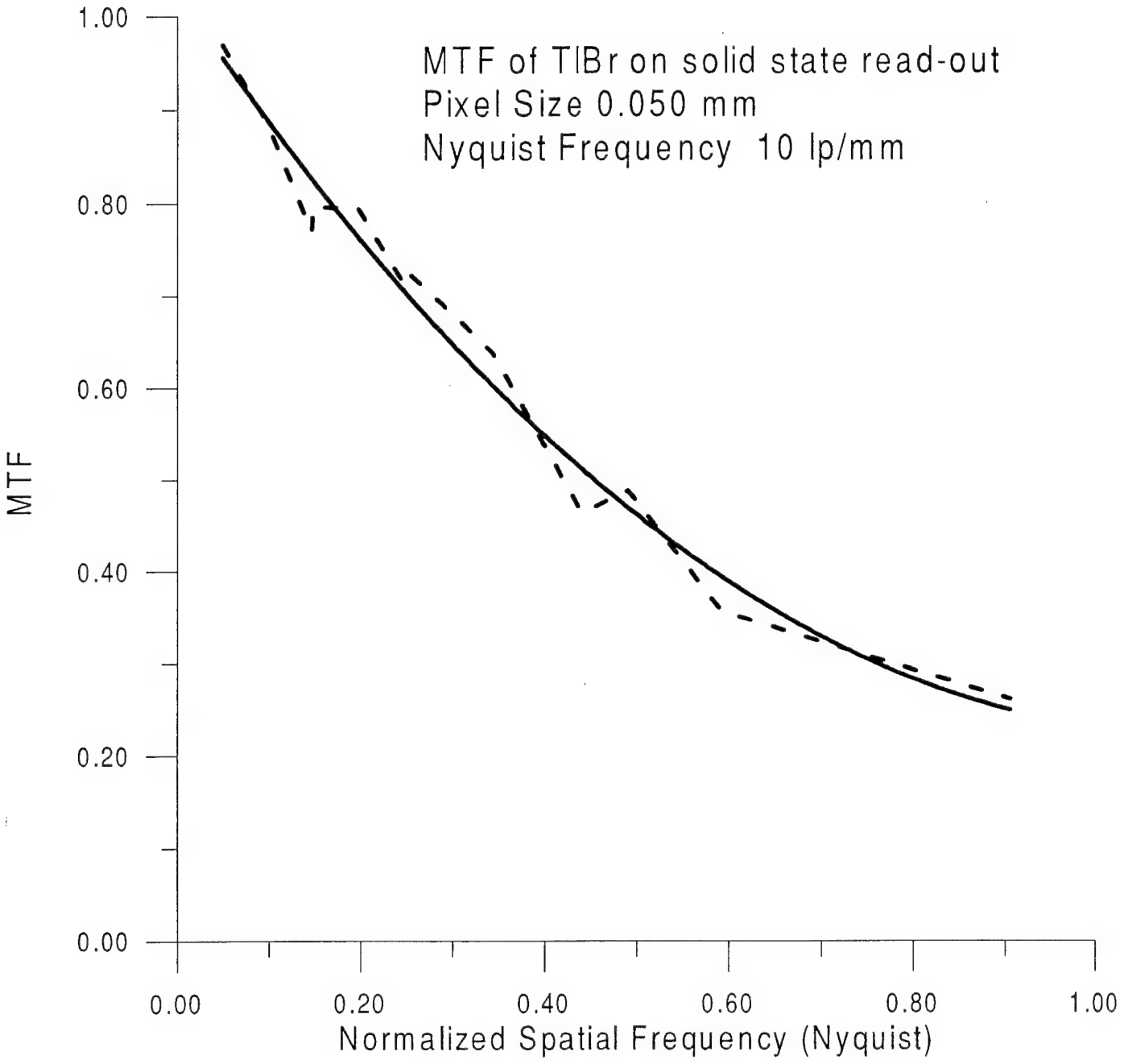

Figure E6: MTF of Thallium Bromide Coated Semiconductor Sensor Array

Appendix F

Abstract SCAR Paper Presented June 5, 1998

ADVANCED DIGITAL MAMMOGRAPHY

Ronald B. Schilling, Ph.D., S.R. Sharma, Ph.D. and John D. Cox, Ph.D.

PrimeX General Imaging Corp.
13650 Paseo del Roble, Los Altos Hills, CA 94022

The current state-of-the-art in screening and diagnostic mammography is still conventional film-screen mammography. However, the efficacy of film-screen mammography is limited by its dynamic range, low contrast resolution, film noise, dose-inefficient scatter reduction and film processing artifacts. It offers low diagnostic specificity in the range of 20% to 30% resulting in a high number of false-positive film-screen initiated biopsies, the cost of which alone is estimated at several hundred million dollars. It is currently estimated that *one out of every four women* screened annually for ten years by film-screen mammography will experience the anxiety and cost of a screening initiated false-positive mammogram (benign biopsy).

Solid-state x-ray sensor technology has the potential to improve the diagnostic quality of mammograms through higher quantum efficiency and spatial resolution than screened film can provide. These improvements in performance can be obtained while lowering the patient exposure dose. The inherently digital output of solid-state detector arrays is ideally suited for PACS (Picture Archiving and Communications Systems) including electronic archiving and image transmission over computer networks, image enhancement and analysis, and computer aided diagnosis (CAD).

PrimeX General Imaging Corp. (PGI) is currently developing a primary x-ray, slot-scanned digital mammography (DXM-1) prototype system based on high performance direct x-ray detection hybrid sensors. The heart of this system is semiconductor x-radiation sensors. Images are acqurired in a similar fashion to a conventional (screen-film) mammography system except for a moving aperture. It consists of a x-ray tube and a beam collimating

Keywords: **Computer Aided Diagnosis, Slot-Scan, Low Dose, Direct Digital Imaging, Conspicuity**

This work was supported by the U.S. Army Medical Research and Materiel Command under DAMD17-96-1-6239

Pre-print SCAR Paper Presented June 5, 1998

Advanced Digital Mammography

J. D. Cox, S. R. Sharma and R. B. Schilling

PrimeX General Imaging Corp. 13650 Paseo Del Roble, Los Altos Hills, CA 94022 USA

1. INTRODUCTION

Mammography is the most demanding of all clinical imaging applications. It requires high contrast, high spatial resolution and high signal to noise ratio at the minimum possible x-radiation dose to the patient. Fundamentally, it is often the minimum contrast of the cancer, relative to its surroundings, which determines the detection of the breast cancer. This can be as low as 0.1%, and averages 6 to 8% at the 18 to 20 KeV x-ray beam energies employed in mammography. The detectable contrast of a cancer is inversely proportional to the signal-to noise ratio of the imaging system. Clusters of much higher contrast microcalcifications are a frequent mammographic presentation of breast cancer requiring high image resolution.

Diagnosing cancer from a mammogram requires skillful and meticulous interpretation. The two primary indicators of breast cancer in a mammogram are the presence of a mass and clustered microcalcifications. Microcalcifications are an important indication of breast cancer because they are present in 30-50% of all cancers found mammographically. Further, microcalcifications are often visible in the mammogram before a mass can be detected clinically by physical examination. However, microcalcifications are often difficult to detect because, radiographically they appear as tiny areas (as small as 0.2 mm in diameter) slightly brighter than the surrounding background. To detect such subtle lesions, radiologists often use a magnifying glass and carefully examine the full breast area of the mammogram which is time consuming and tedious. Although radiologists do find microcalcifications in 30-50% of cases with breast carcinoma, as much as 80% of breast carcinomas reveal microcalcifications in pathologic examination.

Mammography is the most effective method for early detection of breast cancer [1-2] and yet, 10-30% of women who have breast cancer and undergo mammography have negative mammograms. In about two-thirds of these false-negative cases, the radiologist failed to detect a cancer that was evident in retrospect. Low conspicuity of the lesion, eye fatigue, and distraction by other image features are possible causes for these misses. It is expected that if radiologists were alerted to suspicious regions on the mammogram, then the number of missed cancers could be reduced. Furthermore, of the women who are sent to biopsy, only 20-40% actually have breast cancer. Quantitative analysis of the radiographic features of microcalcifications and masses may help radiologists improve their specificity.

Recent developments in the areas of information processing, computer vision, artificial intelligence, neural networks and particularly the high speed computers have permitted development of schemes for automated detection of lesions and characterization of normal and abnormal patterns in mammography. Here computer output is expected to be used as a second

opinion to assist radiologists in their interpretation of radiographic images. The basic concept for this approach to automated detection is called computer-aided diagnosis (CAD). The goals of CAD are to improve diagnostic accuracy by drawing the radiologist's attention to potential lesion sites and enhancing the consistency of image interpretation. Recent work in CAD has demonstrated significantly improved accuracy, mainly due to improved computer vision [3], better methods for film digitization [4] and an increase in the image quality of mammograms [5]. It is for this reason, that CAD is expected to enjoy improved accuracy with the advent of digital imaging systems for mammography, because these systems are expected to be superior to conventional film-screen in image quality. Much of the recent work on CAD was developed at the University of Chicago. Detection of clustered microcalcifications and masses are approached with different strategies.

2. DIGITAL IMAGING MODALITIES

The current state-of-the-art in screening and diagnostic mammography is still conventional film-screen mammography. However, the efficacy of film-screen mammography is limited by its dynamic range, low contrast resolution, film noise, dose-inefficient scatter reduction and film processing artifacts. It offers low diagnostic specificity in the range of 20% to 30% resulting in a high number of false-positive film-screen initiated biopsies, the cost of which alone is estimated at several hundred million dollars. It is currently estimated that *one out of every four women* screened annually for ten years by film-screen mammography will experience the anxiety and cost of a screening initiated false-positive mammogram (benign biopsy).

Solid-state x-ray sensor technology has the potential to improve the diagnostic quality of mammograms through higher quantum efficiency and spatial resolution than screened film can provide. These improvements in performance can be obtained while lowering the patient exposure dose. The inherently digital output of solid-state detector arrays is ideally suited for PACS (Picture Archiving and Communications Systems) including electronic archiving and image transmission over computer networks, image enhancement and analysis, and computer aided diagnosis (CAD).

There are currently several solid-state, digital imaging modalities under development that have applications in mammography. These emerging modalities can be broadly divided into two categories based on how they detect x rays; *primary* sensors which convert the incident x-radiation directly into usable electrical signal and *secondary* sensors which require an intermediate step for first converting the x-radiation into visible light using, e.g., a phosphor screen which then converts the visible light to usable electrical signal. Both of these categories can be further subdivided into area sensors and scanning sensors.

The first digital x-ray sensors to have found application in commercial mammography equipment are the Charge-Coupled Device (CCD) based *secondary*/area sensor systems [5-7]. These systems use CCDs coupled to a phosphor screen, either via a fiber-optic link or a visible light lens system. Limited field-of-view CCD-based digital mammography systems manufactured by Fischer and Lorad received FDA approval in late 1992 for breast imaging during stereotactic core biopsy (5 x 5 cm field). Commercial full-field mammography systems are now under development using this technology in both slot-scanning and area detection configurations.

Recently, General Electric and others have developed an amorphous silicon *secondary*/area sensor system. This system is a full-field imager that employs a scintillating phosphor that illuminates an array of amorphous silicon Schottky diodes connected to polysilicon thin-film transistors. Images acquired with a prototype system were shown at the Radiological Society of North America '96 INFO*Rad* Exhibit, December 1-7, 1996. The images displayed showed resolution comparable to film-screen systems.

PrimeX General Imaging Corp. (PGI) is currently developing two primary x-ray, slot-scanned digital mammography (DXM-1) prototype units based on high performance direct x-ray detection hybrid sensors. The system is schematically shown in Figure 1. The heart of this system is the semiconductor x-radiation sensors. As shown in Figure 1, the transmission is similar to a conventional (screen-film) mammography system except for a moving aperture. It consists of a x-ray tube and a beam collimating aperture that rotates about the tube focal spot. The moving aperture protects the patient from 'unsensed' x-rays by providing a fan shaped beam synchronous in its motion to the sensor assembly on the receptor side.

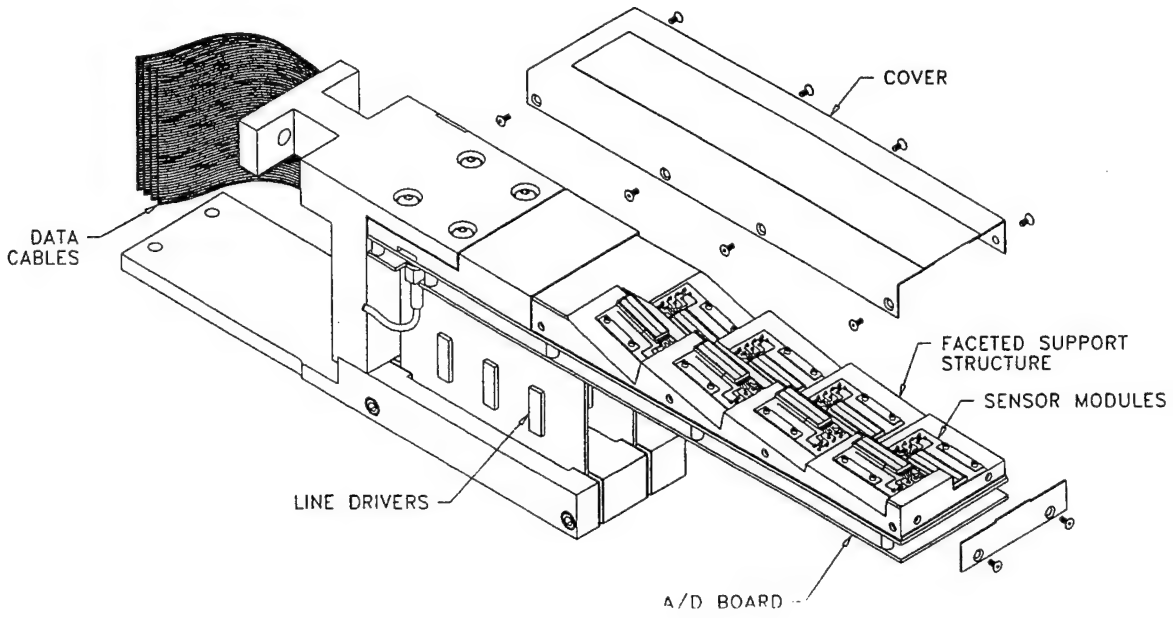

Figure 1. DXM-1 Digital Mammography Camera System

2.1 Comparison of Digital Imaging Modalities

A matrix comparing technologies currently under development for digital mammography is shown in Figure 2. The matrix is divided into 4 quadrants; the 2 quadrants on the left side of the matrix describe area sensors and the 2 quadrants on the right side describe scanning sensors. The quadrants in the upper half of the matrix describe *primary* sensors and the quadrants in the lower half of the matrix describe *secondary* sensors. Accordingly, the upper left quadrant describes *primary*/area sensors, the upper right describes *primary*/scanning sensors, the lower left quadrant describes *secondary*/area sensors and the lower right describes *secondary*/scanning sensors.

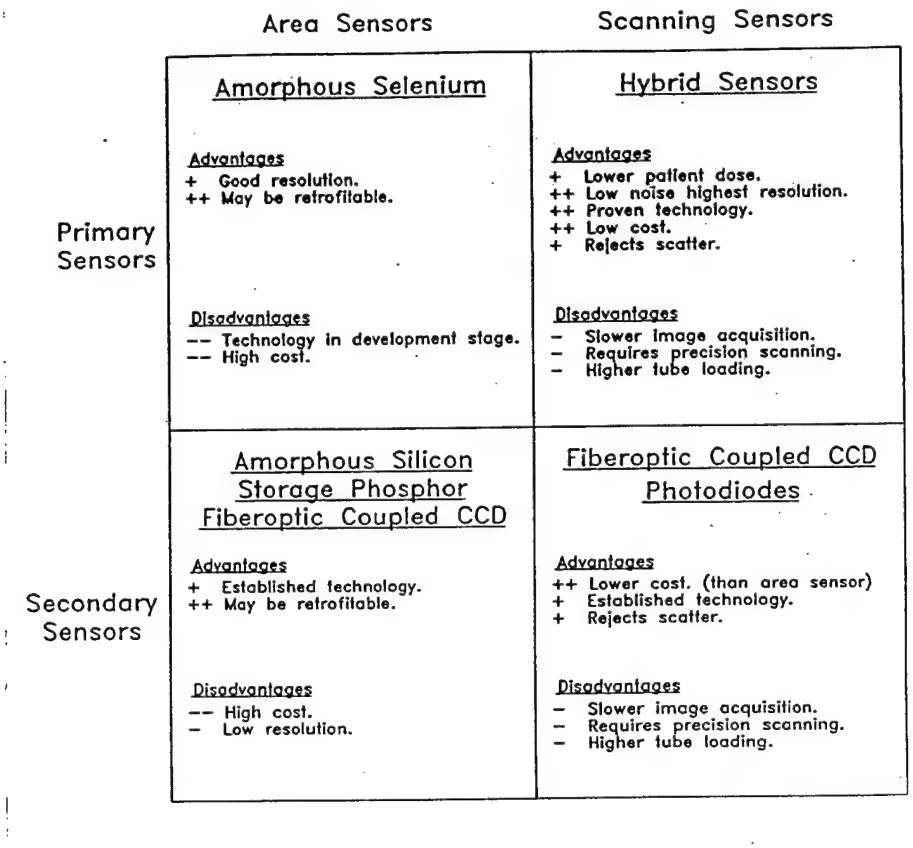

Figure 2. Matrix Comparing Technologies Currently Under Development for Digital Mammography

Within each quadrant the types as well as the advantages and disadvantages of each sensor system is shown. The issues that will drive the acceptance of digital imaging modalities (and the sensor systems they are based on) now under development are principally; cost, image performance and dose. The cost factor is very influential and is driven by how established the technology is and how much it costs to produce. Image performance is driven not only by the intrinsic resolution of the system but how the digital data is managed (i.e., processed and displayed). The dose factor in all cases for developing digital imaging modalities is lower than or equal to screened film. In some cases however, significant dose reduction over screened film is achievable.

System cost for scanning sensors is intrinsically much lower than area sensors due to the fact that scanning systems require a much smaller sensor area. This advantage is off-set somewhat by the requirement to scan the image. The scanning apparatus must not introduce scanning-motion artifacts in the acquired image. Scanning also requires higher x-ray tube output to minimize scanning time. Scanning does however, improve image quality by reducing scatter.

The advantages of area sensors are that they are easier to retrofit into existing mammography gantries and can acquire an image in a single exposure. The two area sensor based systems developed thus far are *secondary* systems that have relatively low resolution compared with *primary* systems and are significantly more expensive than scanning systems.

Based on the advantages and disadvantages described above, a *primary*/scanning system offers the lowest cost, highest performing digital imaging modality for mammography. These advantages can only be realized if the problems of x-ray tube capacity and scanning artifacts can be overcome. At this time x-ray tubes are being manufactured by Varian that have sufficient tube capacity to slot-scan a full-field mammography image in 4 seconds. PGI has acquired images of the ACR/RMI-156 mammography phantom with a prototype slot-scanning system that have no discernable scanning motion artifacts.

2.2 The DXM-1 *Primary*/Scanning Digital Mammography System

Initial testing of the prototype version of the DXM-1 has demonstrated a detective quantum efficiency greater than 80% and a Nyquist image resolution limit of greater than 17 line pairs per millimeter. Images of the ACR/RMI-156 quality assurance breast phantom acquired using these prototype sensors demonstrate image quality superior to film-screen even at exposure levels one-fifth to one-half the normal for film-screen. For instance, at one-fifth the exposure normal for film-screen, thirteen out of the sixteen targets in the breast phantom are clearly visible. At an exposure level of one-half the normal for screen film, all sixteen targets are discernible. In a typical film-screen image of the phantom, on the other hand, only thirteen out of the sixteen targets are visualized on the average. These results were exhibited and presented at the 1994 and 1996 RSNA meetings in Chicago. The peer reviews received were gratifying.

The high DQE of the DXM-1 system allows x-ray patient exposure to be reduced by a factor of up to 5 from the typical film-screen exposures while maintaining the same signal to noise ratio at low spatial frequencies. Even at this reduced exposure, this system will have a better signal to noise ratio at 13 lp/mm than film-screen at 10 lp/mm.

PGI was awarded a contract from the US Army Medical Research and Materiel Command through a Broad Agency Announcement for Breast Cancer Research. The 3-year contract began on July 1, 1996 and will provide approximately $1.6 million in funding to complete the development of the prototype DXM-1 low-dose digital mammography system and pursue a vigorous technical and clinical evaluation. The clinical evaluation will evaluate film screen versus digital mammography using 1,100 women as volunteers.

Two DXM-1 prototype systems will be constructed and evaluated during the study. One unit will be delivered to the University of Arizona for an engineering and technical evaluation which will incorporate some clinical evaluation and the other unit will be delivered to the University of California San Diego. This unit will be used to conduct a three part phase I/II clinical study.

3.0 ADVANCED DIGITAL MAMMOGRAPHY

Digital mammography as a replacement for film has modest advantages based on a cost/benefit analysis when viewed as a film substitute. The real advantage of digital mammography is that digital imaging facilitates CAD, stereo and 3-D imaging and tomography. These techniques are being developed to assist in the diagnosis of breast cancer and have shown encouraging results.

Analysis of digital mammographic data can be divided into three steps: 1) enhancement of mammographic features [8-10]; 2) detection and localization of suspicious areas [11-15]; and 3) classification. Expert-based systems have also been developed using a variety of approaches including the use of texture analysis, neural networks, Fourier descriptors and multitolerance methods [11-16].

Digital imaging modalities coupled with CAD and multidimensional imaging techniques will significantly improve the efficacy of mammography in the early diagnosis of cancer. This prediction is based on the fact that current film-screen based diagnosis suffers from the limitations of the poor DQE of screened film and the difficult nature of interpreting the mammogram. The significant improvement in DQE and the enormous computing power that is available today will provide the radiologist with better tools to make early and accurate diagnosis of breast cancer.

REFERENCES

1. Bassett, L.W., Gold, R.H., Breast Cancer Detection: **Mammography and Other Methods in Breast Imaging**, New York, Grune and Stratton, 198, 82 (1993)
2. Lissner, J., Kessler, M., Anhalt, G, **Early Breast Cancer,** Berlin, Springer-Verlag, (1985), 93-123.
3. Jain, A.K., **Fundamentals of Digital Image Processing**, Englewood Cliffs, NJ, Prentice Hall, 1989
4. Cook, L.T., Giger, M.L., Banitzky, S., Invest. Radiol., 1989, **24**, 910-916
5. Picarro, M.F. and Toker, E., SPIE, **2009**, 1993
6. Toker, E., and Picarro, M.F., SPIE **1901**, 1993
7. Karallas, A., and Harris, L.J., Med. Phys., 1992, 19(4), 1015-1023.
8. McSweeney, M.B., Sprawls, P., and Egan, R.L., **Recent Results in Cancer Research**, vol. 90, New York, Springer-Verlag, 1984, 79-89.
9. Dhawan, A.P., Buelloni, g., and Gordon, R., IEEE Trans. Med Imag., vol MI-5, no.1, 8-15.
10. Dhawan, A.P., and Le Royer, E., Comput. Methods Programs Biomed., vol. 27, 23-35, 1988.
11. Chan, H., Doi, K., Galhotra, S., Vyborny, C, Macmahon, H, and Jokich, P.M., Med. Phys., vol. 14, no. 4, 538-548, July/Aug 1987.
12. Morio, S., and Kawahara, S., et al, Comp. Biol. Med, vol. 19, no. 5, 295-305, 1989
13. Woods, K., Solka, J., Priebe, C, Doss, C., Bowyer, K., and Clarke, L.P., Symp. Electron. Imag.: Sci. Technol. San Jose, CA, USA Jan 31-Feb4 1993.
14. Nishikawa, R.M., et al, Symp. Electron. Imag.: Sci. Technol. San Jose, CA, USA Jan 31-Feb 4 1993.
15. Karssemeijer, N., Image Vision Comp., vol 10, no., 6, 369-375, 1992.
16. Dhwan, A.P., Chitre, Y., Kaiser-Bonasso, C., and Moskowitz, M, IEEE Trans. On Med. Imaging, Vol. 15, No. 3, June, 1996

Pre-print CARS Paper Presented June 24, 1999

Technologies for Digital Mammography

J. D. Cox and R. B. Schilling

PrimeX General Imaging Corp., 13650 Paseo del Roble, Los Altos Hills, CA 94022 USA

A review is provided of the various technologies that are under development for digital mammography. Considerations are given to performance, dose efficiency, cost, comfort factor and patient motion. An update of the current status of clinical results is provided.

1. DIGITAL X-RAY IMAGING MODALITIES

The current state-of-the-art in screening and diagnostic mammography is still conventional film-screen mammography. However, the efficacy of film-screen mammography is limited by its dynamic range, low contrast resolution, film noise, dose-inefficient scatter reduction and film processing artifacts. It offers low diagnostic specificity in the range of 20% to 30% resulting in a high number of false-positive film-screen initiated biopsies. The cost of which alone is estimated at several hundred million dollars. It is currently estimated that one out of every four women screened annually for ten years by film-screen mammography will experience the anxiety and cost of a screening initiated false-positive mammogram (benign biopsy).

Solid-state x-ray sensor technology has the potential to improve the diagnostic quality of mammograms through higher quantum efficiency and spatial resolution than screened film can provide. These improvements in performance can be obtained while lowering the patient exposure dose. The inherently digital output of solid-state detector arrays is ideally suited for PACS (Picture Archiving and Communications Systems) including electronic archiving and image transmission over computer networks, image enhancement and analysis, and computer aided diagnosis (CAD).

There are currently several solid-state, digital imaging modalities under development that have applications in mammography. These emerging modalities can be broadly divided into two categories based on how they detect x rays. There are primary sensors which convert the incident x-radiation directly into usable electrical signal and secondary sensors which require an intermediate step for first converting the x-radiation into visible light using, e.g., a phosphor screen which then converts the visible light to usable electrical signal. Both of these categories can be further subdivided into area sensors and scanning sensors.

Recent developments in the areas of information processing, computer vision, artificial intelligence, neural networks and particularly high speed computers have permitted development of schemes for automated detection of lesions and characterization of normal and abnormal patterns in mammography. Here computer output will be used as a second opinion to assist radiologists in their interpretation of radiographic images.

The basic concept for this approach to automated detection is called computer-aided diagnosis (CAD). Much of the recent work on CAD was developed at the University of Chicago. Detection of clustered micro-calcifications and masses are approached with different strategies. The goals of CAD are to improve diagnostic by drawing the radiologist's attention to potential lesion sites and enhancing the consistency of image interpretation. Recent work in CAD has demonstrated significantly improved accuracy due to improved computer vision [1], better methods for film digitization [2] and an increase in the image quality of mammograms [3]. CAD is expected to enjoy improved accuracy with the advent of digital systems for mammography, because these systems are expected to provide superior quality image data than that which can be provided by conventional film-screen mammograms.

The first digital x-ray sensors to have found application in commercial mammography equipment are the Charge-Coupled Device (CCD) based secondary area sensor systems [4]. These systems use CCDs coupled to a phosphor screen, either via a fiber-optic link or a visible light lens system. Limited field-of-view CCD-based digital mammography systems manufactured by Fischer and Lorad received FDA approval in late 1992 for breast imaging during stereotactic core biopsy (5 x 5 cm field). Commercial full-field mammography systems are now under development using this technology in both slot-scanning (Fischer) and area detection (TREX/Lorad) configurations.

General Electric and others (Siemens) have developed an amorphous silicon secondary/area sensor system for full-field mammography. These systems employ a scintillating phosphor that illuminates an array of amorphous silicon Schottky diodes connected to poly-silicon thin-film transistors. These devices have a pixel size of 100 microns and a 65% fill factor. PrimeX General Imaging Corp. (PGI) has developed a slot-scanning full-field mammography system that employs hybrid silicon-based PIN (primary) sensor arrays. This system has a pixel size of 50 microns and an over-sampling capability to produce a 25-micron pixel size with a 100% fill factor.

1.1 Comparison of Digital X-ray Imaging Modalities

A matrix comparing technologies currently under development for digital mammography is shown in Figure 1. The matrix is divided into 4 quadrants; the 2 quadrants on the left side of the matrix describe area sensors and the 2 quadrants on the right side describe scanning sensors. The quadrants in the upper half of the matrix describe ***primary*** sensors and the quadrants in the lower half of the matrix describe ***secondary*** sensors. Accordingly, the upper left quadrant describes primary/area sensors, the upper right describes primary/scanning sensors, the lower left quadrant describes secondary/area sensors and the lower right describes secondary/scanning sensors.

Within each quadrant the type as well as the advantages and disadvantages of each sensor system are shown. The issues that will drive the acceptance of digital imaging modalities (and the sensor systems they are based on) now under development are principally; cost, image performance and dose. The cost factor is very influential and is driven by how established the technology is and how much it costs to produce. Image performance is driven not only by the intrinsic resolution of the system but how the digital data is managed (i.e., processed and displayed). The dose factor in all cases for developing

digital imaging modalities is lower than or equal to screened film. In some cases however, significant dose reduction over screened film is achievable.

System cost for scanning sensors is intrinsically much lower than area sensors due to the fact that scanning systems require a much smaller sensor area. This advantage is off-set somewhat by the requirement to scan the image. The scanning apparatus must not introduce scanning-motion artifacts in the acquired image. Scanning also requires higher x-ray tube output to minimize scanning time. Scanning does however, improve image quality by reducing scatter. The advantages of area sensors are that they are easier to retrofit into existing mammography gantries and can acquire an image in a single exposure. The two area sensor based systems developed thus far are secondary systems that have relatively low resolution compared with primary systems and are significantly more expensive than scanning systems.

	Area Sensors	Scanning Sensors
Primary Sensors	**Amorphous Selenium** Advantages + Good resolution. ++ May be retrofitable. Disadvantages -- Technology in development stage. -- High cost.	**Hybrid Sensors** Advantages + Lower patient dose. ++ Low noise highest resolution. ++ Proven technology. ++ Low cost. + Rejects scatter. Disadvantages - Slower image acquisition. - Requires precision scanning. - Higher tube loading.
Secondary Sensors	**Amorphous Silicon Storage Phosphor Fiberoptic Coupled CCD** Advantages + Established technology. ++ May be retrofitable. Disadvantages -- High cost. - Low resolution.	**Fiberoptic Coupled CCD Photodiodes** Advantages ++ Lower cost. (than area sensor) + Established technology. + Rejects scatter. Disadvantages - Slower image acquisition. - Requires precision scanning. - Higher tube loading.

Figure 1. Matrix Comparing Technologies Currently Under Development for Digital Mammography

For mammography applications it is likely that a 50-micron pixel will be required. Amorphous silicon flat panel detectors have a very small fill factor (about 15%) when utilizing 50-micron pixels. This makes the use of scintillators impractical due to the fact that the light emitted by the scintillator spreads out and only 15% of the light would be collected. The use of a photoconductor eliminates this problem. X rays are absorbed in the photoconductor liberating electrons and holes which are collected at the electrodes. Shown below is a figure depicting the two processes. As shown in Figure 2, the signal (i.e., electrons) produced by the photoconductor is actually concentrated at the electrode whereas

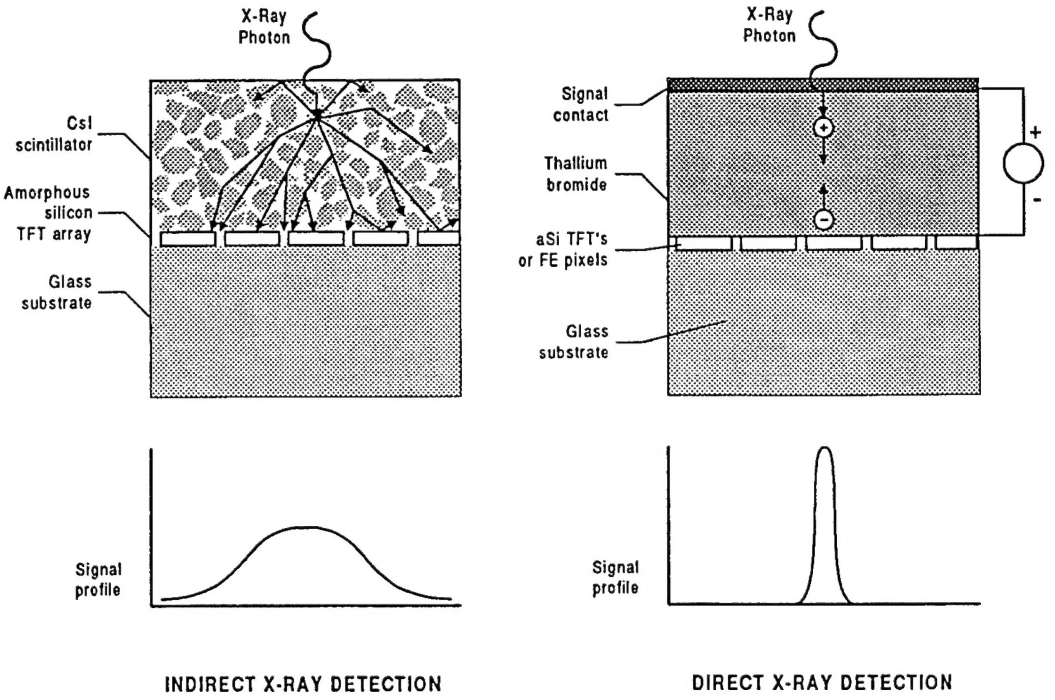

Figure 2. Comparison of resolution in scintillator-based detectors versus photoconductor-based detectors

the signal (i.e., photons) produced by the scintillator spreads out and is diluted requiring a large fill factor to collect it efficiently.

Based on the advantages and disadvantages described above, a primary/scanning system offers the lowest cost, highest performing digital imaging modality for mammography. These advantages can only be realized if the problems of x-ray tube capacity and scanning artifacts can be overcome. At this time x-ray tubes are being manufactured by Varian that have sufficient tube capacity to slot-scan a full-field mammography image in 4 seconds. PGI has acquired images of the ACR/RMI-156 mammography phantom with a prototype slot-scanning system that have no discernable scanning motion artifacts.

TREX medical has entered clinical trials with their full-field fiber-optic coupled CCD digital mammography system. Fischer Imaging Corporation has obtained clinical data for their slot-scanning fiber-optic coupled CCD digital mammography system and showed images at the RSNA '98 meeting in Chicago (Nov 29-Dec 4, 1998). PGI has also obtained clinical images with their slot-scanning hybrid silicon-based PIN diode system.

The TREX medical system is being introduced at a price of $500,000 and has a poor patient comfort aspect due to the large size of the fiber-optic array. The Fischer system is being intoduced at a price of $250,000. The slot-scanning systems being introduced by Fischer and PGI offer improved patient comfort through the use of a curved breast compression plate and reduce motion artifacts due to the slot-scan geometry.

The amorphous silicon-based flat panel mammography systems being introduced by GE and Siemens offer the best solution for a true retrofit option for existing mammography gantries. These digital imaging devices resemble film cassettes and can be interchanged

without any modification to the gantry. As such they offer no changes to the comfort factor or patient motion problems encountered with current film-screen mammography gantries. However, these systems are currently being marketed as new equipment with an estimated price of $250,000-$300,000.

1.2 Other Imaging Modalities

Mammography is fundamental to the examination and detection of breast cancer. Other modalities such as ultrasound, magnetic resonance imaging (MRI), nuclear medicine and positron emission tomography (PET) provide additional insights into the diagnostic process.

Ultrasound is the most useful of the non-ionizing techniques available. Due to the high false-negative rates of x-ray, ultrasound has emerged as the primary modality used by clinicians to provide further evaluation. Ultrasound is also useful during biopsy in distinguishing cysts from solid masses.

The advantages of MRI include improved tissue information reflecting flow and perfusion and the ability to image tomographically. Godd tissue visualization near the chest and in the vicinity of implants can be obtained.

Nuclear medicine and PET can distinguish between tissues that have different metabolic rates after injection of a suitable tracer. PET can provide biochemical-monitoring response to therapy.

2.0 CONCLUSIONS

Digital mammography as a replacement for film has modest advantages based on a cost/benefit analysis when viewed as a film substitute. The real advantage of digital mammography is that digital imaging facilitates CAD, stereo and 3-D imaging and tomography. These techniques are being developed to assist in the diagnosis of breast cancer and have shown encouraging results.

Digital imaging modalities coupled with CAD and multidimensional imaging techniques will significantly improve the efficacy of mammography in the early diagnosis of cancer. This prediction is based on the fact that film-screen based diagnosis suffers from the limitations of the poor DQE of screened film and the difficult nature of interpreting the mammogram. The significant improvement in DQE and the enormous computing power that is available today will provide the radiologist with better tools to make early and accurate diagnosis of breast cancer. CAD is being used to enable the physician to reach a higher level of diagnostic accuracy. CAD is also useful in enabling the health care team in reaching higher levels of productivity.

REFERENCES

1. Jain, A.K., Fundamentals of Digital Imaging Processing, Englewood Cliffs, NJ, (1985), 93-123.
2. Cook, L.T., Giger, M.L., Banitzky, S., Invest. Radiol., 1989, 24, 910-916
3. Bassett, L.W., Gold, R.H., Breast Cancer Detection: Mammography and Other Methods in Breast Imaging, New York, Grune and Stratton, 198,82 (1993)
4. Picarro, M.F. and Toker, E., SPIE 2009, 1993

This work was supported by the U.S. Army Medical Research and Materiel Command under DAMD17-96-1-6239